

1 **Marine Carbohydrates and Other Sea Spray Aerosol Constituents Across**  
2 **Altitudes in the Lower Troposphere of Ny-Ålesund, Svalbard**

3 **Sebastian Zeppenfeld<sup>1\*</sup>, Jonas Schaefer<sup>2</sup>, Christian Pilz<sup>2</sup>, Kerstin Ebell<sup>3</sup>, Moritz Zeising<sup>4</sup>, Frank**  
4 **Stratmann<sup>2</sup>, Holger Siebert<sup>2</sup>, Birgit Wehner<sup>2</sup>, Matthias Wietz<sup>4,5,6</sup>, Astrid Bracher<sup>4,7</sup>, and**  
5 **Manuela van Pinxteren<sup>1</sup>**

6 1 Atmospheric Chemistry Department (ACD), Leibniz Institute for Tropospheric Research (TROPOS),  
7 Leipzig, Germany

8 2 Atmospheric Microphysics (AMP), Leibniz Institute for Tropospheric Research (TROPOS), Leipzig,  
9 Germany

10 3 Institute for Geophysics and Meteorology, University of Cologne, Cologne, Germany

11 4 Alfred Wegener Institute Helmholtz Centre for Polar and Marine Research, Bremerhaven, Germany

12 5 Max Planck Institute for Marine Microbiology, Bremen, Germany

13 6 Institute for Chemistry and Biology of the Marine Environment, University of Oldenburg, Oldenburg,  
14 Germany

15 7 Institute of Environmental Physics, University of Bremen, Bremen, Germany

16

17 \*Correspondence to: Sebastian Zeppenfeld (zeppenfeld@tropos.de)

18

19

20

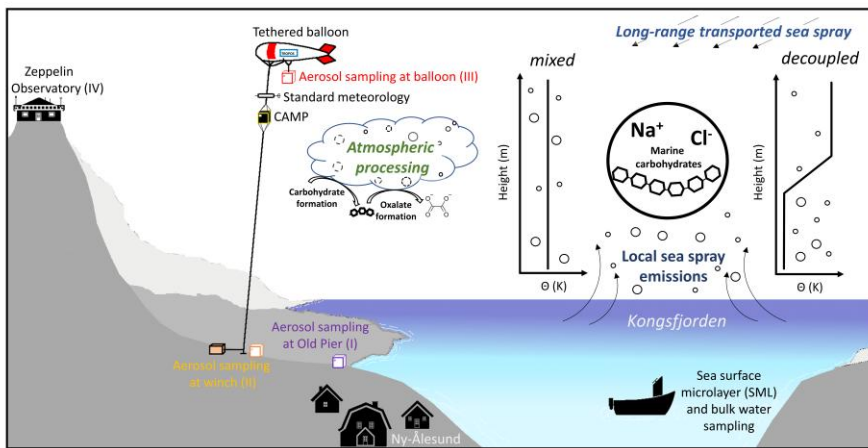
21 **Abstract**

22 Marine combined carbohydrates in aerosol particles (CCHO<sub>aer</sub>) have the potential to influence  
23 cloud formation and properties, but it remains unclear to what extent they reach altitudes  
24 relevant for cloud processes. Balloon-borne measurements of major sea spray aerosol (SSA)  
25 constituents, including sodium (Na<sup>+</sup><sub>aer</sub>) and CCHO<sub>aer</sub>, were conducted in autumn 2021 and  
26 spring 2022 in Ny-Ålesund (Svalbard). Total suspended particles were collected at 321–1112 m,  
27 covering both the marine boundary layer and the free troposphere, with Na<sup>+</sup><sub>aer</sub> ranging 23–  
28 850 ng m<sup>-3</sup> and CCHO<sub>aer</sub> 3.8–274 ng m<sup>-3</sup>. The chemical composition of balloon-borne aerosol  
29 samples was compared with synchronized ground level measurements at the balloon's winch  
30 (Na<sup>+</sup><sub>aer</sub>: 35–3710 ng m<sup>-3</sup>; CCHO<sub>aer</sub>: 1.9–194 ng m<sup>-3</sup>), and at the Old Pier (Na<sup>+</sup><sub>aer</sub>: 140–1470 ng m<sup>-3</sup>;  
31 CCHO<sub>aer</sub>: 1.6–10.0 ng m<sup>-3</sup>), where freshly emitted SSA particles were sampled. Surface  
32 seawater from the Kongsfjorden was analyzed to evaluate the sea-air transfer of marine  
33 CCHO. Air mass histories, atmospheric mixing, and cloud conditions were evaluated for three  
34 selected cases to explain vertical concentration patterns. A strong correlation (R=0.78,

35  $p < 0.001$ ) between combined xylose ( $< 0.2\text{--}14.1 \text{ ng m}^{-3}$ ) in  $\text{CCHO}_{\text{aer}}$  and oxalate $_{\text{aer}}$  ( $< 1\text{--}67 \text{ ng m}^{-3}$ )  
 36  $^3$ ) across all altitudes, suggests either coproduction or a connection through atmospheric  
 37 processing. These results provide a first comprehensive picture of local primary sea-air  
 38 transfer of marine combined carbohydrates and highlight the roles of long-range transport,  
 39 in-situ formation, and atmospheric chemical aging/processing in shaping their atmospheric  
 40 distribution.

41

42



43

## 44 1. Introduction

45 Aerosol particles in the High Arctic atmosphere originate from a complex interplay of primary  
46 and secondary emissions from oceanic, terrestrial, cryospheric, and anthropogenic sources,  
47 followed by diverse atmospheric processes (Schmale et al., 2021). They play a crucial role in  
48 the radiation balance, ~~both~~ directly by scattering and absorbing ~~sunlight shortwave and~~  
49 ~~longwave radiation~~, and indirectly by influencing cloud formation and phase state ~~through~~  
50 ~~functioning~~ as cloud condensation nuclei (~~CCNs~~) and ice-nucleating particles (~~INPs~~) (Lohmann  
51 and Feichter, 2005; Penner et al., 2001; Quinn et al., 2015; Yu et al., 2006). These effects are  
52 strongly governed by the particles' size distribution and chemical composition (Dusek et al.,  
53 2006; Farmer et al., 2015; Kanji et al., 2017; Pilinis et al., 1995).

54 The High Arctic predominantly consists of marine areas, characterized by a seasonally variable  
55 extent of sea ice cover and open waters. Consequently, sea spray aerosol (SSA) particles  
56 represent a key group of primary aerosol particles in this region (Heutte et al., 2025; Kang et  
57 al., 2025; Schmale et al., 2022). As Arctic sea ice coverage continues to decline due to global  
58 warming, enhanced by Arctic amplification (Cai et al., 2021; Francis and Wu, 2020; Wendisch  
59 et al., 2017, 2023), larger expanses of open ocean are anticipated to become significant  
60 sources of SSA emissions (Browse et al., 2014; Struthers et al., 2011). Although direct  
61 measurements remain sparse, Sharma et al. (2019) readily observed increasing sea salt  
62 aerosol production from sea spray over 34 years at the Arctic air chemistry observatory in  
63 Alert, Canada.

64 SSA particles are generated through wind-driven wave action, which causes bubbles at the sea  
65 surface to burst, ejecting film and jet droplets into the atmosphere (Veron, 2015). SSA  
66 particles primarily consist of inorganic sea salt ions, mainly sodium and chloride, along with  
67 organic matter (OM), including significant amounts of marine carbohydrates originating from  
68 the sea surface microlayer (SML) and the underlying bulk seawater (Müller et al., 2010; van  
69 Pinxteren et al., 2023; Quinn et al., 2015; Russell et al., 2010). In seawater, carbohydrates are  
70 produced by ~~both unicellular and multicellular photoautotrophic~~ organisms, predominantly as  
71 linear or branched oligo- and polysaccharides (Aluwihare et al., 1997; Borch and Kirchman,  
72 1997; Engel and Händel, 2011; Khadem, 2012), collectively referred to as combined  
73 carbohydrates (CCHO). They also exist as ~~monosaccharides, known as~~ dissolved free  
74 carbohydrates (DFCHO). ~~Both DFCHO and CCHO, monosaccharides are often rapidly~~

75 consumed or transformed by heterotrophic organisms, with turnover rates largely  
76 determined by the molecular structure and composition of the carbohydrates~~bacteria~~ (Arnosti  
77 et al., 2021; Engel and Händel, 2011; Ittekkot et al., 1981; Kirchman et al., 2001).

78 Sodium in aerosol particles ( $\text{Na}^+_{\text{aer}}$ ) is highly abundant in the marine boundary layer, with only  
79 minor terrestrial sources and greater atmospheric stability compared to chloride ( $\text{Cl}^-_{\text{aer}}$ ) (Chi  
80 et al., 2015; Keene et al., 1986; Manders et al., 2010; Sander et al., 2003). This makes it a  
81 valuable conservative tracer for studying the sea-to-air transfer and atmospheric  
82 transformation of organic compounds, including marine carbohydrates, as well as other  
83 inorganic SSA constituents. Notably, the ratio of OM to  $\text{Na}^+$  is significantly higher in SSA  
84 particles than in seawater, reflecting not only the preferential enrichment of surface-active  
85 substances at the interface but also a more complex interplay of factors such as water  
86 solubility, biological activity within the ocean surface, and co-adsorption processes involving  
87 matrix constituents (Burrows et al., 2014; Gantt et al., 2011; Hasenecz et al., 2020, 2019;  
88 Hoffman and Duce, 1976; Jayarathne et al., 2016; van Pinxteren et al., 2017; Quinn et al., 2015;  
89 Russell et al., 2010; Schill et al., 2018). This enrichment is particularly pronounced in  
90 submicron particles compared to supermicron particles. Furthermore, following the sea-to-air  
91 transfer of OM and CCHO, recent laboratory (Hasenecz et al., 2020; Malfatti et al., 2019) and  
92 field (Zeppenfeld et al., 2021, 2023) observations suggest their molecular transformation or  
93 additional in-situ formation, driven by abiotic, microbial or enzymatic activities in the  
94 atmosphere.

95 SSA particles are known to function as both CCNs-cloud condensation nuclei (Orellana et al.,  
96 2011; Xu et al., 2022) and INPs-ice-nucleating particles (Alpert et al., 2022; DeMott et al., 2016;  
97 Hill et al., 2023; Mirrielees et al., 2024), underscoring their important role in cloud  
98 microphysics, cloud formation, and precipitation processes. Recently, Hartmann et al. (2025)  
99 demonstrated, through a combination of lab and field data, that SSA particles' ice-nucleating  
100 activity is likely attributable to the polysaccharides they contain. Model simulations further  
101 indicated that the ice-nucleating activity of marine polysaccharides is particularly significant  
102 within the temperature range between  $-20$  and  $-15^\circ\text{C}$  in remote oceanic regions, where  
103 contributions from terrestrial ~~INP sources~~ ice-nucleating particles are minimal or absent.  
104 Furthermore, Rocchi et al., (2024) demonstrated that the presence of glucose-rich CCHO, in  
105 combination with sea salt, significantly enhances SSA production in eastern Arctic waters. This  
106 finding may improve the predictability of SSA emissions in marine models.

107 In the field, marine combined carbohydrates in aerosol particles (CCHO<sub>aer</sub>) have been  
108 predominantly measured at ship-based or coastal locations, which are in close proximity to  
109 local marine emission sources both horizontally and vertically (Leck et al., 2013; van Pinxteren  
110 et al., 2023; Zeppenfeld et al., 2021, 2023). In contrast, only a few studies have investigated  
111 CCHO<sub>aer</sub> (Karl et al., 2019; Yttri et al., 2024) at an elevated mountain site in a marine-influenced  
112 setting, aiming to assess atmospheric concentrations at higher altitudes. Vertically resolved  
113 field data comparing ground-level and elevated altitudes using mobile platforms, however,  
114 have been unavailable for marine CCHO<sub>aer</sub> in the past. As a result, it remains unclear to what  
115 extent and under which conditions CCHO<sub>aer</sub> reach the upper marine boundary layer and the  
116 free troposphere. This is due to several challenges, including low atmospheric concentrations  
117 pushing the instruments' detection capabilities for offline analyses to their limits, the lack of  
118 highly resolving online detection techniques for CCHO<sub>aer</sub>, and in particular the absence of  
119 lightweight yet powerful pumps with high flow rates. Additionally, the very short sampling  
120 times typically available on mobile airborne measurement platforms pose a further obstacle  
121 for measuring marine CCHO<sub>aer</sub> in aerosol particles across altitudes within the troposphere. This  
122 lack of vertical field data leaves high uncertainty about the broader relevance of these  
123 biomolecules in cloud formation and glaciation beyond a controlled laboratory setup.

124 Previous airborne measurements around Svalbard (Hara et al., 2003; [Simon et al., 2025](#)) and  
125 the Canadian Arctic (Köllner et al., 2017) demonstrated that SSA particles, identified by Na<sup>+</sup>  
126 and Cl<sup>-</sup>, are present in higher altitudes of the lower troposphere, and, to a lesser extent,  
127 reach the middle free troposphere (3–6 km a.s.l.). Some of these aerosol particles showed  
128 signs of atmospheric aging, such as the replacement of chloride with nitrate and sulfate in the  
129 SSA particles. While vertically resolved data exists for major inorganic SSA constituents, such  
130 extended information is lacking for marine CCHO<sub>aer</sub>.

131 Recent methodological advances now allow for a more detailed investigation of the transport  
132 mechanisms and atmospheric chemical fate of marine carbohydrates. In this study, we  
133 present atmospheric concentrations of these biomolecules alongside common inorganic SSA  
134 constituents. Measurements were conducted from ground level up to various altitudes within  
135 the boundary layer and lower free troposphere using a tethered helium balloon in Ny-Ålesund  
136 on Svalbard during autumn 2021 and spring 2022. For selected cases, we examined the  
137 influence of mixing state, meteorological conditions, and air mass history on the observed  
138 aerosol composition. Finally, this study addresses the potential atmospheric processing and

139 transformation of marine carbohydrates, with a focus on their possible contribution to  
140 secondary aerosol formation and their implications for atmospheric chemistry and cloud-  
141 relevant processes.

142

## 2. Experimental

143

An overview of all analytical and modelling methods applied in this study is provided in

144

Table 1.

145

Table 1. Overview of parameters, methods and sample/media types used in this study.

<u>Category</u>	<u>Parameters</u>	<u>Method/Instrument</u>	<u>Sample/Medium</u>
<u>Major inorganic ions</u>	<u>Na<sup>+</sup>, K<sup>+</sup>, Mg<sup>2+</sup>, Ca<sup>2+</sup>, Cl<sup>-</sup>, SO<sub>4</sub><sup>2-</sup>, oxalate</u>	<u>Ion chromatography</u>	<u>Bulk seawater, SML, aerosol particles (filter)</u>
<u>Free and combined carbohydrates</u>	<u>Fuc, Rha, Ara, Gal, Glc, Xyl, Man, Fru, GalN, GlcN, MurAC, GalAC, GlcAC</u>	<u>HPAEC-PAD</u>	<u>Bulk seawater, SML, aerosol particles (filter)</u>
<u>Sea surface temperature</u>	<u>SST</u>	<u>Digital Thermometer</u>	<u>Ocean surface</u>
<u>Aerosol number concentration</u>	<u>N<sub>550</sub> (150-2900 nm)</u>	<u>POPS (CAMP)</u>	<u>Atmospheric column</u>
<u>Meteorology</u>	<u>T, U, WD, RH, p, wind, θ, q</u>	<u>Standard meteorology package + thermodynamic equations</u>	<u>Atmosphere at ground (AWIPEV), atmospheric column</u>
<u>Cloud properties</u>	<u>Clouds and hydrometer types, IWP, LWP, IWV</u>	<u>Cloudnet + HATPRO</u>	<u>Atmospheric column</u>
<u>Biogeochemistry (model)</u>	<u>TChl-a, dissolved acidic polysaccharides</u>	<u>FESOM2.1-REcoM3</u>	<u>Ocean surface</u>
<u>Air mass origin</u>	<u>48-h back-trajectories</u>	<u>NOAA HYSPLIT</u>	<u>Several altitudes of atmosphere</u>

146

147

### 2.1 Study area: Ny-Ålesund as an atmospheric observation site

148

Ny-Ålesund, located at 78.9°N at the Kongsfjorden in Svalbard (Norway), belongs to the

149

world's northernmost permanently inhabited settlements with a year-round accessibility. It

150

serves as a key research site for studying Arctic climate change and Arctic amplification. Ny-

151

Ålesund hosts long-term monitoring sites for aerosols and meteorology, such as the Zeppelin

152

Observatory (Platt et al., 2022), Gruvebadet (Amore et al., 2022), and the AWIPEV Observatory

- hat formatiert ...
- hat formatiert ...
- hat formatiert ...
- Formatiert ...
- hat formatiert ...
- hat formatiert ...
- hat formatiert ...
- Formatiert ...
- Formatiert ...
- Formatierte Tabelle ...
- Formatiert ...
- hat formatiert ...
- hat formatiert ...
- Formatiert ...
- hat formatiert ...
- Formatiert ...
- hat formatiert ...
- Formatiert ...
- hat formatiert ...
- hat formatiert ...
- Formatiert ...
- hat formatiert ...
- hat formatiert ...
- hat formatiert ...
- hat formatiert ...
- Formatiert ...
- hat formatiert ...
- hat formatiert ...
- hat formatiert ...
- Formatiert ...
- Formatiert ...
- hat formatiert ...
- hat formatiert ...
- Formatiert ...
- Formatiert ...
- hat formatiert ...
- hat formatiert ...
- hat formatiert ...
- Formatiert ...
- Formatiert ...
- hat formatiert ...

153 (Maturilli et al., 2013, 2015). These, along with additional research stations operated by  
154 various international institutions, provide valuable data for both long-term atmospheric  
155 studies and short-term investigations like the present one.

156 However, Ny-Ålesund is not representative of the entire High Arctic. Its distinct topography,  
157 situated within a fjord and surrounded by high mountains up to 800 m, leads to complex  
158 atmospheric dynamics, including foehn-like effects (Shestakova et al., 2021). The local  
159 boundary layer is relatively shallow characterized by an average mixing layer height below  
160 700 m and a strong influence by orographic effects (Chang et al., 2017; Dekhtyareva et al.,  
161 2018; Gierens et al., 2020). While free-tropospheric winds are predominantly westerly,  
162 surface winds result from an interplay of land-sea breeze circulations, southeasterly  
163 channeled winds along the fjord axis, and katabatic flows from the Zeppelin mountain range,  
164 the Broeggerbreen glacier, or the Kongsvegen glacier (Esau and Repina, 2012; Gierens et al.,  
165 2020). Additionally, large wind shear has been observed to generate turbulence, leading to  
166 frequent neutral stratification (Gierens et al., 2020). Furthermore, boundary layer mixing can  
167 occur even when a positive gradient in potential temperature suggests a more stable  
168 stratification. During the present field campaign, we observed that near-surface winds often  
169 shift unpredictably, changing direction without a clear pattern, making airflow dynamics  
170 challenging to interpret.

171 From an oceanographic perspective, Svalbard is similarly exceptional. The region is influenced  
172 by the cold Arctic waters of the Spitsbergen Polar Current and the warm waters of the West  
173 Spitsbergen Current (Feltracco et al., 2021). Kongsfjorden, located on the western coast of  
174 Spitsbergen, lies at the interface of High Arctic and Atlantic influences, making it a dynamic  
175 and variable environment (Bischof et al., 2019).

176 Therefore, findings from Ny-Ålesund may not be fully transferable to atmospheric processes  
177 over sea ice or the open ocean in the High Arctic. However, in general, the representativeness  
178 of any single Arctic site is highly questionable, as Freud et al., (2017) found significant  
179 heterogeneity in aerosol particle size distribution across all Arctic sites in their study.

180

Formatiert: Block, Abstand Vor: 6 Pt., Nach: 6 Pt.

## 2.2 Field sampling

The field samples (aerosol particles, bulk seawater and SML) for this study were collected near Ny-Ålesund and from the adjacent Kongsfjorden during autumn 2021 and spring 2022.

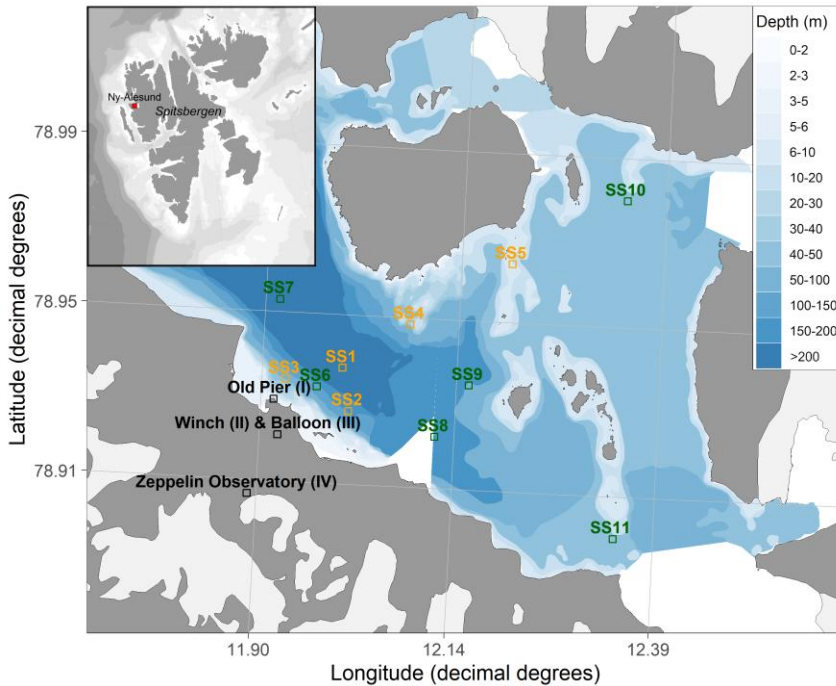


**Figure 1.** Map of the sampling locations. Aerosol particles were collected at: (I) the Old Pier, representing fresh SSA emissions; (II) the winch, representing ground measurements; (III) the tethered balloon at various altitudes; and (IV) the Zeppelin Observatory, serving as a reference for comparison. Bulk and SML samples were collected from different locations within Kongsfjorden. Orange squares (SS1-SS5) indicate autumn 2021 samples, while green squares (SS6-SS11) represent spring 2022 samples. Blue shading indicates water depth.

### a) Bulk seawater and SML sampling

In total, 11 bulk surface seawater and 11 SML samples were taken from a small boat at various dates and locations across the Kongsfjorden (Figure 1, Table S1). Bulk water samples were obtained from a depth of 1 m using low-density polyethylene (LDPE) bottles secured to a telescopic rod. The corresponding SML samples were collected using the glass plate technique (Cunliffe and Wurl, 2014; van Pinxteren et al., 2012). A glass plate measuring

Formatiert: Seitenumbruch oberhalb

192 50 cm × 20 cm × 0.5 cm, with an oval sampling area of 2000 cm<sup>2</sup>, was immersed vertically into  
193 the surface of the fjord seawater and withdrawn at a steady rate of 15 cm s<sup>-1</sup>. The SML film  
194 attached to the glass surface was drained into a precleaned wide-neck plastic bottle using a  
195 funnel and a framed Teflon wiper. Water samples were filtered through 0.2 μm polycarbonate  
196 filters (Whatman® Nuclepore™, 47 mm diameter) to separate dissolved and particulate  
197 fractions. The filtrate, filters and field blanks were preserved at -20°C until chemical analyses  
198 (inorganic ions, carbohydrates). Sea surface temperature (SST) was measured directly from  
199 the boat at a depth of approximately 10 cm using a digital thermometer.

200 *b) Aerosol particle sampling in the surroundings of Ny-Ålesund*

201 Total suspended aerosol particles (TSP) were captured on polycarbonate filters (0.8 μm,  
202 Whatman® Nuclepore™, 47 mm diameter) at four locations (**Figure 1**): (I) Near the Old Pier  
203 next to Kongsfjorden (8 samples), representing fresh SSA emissions; (II) near the balloon winch  
204 close to the AWIPEV Observatory (17 samples), representing ground measurements; (III) at  
205 high altitudes at the tethered balloon (14 samples); and (IV) at the Zeppelin Observatory  
206 (1 sample), serving as a reference for comparison. **Table S2** provides details of individual  
207 aerosol particle samplings near the Old Pier (I), while **Table S3** presents the sampling times,  
208 locations and heights of all the individual high-altitude aerosol samples (III & IV), along with  
209 the corresponding simultaneous ground-level samples (II) taken near the winch.

210 For sampling aerosol particles at the Old Pier (4 m above sea level), a filter holder with a  
211 polycarbonate filter attached to a pump was used. Sampling lasted between 4 and 7 days.  
212 Flow rates, measured at the beginning and the ending of the sampling with a flowmeter,  
213 ranged from 5 to 10 L min<sup>-1</sup>, with total air volumes between 44 and 82 m<sup>3</sup>. The estimated  
214 diameter-dependent collection efficiency of this TSP sampling setup, assuming a 90°  
215 aspiration angle, is shown in **Figure S1**. To reduce the risk of pump failure due to cold  
216 temperatures or snow, the pumps were housed in a Zarges box for protection.

217 High-altitude TSP samples were collected using the helium-filled tethered balloon BELUGA, as  
218 described in detail by Pilz et al. (2023). The balloon's altitude was controlled using an electric  
219 winch located near the AWIPEV Observatory, with ascent and descent rates from 1 to 3 m s<sup>-1</sup>.  
220 The tethered balloon operated under various meteorological conditions, including both clear  
221 and cloudy skies. At a specified altitude, a HALFBAC (High-volume And Light-weight Filter  
222 sampler for BALloon-borne appliCation) (Grawe et al., 2023) collected aerosol particles 2-3 m

223 below the balloon. The HALFBAC is a custom-designed, lightweight aerosol particle sampler  
224 operating at a pump flow between 25 and 35 L min<sup>-1</sup>. It is capable of collecting sufficient  
225 aerosol mass on filters at high altitudes for subsequent offline chemical and microphysical  
226 analyses. Simultaneously, another HALFBAC collected ground-level aerosol particles near the  
227 electric winch (20 m above sea level). Additionally, one aerosol sample (Filter ID 62, sampling  
228 date: 10/05/2022) was collected at the Zeppelin Observatory, a permanent monitoring station  
229 located at 474 m a.s.l. on Zeppelinfjellet, using the HALFBAC. Synchronized aerosol particle  
230 sampling at the winch and the balloon typically lasted around two hours, as detailed in **Table**  
231 **S3**. The collection efficiency for TSP sampling using HALFBAC is discussed in the supplement  
232 (A1) and **Figure S1**.

233

### 234 **2.3 Chemical analyses from offline aerosol particle filters and seawater**

235 For the analysis of major cations, anions and marine carbohydrates in aerosol particles, the  
236 complete polycarbonate filters were extracted in 6-7 mL of ultrapure water  
237 (resistivity > 18.2 MΩ) for two hours followed by a filtration through a 0.45 μm syringe filter.  
238 Frozen seawater samples were gently thawed at 4°C one day before analysis.

#### 239 *a) Major cations and anions*

240 Major inorganic ions, including sodium (Na<sup>+</sup>), potassium (K<sup>+</sup>), magnesium (Mg<sup>2+</sup>), calcium  
241 (Ca<sup>2+</sup>), chloride (Cl<sup>-</sup>), sulfate (SO<sub>4</sub><sup>2-</sup>SO<sub>4</sub><sup>2-</sup>), and oxalate, were quantified in 0.45 μm filtered  
242 aqueous aerosol extracts, bulk seawater and SML samples using ion chromatography (Dionex  
243 ICS-6000, Thermo Scientific) as described by Zeppenfeld et al. (2021). Cations were separated  
244 isocratically with a 36 mM methanesulfonic acid eluent on a Dionex IonPac CS16-4 μm column  
245 (2 mm × 250 mm), paired with a Dionex IonPac CG16-4 μm guard column (2 mm × 50 mm).  
246 For anion separation, a gradient from 4 to 40 mM KOH was applied on a Dionex IonPac AS18  
247 column (2 mm × 250 mm), along with a Dionex IonPac AG18 guard column (2 mm × 50 mm).  
248 The analytical uncertainty for each ion was below 5%. Aerosol extracts were measured  
249 undiluted, while bulk seawater and SML samples were analyzed at a 1:15,000 dilution.

250

251 *b) Dissolved free and combined carbohydrates*

252 Carbohydrates in seawater and aerosol particle extracts were measured according to the  
253 protocols outlined by Zeppenfeld et al. (2020, 2021), utilizing high-performance anion-  
254 exchange chromatography with pulsed amperometric detection (HPAEC-PAD). The system  
255 was equipped with a Dionex CarboPac PA20 analytical column (3 mm × 150 mm) and a Dionex  
256 CarboPac PA20 guard column (3 mm × 30 mm). The applied eluent gradient separated the  
257 following monosaccharide units: fucose (Fuc), rhamnose (Rha), arabinose (Ara), galactose  
258 (Gal), glucose (Glc), xylose (Xyl), mannose (Man), fructose (Fru), galactosamine (GalN),  
259 glucosamine (GlcN), muramic acid (MurAc), galacturonic acid (GalAc), and glucuronic acid  
260 (GlcAc). The analytical uncertainty for each monosaccharide was below 10%. dFCHO  
261 represents the total of identifiable free monosaccharides, whereas CCHO include only those  
262 monosaccharides released through acid hydrolysis (0.8 M HCl, 100°C, 20 h). For seawater  
263 samples, particulate combined carbohydrates (pCCHO, >0.2 μm) were measured from 0.2 μm  
264 polycarbonate filters, while dissolved combined carbohydrates (dCCHO, <0.2 μm) were  
265 measured from the filtrate after desalination via electro dialysis. Both fractions were later  
266 summed to represent the total CCHO. For the winch and balloon samples, the limited air  
267 volume and resulting low aerosol mass collected on the filters permitted quantification only  
268 of the major monosaccharides (typically Glc, Xyl, Gal, Ara), while minor monosaccharides  
269 remained largely below the instrumental detection limits. In contrast, samples from the Old  
270 Pier and surface seawater provided sufficient analyte mass to quantify the full suite of the  
271 CCHO monosaccharides.

Formatiert: Seitenumbruch oberhalb

hat formatiert: Nicht Hervorheben

274 **2.4 Vertical profiles from online measurements**

275 *a) Size-resolved aerosol particles number concentrations*

276 An optical particles size spectrometer (POPS, Handix), integrated into the Cubic Aerosol  
277 Measurement Platform (CAMP) as described by Pilz et al. (2022), provided the integrated total  
278 number concentrations ( $N_{150}$ ) for aerosol particles between 150 and 2900 nm at a temporal  
279 resolution of 1 second. On selected dates of HALFBAC sampling, CAMP was operated  
280 simultaneously 25 m below the balloon providing insight into the vertical profile of  $N_{150}$  during  
281 specific events. Vertical profiles are presented as rolling averages over 30 seconds.

282

283

284 *b) Meteorological observations and calculations*

285 Standard meteorological parameters—including altitude, ambient temperature (T), wind  
 286 speed (U), wind direction (WD), air pressure (p), and relative humidity (RH)—were measured  
 287 for the elevated-altitude samples using a standard meteorology package positioned  
 288 approximately 20 m below the balloon (Pilz et al., 2023). The potential temperature ( $\theta$ ) within  
 289 the atmospheric column - as a measure of the static stability of the unsaturated atmosphere  
 290 - was calculated using Eq. I, where T is the ambient temperature (K), p is the atmospheric  
 291 pressure (hPa),  $p_0$  is the reference pressure (1000 hPa), R is the specific gas constant (287 J kg<sup>-1</sup>  
 292 K<sup>-1</sup>) and  $c_p$  is the specific heat capacity of dry air at constant pressure (1004 J kg<sup>-1</sup> K<sup>-1</sup>).

$$293 \quad \theta = T \left( \frac{p_0}{p} \right)^{\frac{R}{c_p}} \quad (\text{Eq. I})$$

294 Specific humidity (q)—remaining constant during adiabatic ascent or descent as long as no  
 295 phase changes occur—was calculated using Eq. II from Egerer et al. (2021), where  $R_d/R_v$  (the  
 296 ratio of specific gas constants for dry air and water vapor) is approximately 0.622, and  $e_s(T)$   
 297 represents the temperature-dependent saturation vapor pressure.

$$298 \quad q = \frac{R_d/R_v \cdot e_s(T) \cdot RH}{p - (1 - R_d/R_v) \cdot e_s(T) \cdot RH} \quad (\text{Eq. II})$$

299 Meteorological data measured 2 m above the ground (13 m above sea level) at the AWIPEV  
 300 Atmospheric Observatory (Maturilli, 2020), represented the weather conditions during  
 301 aerosol sampling at the winch.

## 302 2.5 Supporting observations and model calculations

303 Major inorganic ions measured at the Zeppelin Observatory with a 24-hour resolution using a  
304 statically installed aerosol sampler (Filter\_3pack) as part of the European Monitoring and  
305 Evaluation Programme (Tørseth et al., 2012) by the Norwegian Polar Institute (NPI) and the  
306 Norwegian Institute for Air Research (NILU) were obtained from the EBAS database for the  
307 study duration (Aas et al., 2022, 2023). The Filter\_3pack data were utilized in two ways:

- 308 1. **Comparing sampling techniques:** Data from the Filter\_3pack were compared with one  
309 HALFBAC aerosol particle sample collected directly at the Zeppelin Observatory (Filter  
310 ID 62, 10\_May\_05/2022) to evaluate potential artifacts arising from differences in  
311 sampling techniques and filter media. Despite variations in time resolution and  
312 methods, sodium, potassium, chloride, and sulfate concentrations showed strong  
313 agreement (detailed in the supplement A2 and **Figure S2**).
- 314 2. **Comparison with balloon data:** Sodium concentrations measured at the Zeppelin  
315 Observatory were directly compared with those obtained from the tethered balloon  
316 sampling.

317 Information on the occurrence of clouds and hydrometeor types at Ny-Ålesund were taken  
318 from the Cloudnet classification product (Illingworth et al., 2007; Nomokonova et al., 2019),  
319 which is based on a combination of ground-based cloud radar, ceilometer, and numerical  
320 weather prediction output. Vertically integrated ice water content (IWC), i.e. ice water path  
321 (IWP), has been calculated from the Cloudnet IWC product following Hogan et al. (2006).  
322 Vertically integrated cloud liquid water (liquid water path; LWP) and water vapor (IWV) were  
323 taken from zenith HATPRO microwave radiometer measurements (Nomokonova et al., 2019).

324 The 48-hour back-trajectories for the aerosol sampling periods were generated using the  
325 NOAA HYSPLIT model (Stein et al., 2015). Trajectories were calculated hourly based on GDAS1  
326 meteorological data (Global Data Assimilation System; 1° spatial resolution; 3-hour intervals)  
327 for various arrival heights: 50 m (ground level), 474 m (Zeppelin Observatory), and the specific  
328 balloon sampling altitudes. Sea ice concentration data were obtained from the NOAA-  
329 maintained ERDDAP server (Environmental Research Division's Data Access Program). The  
330 back-trajectories were used to assess the relative influence of distant sources, such as the  
331 marginal ice zone, versus local ice-free oceanic emissions on the aerosol chemical  
332 composition. Given the rather short atmospheric residence times of [supermicron](#) SSA particles

~~—typically less than two days for supermicron particles (Madry et al., 2011; Veron, 2015), which, which account for most of the SSA mass in TSP, —and- the increasing uncertainties associated with longer back-trajectory periods, we considered a 48-hour back-trajectory length appropriate for this analysis.the increasing uncertainties associated with longer back-trajectory periods, we consider 48 hours back-trajectory length appropriate for this analysis.~~

Ocean surface concentrations for total chlorophyll *a* (TChl-*a*) and dissolved acidic polysaccharides were obtained by a coupled setup of the ocean sea ice biogeochemistry model FESOM2.1-REcoM3 (Gürses et al., 2023), to which additional state equations have been added to simulate dissolved and particulate organic carbon following Engel et al. (2004) and Schartau et al. (2007). The simulation was set up following Gürses et al. (2023) and using the Arctic-specific tuning of Oziel et al. (2022). Monthly model output was obtained on an irregular grid with approximately 4.5 km resolution in the Arctic Ocean. This configuration has already been applied successfully in Leon-Marcos et al. (2025).

## 2.6 Statistics, data processing, visualization and text optimization

Statistical analyses, calculations and visualization were conducted using OriginPro 2024, Microsoft Excel, IDL, python3 and R version 4.2.1 with the ncdf4 (Pierce, 2023), openair (Carslaw and Ropkins, 2012), reshape2 (Wickham, 2007), scales (Wickham et al., 2023b), lubridate (Grolemund and Wickham, 2011), cmocean (Thyng et al., 2016), maps (Brownrigg, 2023), mapdata (Brownrigg, 2013), rgdal (Bivand et al., 2022), raster (Hijmans, 2023), RColorBrewer (Neuwirth, 2022), sp (Bivand et al., 2013), dplyr (Wickham et al., 2023a), ggplot2 (Wickham, 2016), and PlotSvalbard (Vihtakari, 2020) packages. Box-and-whisker plots illustrate the interquartile range (box), the median (horizontal line inside the box), the mean (open square), the minimum and maximum values (whiskers). Text and language were optimized using Open AI's ChatGPT-4 Turbo.

### 358 3. Results and Discussion

#### 359 3.1 Chemical constituents in marine aerosol particles from their oceanic source 360 to elevated altitudes

##### 361 *Sodium in aerosol particles ( $\text{Na}^+_{\text{aer}}$ )*

362 Sodium, a dominant and chemically stable component of SSA, is commonly used as a tracer  
363 for tracking ocean-derived emissions in atmospheric studies (Manders et al., 2010; van  
364 Pinxteren et al., 2017; White, 2008). In this study, consistently high  $\text{Na}^+_{\text{aer}}$  concentrations were  
365 observed on the TSP filters at the Old Pier next to Kongsfjorden in both autumn 2021 and  
366 spring 2022 (**Figure 2a**), ranging from 140 to 1470  $\text{ng m}^{-3}$  (median: 495  $\text{ng m}^{-3}$ ;  $n=8$ ). The area  
367 around Ny-Ålesund, especially the Old Pier, remained largely ice-free, indicating a negligible  
368 influence of local sea ice on SSA emissions.

~~369 During the campaign, sea ice coverage in Kongsfjorden varied; however, significant areas  
370 around Ny-Ålesund—particularly near the Old Pier—remained ice-free, suggesting that local  
371 sea ice likely had only little influence on sea spray emissions.~~

372  $\text{Na}^+_{\text{aer}}$  concentrations measured at the winch site, located further inland but still at ground  
373 level (35–3710  $\text{ng m}^{-3}$ ; median: 155  $\text{ng m}^{-3}$ ;  $n=17$ ), and at their elevated HALFBAC  
374 balloons samples between 321 and 1112 m; (23–850  $\text{ng m}^{-3}$ ; median: 124  $\text{ng m}^{-3}$ ;  $n=15$ ) was  
375 generally lower than at the Old Pier, though episodic high events occurred at all sites. were  
376 generally lower in both minimum and median values compared to those at the Old Pier.  
377 Nevertheless, occasional high concentration events were observed across all three sampling  
378 locations. This wide variability from low  $\text{ng m}^{-3}$  to a few  $\mu\text{g m}^{-3}$  agrees with observations from  
379 other marine environments and altitudes. The large variability in  $\text{Na}^+_{\text{aer}}$  concentrations, ranging  
380 from the lower  $\text{ng m}^{-3}$  to a few  $\mu\text{g m}^{-3}$ , aligns with other marine sampling locations and  
381 altitudes (Fomba et al., 2014; Li et al., 2024; Ooki et al., 2002; Theodosi et al., 2010; Triesch et  
382 al., 2021; Zeppenfeld et al., 2021, 2023).

383 Since ~~aerosol particle sampling at the winch and the balloon sampling was~~ were always  
384 synchronized, direct comparisons ~~between the two sites~~ were possible (**Figure 3**). Several  
385 events showed nearly identical  $\text{Na}^+_{\text{aer}}$  sodium concentrations ~~at both locations (winch vs.  
386 balloon)~~, (e.g. e.g., 30 September: 191  $\text{ng m}^{-3}$  ~~at the winch and vs.~~ 207  $\text{ng m}^{-3}$  ~~at the balloon~~; 2  
387 October: 35  $\text{ng m}^{-3}$  ~~vs.~~ ~~at the winch and~~ 36  $\text{ng m}^{-3}$  ~~at the balloon~~; 9 October: 59  $\text{ng m}^{-3}$  ~~vs.~~ ~~at the~~

hat formatiert: Schriftart: Fett

hat formatiert: Schriftart: (Standard) + Textkörper  
(Calibri), Englisch (Vereinigtes Königreich)

388 ~~winch and~~ 60 ng m<sup>-3</sup> ~~at the balloon;~~ 12 November: 240 ng m<sup>-3</sup> ~~vs. at the winch and~~ 223 ng m<sup>-3</sup>  
389 ~~at the balloon).~~ In contrast, other ~~dates periods revealed significant differences~~ exhibited  
390 ~~strong vertical gradients, with much lower concentrations at higher altitudes than at the~~  
391 ~~ground with higher ground-level concentrations~~ (e.g., 27 September: 1840 ng m<sup>-3</sup> ~~at the winch~~  
392 ~~and vs.~~ 23 ng m<sup>-3</sup> ~~at the balloon;~~ 5 April: 84 ng m<sup>-3</sup> ~~at the winch and vs.~~ 54 ng m<sup>-3</sup> ~~at the balloon;~~  
393 11 May: 496 ng m<sup>-3</sup> ~~at the winch and vs.~~ 125 ng m<sup>-3</sup> ~~at the balloon~~), ~~but also two instances while~~  
394 ~~two cases showed higher values of even higher concentrations recorded~~ at the balloon (24  
395 September: 47 ng m<sup>-3</sup> ~~at the winch and vs.~~ 99 ng m<sup>-3</sup> ~~at the balloon;~~ 3 April: 77 ng m<sup>-3</sup> ~~at the~~  
396 ~~winch and vs.~~ 194 ng m<sup>-3</sup> ~~at the balloon~~). These variations ~~can be~~ likely ~~be attributed to~~ driven  
397 ~~by~~ atmospheric depletion processes, including dry and wet deposition (Farmer et al., 2021),  
398 ~~atmospheric~~ dilution during vertical and horizontal transport from the emission region (Wong  
399 et al., 2019), vertical mixing ~~conditions~~ (Pilz et al., 2024) and differ~~ing~~ ~~ences in~~ air mass  
400 histories (Willis et al., 2018), ~~which will be examined in detail.~~ ~~The influence of atmospheric~~  
401 ~~meteorological conditions on the vertical distribution of chemical compounds will be analyzed~~  
402 ~~and discussed in detail~~ for three selected cases later in this study.

403 ~~Na<sup>+</sup><sub>aer</sub> Concentrations measured~~ at the Zeppelin Observatory, ~~where Na<sup>+</sup><sub>aer</sub> is routinely~~  
404 ~~monitored,~~ were largely ~~agreed~~ consistent with ~~those observed in~~ the balloon  
405 ~~samples measurements,~~ showing an ~~(overall agreement ranging between 56 and 213%~~  
406 ~~overall;~~ ~~with five events demonstrating excellent agreement of 92–107% in five events;~~  
407 ~~(Table S6), despite differences in.~~ This similarity is remarkable considering the differences in  
408 ~~sampling,~~ time resolution (24 h ~~at Zeppelin vs. 1–2 h for the balloon~~), sampling altitudes, the  
409 horizontal distance between the sites, ~~Svalbard's~~ the complex topography ~~of Svalbard~~ (Gierens  
410 et al., 2020; Shestakova et al., 2021), and the fact that meteorological conditions and  
411 atmospheric mixing states have not yet been considered.

412

413

414

415

416

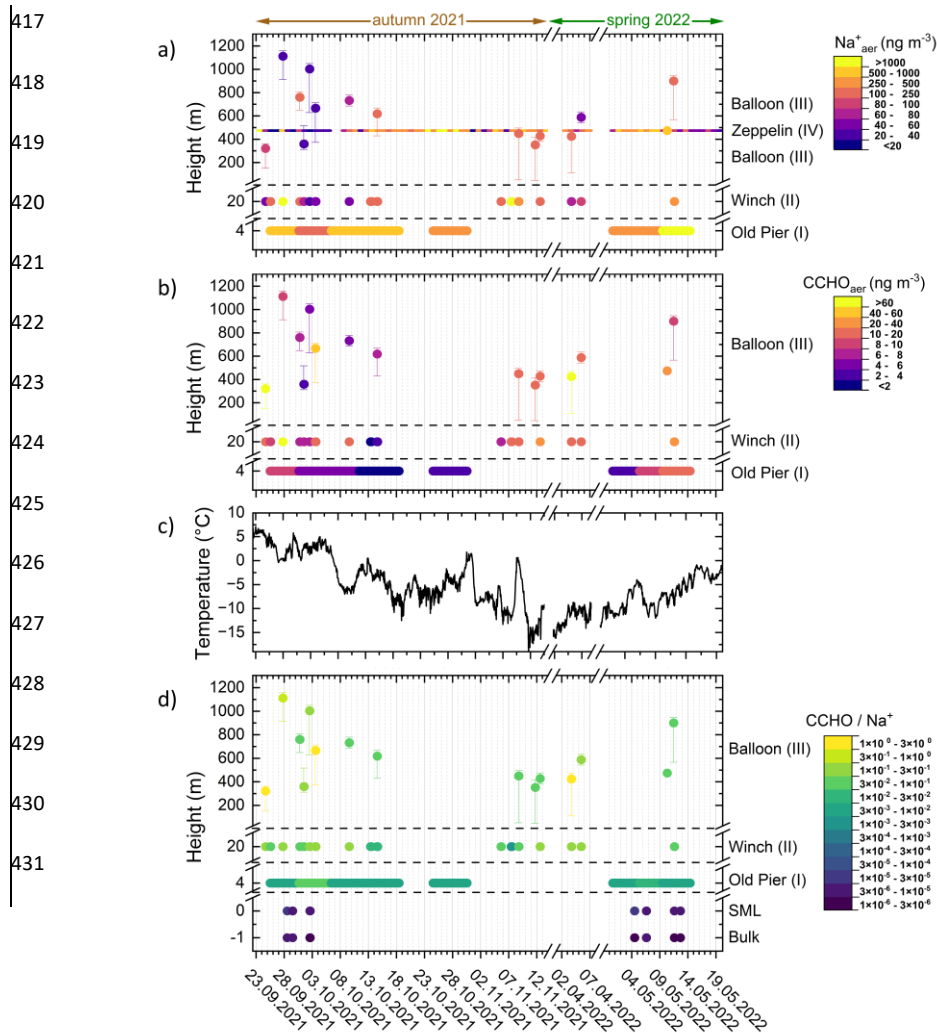


**Figure 2.** Time-resolved atmospheric concentrations of a) sodium- $\text{Na}^+_{\text{aer}}$  and b)  $\text{CCHO}_{\text{aer}}$  in aerosol particles (TSP) collected in autumn 2021 and spring 2022 in Ny-Ålesund at several heights (m a.s.l.) from four sites: Old Pier, winch near the AWIPEV Observatory, balloon and the Zeppelin Observatory. Dots represent the median height during the total sampling time and vertical error bars represent maximum and minimum height of the sampler during the active sampling. The x-axis ticks represent the start of each date at midnight. c) Air temperature (2 m above ground) measured at the AWIPEV Observatory. d)  $\text{CCHO}/\text{Na}^+$  ratios within the bulk seawater, the SML and in the aerosol particles at several heights. In panel (a), the label "Balloon (III)" appears twice because balloon sampling for sodium measurements occurred both below and above the fixed altitude of the Zeppelin Observatory.

hat formatiert: Schriftart: 9 Pt., Nicht Kursiv, Schriftfarbe: Automatisch

432 Overall,  $\text{Na}^+_{\text{aer}}$  was detectable up to 1100 m altitude, encompassing both the boundary layer  
 433 and the free troposphere, sodium was detectable and quantifiable, sometimes at  
 434 concentrations levels comparable to those near the emission source, indicating effective  
 435 vertical mixing or transport to cloud-relevant heights via advection. This indicates that SSA  
 436 compounds are either effectively mixed throughout the vertical atmospheric column, or reach  
 437 heights relevant for cloud formation through advection. Such observations This vertical  
 438 distribution is are consistent with the aircraft-based sodium-SSA measurements reported by  
 439 Hara et al. (2003) and Köllner et al. (2017).

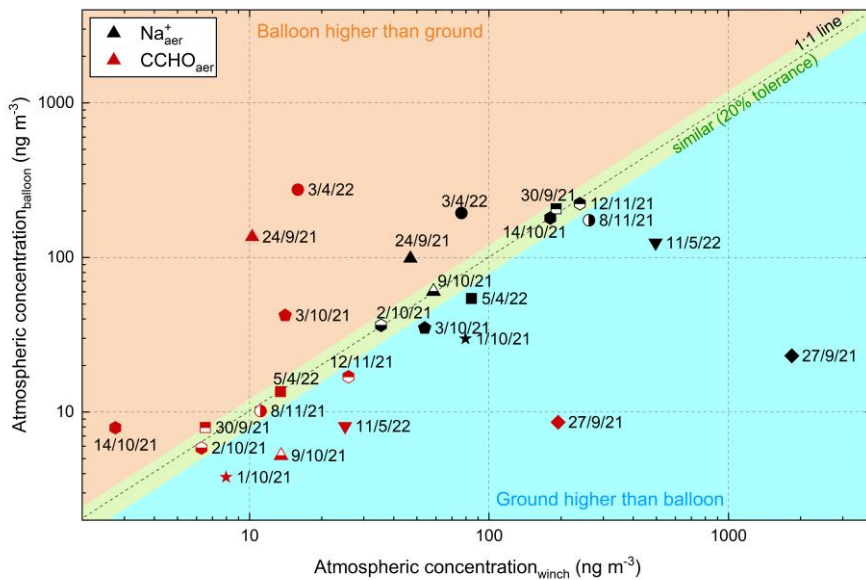


Figure 3. Scatter plot showing  $\text{Na}^+_{\text{aer}}$  (black symbols) and  $\text{CCHO}_{\text{aer}}$  (red symbols) concentrations in TSP measured at the winch, and balloon levels. Data points are categorized to indicate whether values were similar, higher at the balloon, or higher at the ground.

440 The longer atmospheric residence increases the exposure of SSA particles to remain in the  
 441 atmosphere, the greater their exposure to atmospheric aging processes processing, which can  
 442 alter their impact on cloud formation. While  $\text{Na}^+_{\text{aer}}$  in SSA is considered chemically stable, co-  
 443 emitted OM including carbohydrates may undergo physical, chemical and microbial  
 444 change transformations, as suggested by Zeppenfeld et al. (2021, 2023). This aspect will be  
 445 explored further in the following section 3.3s.

hat formatiert: Schriftart: Nicht Kursiv, Englisch (Vereinigtes Königreich)

Formatiert: Beschriftung, Block, Abstand Vor: 0 Pt., Nach: 0 Pt., Zeilenabstand: einfach

446

447

448

449

450

451

452

453

454

455

456

457

458

459

460

461

462

463

464

465

466

467

468

469

470  
471  
472  
473  
474  
475  
476

477 ***Combined carbohydrates in fresh SSA and their oceanic origin***

478 Similar to sodium, CCHO<sub>aer</sub> were detected ~~at in all atmospheric samples across~~ all sites and  
479 altitudes (**Figure 2b**). At the Old Pier, CCHO<sub>aer</sub> concentrations ranged from 1.6 to 10.0 ng m<sup>-3</sup>  
480 (median: 5.0 ng m<sup>-3</sup>; n=8), ~~showing a seasonal pattern. A seasonal pattern emerged,~~ with the  
481 highest values ~~observed~~ at the beginning (~~end of~~ September 2021) and end (~~mid of~~ May 2022)  
482 of the study ~~period, and lower values while lower concentrations were recorded during the~~  
483 ~~colder, darker in months in between October 2021 (Figure 2c).~~ However, it ~~No samples were~~  
484 ~~collected between November and April, so winter trends remain unknown. should be noted~~  
485 ~~that no aerosol samples were collected during the coldest winter months.~~

486

487 The seasonal variation of CCHO<sub>aer</sub> at the Old Pier may be linked to the seasonal dynamics of  
488 marine CCHO in the surface water of Kongsfjorden, ~~their most probable only~~ local emission  
489 source ~~offer~~ SSA. These dynamics are likely driven by seasonal shifts in primary production  
490 and phytoplankton composition ~~as well as overall primary production~~ (Assmy et al., 2023;  
491 Mayot et al., 2018). ~~Reduced or absent production in Kongsfjorden during the winter and early~~  
492 ~~spring, as indicated by low phytoplankton and TChl a concentrations, contrasts with~~  
493 ~~significantly higher values from mid-spring to mid-autumn (van de Poll et al., 2021).~~

494 Similar seasonality was observed for selected monosaccharides among ~~the~~ dissolved  
495 combined carbohydrates (dCCHO) in Kongsfjorden seawater, ~~the primary source of~~  
496 ~~atmospheric CCHO<sub>aer</sub>.~~ In particular, fucose, galactosamine, and rhamnose in bulk water

497 dCCHO exhibited a distinct pattern, closely following SST. Their concentrations peaked in late  
498 September/early October, while being much lower (44-67%) in early to mid-May (**Figure S34**).

499 This pattern was weaker for glucose in bulk dCCHO and even less pronounced in the SML for  
500 most monosaccharides. However, this trend was less pronounced for glucose in bulk water  
501 dCCHO and even weaker in the SML across most monosaccharide units (**Figure S43**).

502 In contrast, particulate combined carbohydrates (pCCHO) showed no clear seasonal trend in  
503 seawater (**Figure S3**). While dCCHO in bulk water exhibited relatively low spatial and intra-  
504 seasonal variability, pCCHO and SML samples were considerably more variable, even among  
505 samples from the same season (**Figure S4**). This likely reflects the rapid dynamics of pCCHO's  
506 in relation to phytoplankton blooms (Becker et al., 2020; Engel et al., 2012; Fabiano et al.,  
507 1993), TEP formation from dCCHO in turbulent waters, and vertical transport of pCCHO  
508 through sedimentation (e.g., as marine snow) or its accumulation in the SML depending on  
509 buoyancy (Burns et al., 2019; Engel, 2004; Robinson et al., 2019b, a; Wurl and Holmes, 2008).  
510 The SML, in particular, may be more sensitive to these dynamics than the bulk water,  
511 potentially explaining its greater fluctuations.

512  
513  
514  
515  
516  
517  
518  
519  
520  
521

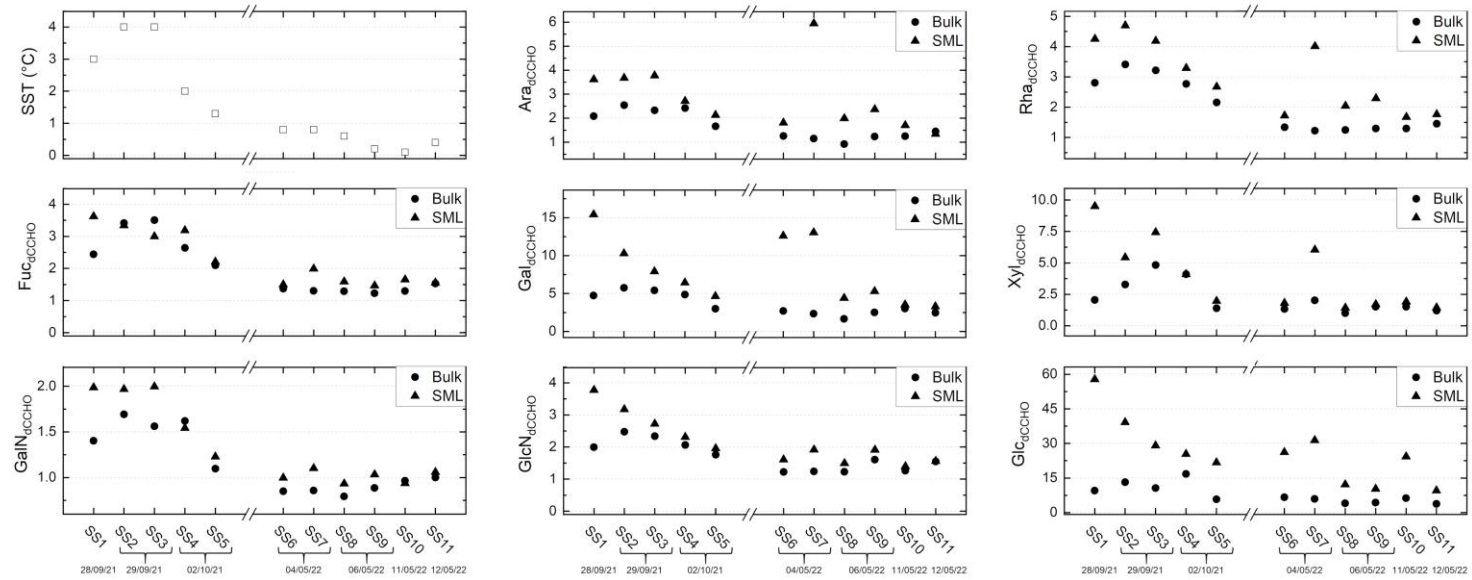


**Figure S43.** Concentration of measured monosaccharide units in dCCHO from bulk and SML samples collected in Kongsfjorden during autumn 2021 and spring 2022, along with SST measurements taken from bulk samples at the time of sampling.

522  
523 ~~In contrast, particulate combined carbohydrates (pCCHO) including contributions from~~  
524 ~~transparent exopolymer particles (TEPs), detritus, and dead or living cells showed no clear~~  
525 ~~seasonal trend in seawater (Figure S4). While dCCHO in bulk water exhibited relatively low~~  
526 ~~spatial and intra-seasonal variability, pCCHO and SML samples were considerably more~~  
527 ~~variable among all samples, even among samples from the same season (Figure S5). This~~  
528 ~~variability likely reflects pCCHO's rapid dynamics in relation to phytoplankton blooms (Becker~~  
529 ~~et al., 2020; Engel et al., 2012; Fabiano et al., 1993). Additional drivers include the~~  
530 ~~spontaneous formation of TEPs from dCCHO precursors in turbulent waters, as well as the~~  
531 ~~vertical transport of pCCHO through sedimentation (e.g., as marine snow) or its accumulation~~  
532 ~~in the SML depending on its buoyancy (Burns et al., 2019; Engel, 2004; Robinson et al., 2019b,~~  
533 ~~a; Wurl and Holmes, 2008). The SML, in particular, may be more sensitive to these dynamics~~  
534 ~~than the more stable bulk water, potentially explaining the greater fluctuations.~~

535 On the other hand, dCCHO ~~measured~~ in bulk water ~~is similar to~~ like dissolved organic carbon  
536 (Hansell, 2013; Keene et al., 2017) ~~is likely~~ may be generally dominated by recalcitrant and  
537 semi-recalcitrant compounds, ~~while~~ ~~the~~ labile fraction ~~of dCCHOs is likely more~~ rapidly  
538 consumed by heterotrophic bacteria (Goldberg et al., 2011) ~~and the remaining dCCHOs~~  
539 ~~presumably represent substrates that are less available to microbial metabolism.~~ Notably,  
540 combined glucose showed high variability in both dCCHO and pCCHO, likely due being the  
541 main constituent of abundant storage macromolecules such as laminarin (Becker et al., 2020)  
542 during periods of photosynthetic overflow (Barthelmeß et al., 2025), as well as its relatively  
543 rapid microbial utilization (Kharbush et al., 2020).

544 In conclusion, ~~the seasonal variation of CCHO<sub>aer</sub> aligns with certain marine carbohydrates in~~  
545 ~~Kongsfjorden, suggesting surface dCCHO as the main source of freshly emitted CCHO<sub>aer</sub>.~~

546 ~~the seasonal variation of CCHO<sub>aer</sub> aligns with the observed seasonality of certain marine~~  
547 ~~carbohydrates in the Kongsfjorden, indicating that dCCHO in surface seawater may be the~~  
548 ~~major origin of freshly emitted CCHO<sub>aer</sub>.~~

549 **CCHO<sub>aer</sub> at the winch and higher altitudes**

hat formatiert: Tiefgestellt

hat formatiert: Tiefgestellt

550 CCHO<sub>aer</sub> ~~concentrations were also measured~~ at the winch site (1.9–194 ng m<sup>-3</sup>; median:  
551 10.6 ng m<sup>-3</sup>; n=17) and at the balloon (3.8–274 ng m<sup>-3</sup>; median: 10.2 ng m<sup>-3</sup>; n=15), showing  
552 a broader range and significantly higher median and maximum values ~~than at compared to~~  
553 the Old Pier (Figure 2b), suggesting sources beyond primary sea-air transfer. ~~The higher~~  
554 ~~concentrations, found more inland and at higher altitudes, compared to the Old Pier were~~  
555 ~~unexpected and suggest sources beyond an exclusive primary sea-air transfer, which will be~~  
556 ~~discussed below. Unlike the Old Pier, no clear seasonal pattern or altitude dependence was~~  
557 ~~observed, likely due to the winch site's inland location. Unlike the Old Pier samples, no clear~~  
558 ~~seasonal pattern was evident in these locations, nor was there any apparent dependence on~~  
559 ~~sampling height. The lacking seasonality at the Winch site, unlike at the Old Pier, may be due~~  
560 ~~to its more inland position~~, making it more sensitive to wind direction and changing weather.  
561 ~~Also~~ Also, the higher temporal resolution of the samples likely captured short-term  
562 fluctuations rather than integrated seasonal trends. In addition, atmospheric processing  
563 during transport and the lack of true winter samples may have further obscured any clear  
564 seasonal signal.

hat formatiert: Schriftart: Nicht Fett

565 Similar to sodium, ~~certain some~~ events (Figure 3) showed comparable ~~CCHO<sub>aer</sub> at the winch~~  
566 ~~and balloon concentrations between the winch and balloon samples~~ (e.g., 30 September:  
567 6.5 ng m<sup>-3</sup> ~~at the winch and vs.~~ 8.0 ng m<sup>-3</sup> ~~at the balloon~~; 2 October: 6.3 ng m<sup>-3</sup> ~~vs. at the winch~~  
568 ~~and 5.8 ng m<sup>-3</sup> at the balloon~~; 8 November: 11.1 ~~vs. ng m<sup>-3</sup> at the winch and~~ 10.2 ng m<sup>-3</sup> ~~at the~~  
569 ~~balloon~~; 12 November: 26 ng m<sup>-3</sup> ~~at the winch and 17 ng m<sup>-3</sup> at the balloon~~), ~~while on~~ on other  
570 dates, ~~however, CCHO<sub>aer</sub> concentrations were markedly lower at higher altitudes~~ (e.g.,  
571 27 September: 194 ~~vs. ng m<sup>-3</sup> at the winch and~~ 8.6 ng m<sup>-3</sup> ~~at the balloon~~; 11 May: 25 ~~vs. ng m<sup>-3</sup>~~  
572 ~~at the winch and 8.1 ng m<sup>-3</sup> at the balloon~~), ~~or conversely, higher aloft. Interestingly, there~~  
573 ~~were also instances where CCHO<sub>aer</sub> concentrations were much higher at elevated altitudes~~  
574 ~~than at ground level~~ (e.g., 24 September: 10.2 ~~vs. ng m<sup>-3</sup> at the winch and~~ 136 ng m<sup>-3</sup> ~~at the~~  
575 ~~balloon~~; 3 April: 15.9 ~~vs. ng m<sup>-3</sup> at the winch and~~ 275 ng m<sup>-3</sup> ~~at the balloon~~). In most cases,  
576 CCHO<sub>aer</sub> covaried with ~~sodium sodium except on 03 Oct. However, a notable exception~~  
577 ~~occurred on 3 October, when Na<sup>+</sup><sub>aer</sub> concentrations were slightly higher/lower~~ at the  
578 ~~ground/balloon (5435 vs. ng m<sup>-3</sup>) than at the ground (3554 ng m<sup>-3</sup>)~~, whereas CCHO<sub>aer</sub> showed  
579 ~~the opposite pattern, with higher concentrations was higher~~ at the balloon (42 ng m<sup>-3</sup>) than at  
580 the winch (14 ng m<sup>-3</sup>).

hat formatiert: Schriftart: Fett

581 To investigate ~~the oceanic emission processes from the ocean~~ and the atmospheric fate of  
582 marine CCHO, CCHO/Na<sup>+</sup> ratios were calculated for all aerosol ~~particle~~, bulk seawater and SML  
583 samples, representing the primary sources of the SSA particle constituents studied here  
584 **(Figure 2d)**. ~~Bulk seawater showed the lowest ratios ( $2.0 \times 10^{-6} - 6.0 \times 10^{-6}$ ) with minimal~~  
585 ~~variability, while the SML had slightly higher ratios ( $3.3 \times 10^{-6} - 2.5 \times 10^{-5}$ ) due to CCHO~~  
586 ~~enrichment. The lowest ratios, with minimal CCHO/Na<sup>+</sup> variability, were observed in bulk~~  
587 ~~seawater ( $2.0 \times 10^{-6}$  to  $6.0 \times 10^{-6}$ ). Slightly higher ratios were found in the SML ( $3.3 \times 10^{-6}$  to~~  
588  ~~$2.5 \times 10^{-5}$ ), which can be explained with the known enrichment of CCHO in the SML compared~~  
589 ~~to bulk seawater. Specifically, the enrichment factors (EF<sub>SML</sub>) ranged between 1.3 and 4.1~~  
590 ~~for dCCHO and between 0.9 and 6.8 for pCCHO (Figure S45), which aligns well with the~~  
591 ~~typical single-digit and occasionally two-digit enrichment factors reported in~~ previous studies  
592 (Engel and Galgani, 2016; Gao et al., 2012; Zäncker et al., 2021; Zeppenfeld et al., 2021, 2023).

593 At the Old Pier, where fresh SSA was sampled, the ratios were significantly higher, ~~ranging~~  
594 ~~from ( $6.2 \times 10^{-3}$  to  $3.3 \times 10^{-2}$ ), indicating the chemo-selective sea-air transfer that enriches~~  
595 ~~surface-active organics relative to sodium in aerosol particles. This pronounced enrichment of~~  
596 ~~CCHO relative to sodium in SSA particles compared to seawater has been discussed previously~~  
597 ~~and is attributed to a chemo-selective sea-air transfer (Hasenecz et al., 2020, 2019; Jayarathne~~  
598 ~~et al., 2016; Schill et al., 2018; Zeppenfeld et al., 2021, 2023). This process preferentially~~  
599 ~~transfers surface active organics during bubble bursting to the atmosphere, while highly~~  
600 ~~water-soluble inorganic ions of the sea salt remain in the seawater. The enrichment effect is~~  
601 typically more pronounced in submicron particles, which have a higher relative contribution  
602 of organics than inorganic ions (Quinn et al., 2015). In contrast, supermicron particles are  
603 predominantly composed of sea salts, although organic substances are still notably enriched  
604 compared to the surface seawater. ~~As total suspended particles were measured here, and~~  
605 ~~most SSA mass resides in the supermicron range (Facchini et al., 2008; O'Dowd et al., 1997),~~  
606 ~~our results primarily reflect supermicron aerosol composition. Since this study measured total~~  
607 ~~suspended particles, and the majority of SSA particle mass typically resides in the supermicron~~  
608 ~~size range (Facchini et al., 2008; O'Dowd et al., 1997), our results could be considered more~~  
609 ~~representative of supermicron aerosol particles.~~

610 At the winch sampling station, located at ground level but further inland, the CCHO/Na<sup>+</sup> ratios  
611 ~~within in~~ TSP aerosol particles ranged from  $2.9 \times 10^{-3}$  to  $2.6 \times 10^{-1}$ , ~~being either similar to or~~  
612 slightly higher ~~than than those~~ at the Old Pier. In contrast, balloon samples from elevated

613 altitudes showed higher  $\text{CCHO}/\text{Na}^+$  ratios (~~ranging from  $3.9 \times 10^{-2}$  to  $1.4 \times 10^0$~~ ), likely due  
614 ~~to depletion of salt-rich supermicron particles during dry and wet deposition (Croft et al.,~~  
615 ~~2009; Hoppel et al., 2002; O'Dowd and de Leeuw, 2007), increasing the relative contribution~~  
616 ~~of OM-dominated submicron particles. This increase possibly results from the depletion of~~  
617 ~~larger, salt-dominated supermicron SSA particles through dry and wet deposition (Croft et al.,~~  
618 ~~2009; Hoppel et al., 2002; O'Dowd and de Leeuw, 2007), leading to a relatively greater~~  
619 ~~contribution of OM-dominated submicron particles during transport and with extended~~  
620 ~~atmospheric residence time.~~ Furthermore, the increasing absolute concentration of CCHO at  
621 higher altitudes (**Figure 2b**) suggests an atmospheric formation process contributing to the  
622 elevated  $\text{CCHO}/\text{Na}^+$  ratios, potentially linked to microbial activity in the atmosphere (~~see, as~~  
623 ~~discussed in detail in section 3.3~~). However, because only the major monosaccharides  
624 (typically Glc, Xyl, Gal, Ara) could be quantified reliably in the winch and balloon samples,  
625 relative CCHO compositions were not assessed across the entire vertical sample set.  
626 Therefore, they were not used to further substantiate this conclusion, as it has been done in  
627 Zeppenfeld et al. (2021, 2023).

628 The  $\text{CCHO}/\text{Na}^+$  ratios observed at the Old Pier and the Winch closely align with ship-based  
629 measurements in the High Arctic during the PASCAL cruise ( $2 \times 10^{-3}$  to  $2 \times 10^{-1}$  for  $\text{PM}_{10}$  from  
630 summed Berner impactor stages) conducted in May–July 2017 (Zeppenfeld et al., 2023). In  
631 contrast, the very high  $\text{CCHO}/\text{Na}^+$  values ( $>1 \times 10^0$ ) observed at some elevated altitudes in this  
632 study were reported only occasionally for submicron particles (0.14–0.42  $\mu\text{m}$ ) during PASCAL.  
633 This may support the idea that supermicron particle deposition caused the shift in balloon  
634 sample ratios, though microbial contributions in the atmosphere are also possible. Moreover,  
635 these ratios far exceed those from the Southern Ocean near the western Antarctic Peninsula  
636 ( $8 \times 10^{-4}$  to  $7 \times 10^{-3}$ ) (Zeppenfeld et al., 2021), likely due to differences in surface seawater  
637 productivity.

638 Overall, it can be concluded that both  $\text{Na}_{\text{aer}}^+$  and  $\text{CCHO}_{\text{aer}}$  are transported from the marine  
639 emission source to elevated heights within the lower troposphere. However, with longer  
640 atmospheric residence times, the chemical composition of aerosol particles appears  
641 increasingly altered in certain samples. As a key factor influencing these observations, the role  
642 of meteorological conditions and atmospheric mixing in linking ground and balloon samples  
643 will be discussed in the next section.

644 **3.2 Impact of meteorological conditions on SSA particle constituents in higher**  
 645 **altitudes**

646 To examine how meteorological conditions and atmospheric mixing influenced  $\text{Na}^+_{\text{aer}}$  and  
 647  $\text{CCHO}_{\text{aer}}$  at elevated altitudes, three distinct cases with distinct, unvarying constant weather  
 648 conditions were selected (**Figure 53**). These conditions allow for a detailed interpretation of  
 649 the observed chemical values.

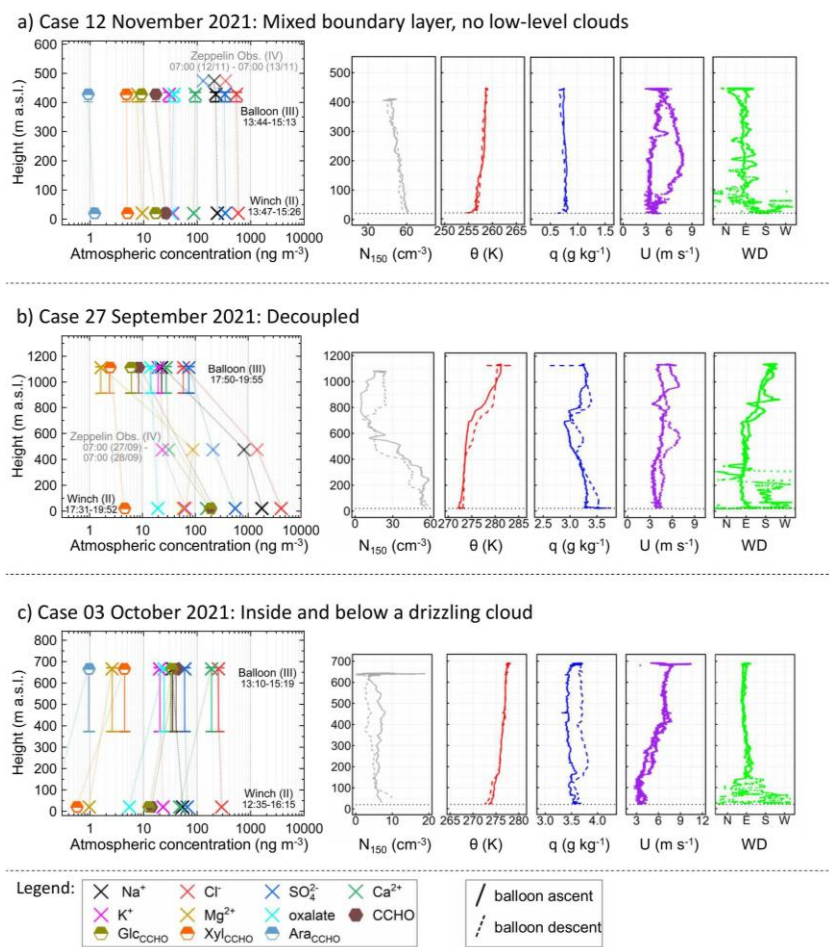


**Figure 53.** Vertical profiles of three atmospheric cases showing mass concentrations of chemical constituents (inorganic ions, oxalate, total  $\text{CCHO}_{\text{aer}}$ , and major monosaccharides within  $\text{CCHO}_{\text{aer}}$ ) in aerosol particles, measured on the ground (winch) and aloft (balloon) using offline filters. Vertical error bars indicate the range between minimal and maximal heights during active sampling at the balloon, while the symbols denote the median sampling heights. Data from the Zeppelin Observatory are also included when available and above detection limits, albeit with a 24-hour resolution. Dotted lines are included to aid in reading the vertical distribution of individual chemical substances. These profiles are complemented by aerosol particle number concentrations of particles bigger than 150 nm ( $N_{150}$ ), potential temperature ( $\theta$ ), specific humidity ( $q$ ), wind speed ( $U$ ), and wind direction ( $WD$ ) measured during the ascents (solid lines) and descents (dashed lines) of the balloon.

650 To assess atmospheric stability and layering in these cases, vertical profiles of potential  
 651 temperature were utilized. To further confirm aerosol mixing conditions, additional  
 652 meteorological parameters (specific humidity, wind speed and direction), vertical aerosol  
 653 particle number concentrations of particles larger than 150 nm ( $N_{150}$ ) (Figure S53), cloud  
 654 conditions (Figure S56) and back-trajectory analyses (Figure 64) were considered. The  
 655 selected cases include (a) a cloud-free mixed boundary layer (12 November 2021), (b) a free  
 656 troposphere decoupled from the ground (27 September 2021), and (c) a boundary layer  
 657 capped by precipitating clouds (03 October 2021).

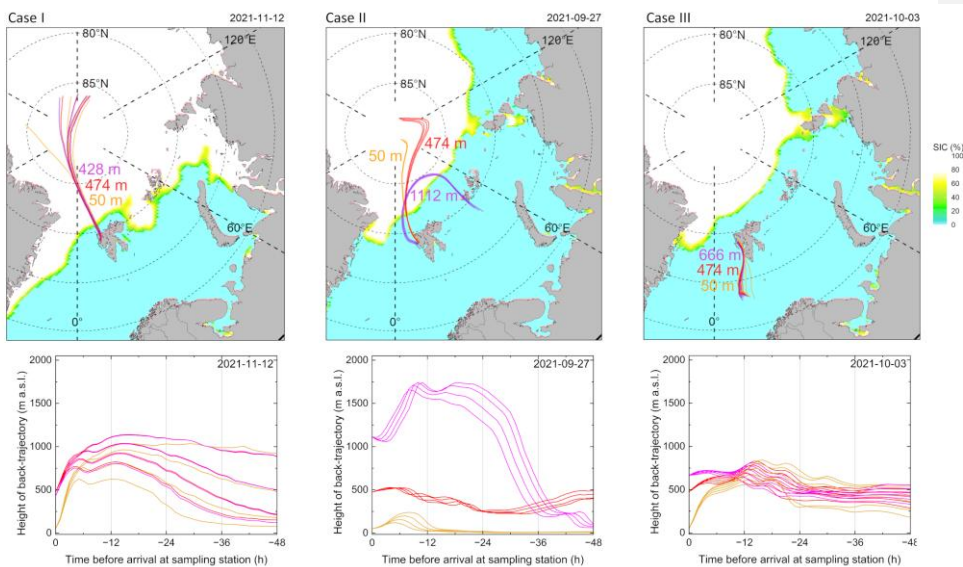


Figure 64. 48-hour back-trajectories calculated on an hourly basis for three arrival heights: orange (50 m, ground-level air masses), red (474 m, height of the Zeppelin Observatory), and purple (variable arrival height, high-altitude air masses sampled at tethered balloon). These are accompanied by daily sea ice concentration (SIC) maps (top) and height profiles (bottom) for three selected aerosol particle sampling cases.

658 **Case I: Mixed boundary layer & no low-level clouds**

659 On 12 November 2021, during the polar night, two HALFBACs were ~~simultaneously~~ operated  
 660 simultaneously at the ground and the balloon (median altitude of 428 m) for approximately  
 661 90 minutes. Ground-level conditions were  $-16.7^{\circ}\text{C}$ , 69% RH, and  $1.5\text{ m s}^{-1}$  wind mainly from  
 662 the southwest. At the balloon, sampling occurred at a similar temperature ( $-17.5^{\circ}\text{C}$ ) and RH  
 663 (72%), but higher wind speeds ( $4.3\text{ m s}^{-1}$ ) from the northeast to southeast. With  $\text{IWV} < 3\text{ kg m}^{-2}$ ,  
 664 the atmosphere was very dry (Figure S5a), and only a thin mixed-phase cloud layer at 4.5–5

665 km altitude was present, with negligible LWP and IWP (Figure S5a), unlikely to affect aerosol  
666 chemistry within the boundary layer.

667 ~~During active sampling at the ground, the average temperature was 16.7°C with a relative~~  
668 ~~humidity of 69% and a wind speed of 1.5 m s<sup>-1</sup> mostly from the southwest. At the balloon,~~  
669 ~~sampling occurred at a similar average temperature of 17.5°C, a relative humidity of 72%, but~~  
670 ~~a higher wind speed of 4.3 m s<sup>-1</sup> from the northeast and southeast. With an IWV of less than~~  
671 ~~3 kg m<sup>-2</sup>, the atmosphere was in general very dry (Figure S6a). The sky near the balloon was~~  
672 ~~clear of low-level clouds, with only a very thin mixed-phase cloud layer from 4.5 to 5 km~~  
673 ~~altitude with insignificant LWP and IWP values (Figure S6a). While these clouds may have had~~  
674 ~~some radiative effects, they were not expected to influence aerosol chemistry measurements~~  
675 ~~within the boundary layer.~~

676 ~~During the balloon's ascent to the aerosol sampling height, potential temperature increased~~  
677 ~~from 255 K to 258 K, with the strongest gradient near the surface ground. Using the wind speed~~  
678 ~~profile and the Richardson number approach (Akansu et al., 2023), a very shallow surface~~  
679 ~~mixing layer of ~12 m was estimated, likely caused by recent surface cooling. Together with~~  
680 ~~the wind speed profile, this allowed to estimate the surface mixing layer height using the~~  
681 ~~Richardson number approach (Akansu et al., 2023), resulting in a very low value of~~  
682 ~~approximately 12 m, likely due to recent surface cooling. Although this surface inversion and~~  
683 ~~the slightly stable to near-neutral stratification above would limit instantaneous vertical~~  
684 ~~mixing, surface mixing layer height reflects only momentary conditions, whereas aerosol and~~  
685 ~~humidity profiles integrate mixing over longer timescales. The coupling state at the time of~~  
686 ~~measurement is therefore not a reliable indicator of the effective boundary-layer mixing~~  
687 ~~state. This surface inversion, together with the slightly stable to near neutral part of the~~  
688 ~~boundary layer above, would limit recent vertical mixing of aerosols from the ground into~~  
689 ~~higher layers of the troposphere. However, while surface mixing layer height reflects~~  
690 ~~momentary conditions and can vary within minutes to hours, the aerosol and humidity profiles~~  
691 ~~represent the integrated effects of mixing over longer time scales. We therefore concluded~~  
692 ~~that the current coupling state is not a reliable indicator of the actual mixing state of the~~  
693 ~~atmospheric boundary layer.~~

694 Furthermore, as noted in Section 2.1, Ny-Ålesund's complex orography can induce localized  
695 turbulent mixing even under stable stratification. In addition, a low-level jet observed during

696 descent, with wind speeds at least  $2 \text{ m s}^{-1}$  higher than above and below, provided a significant  
697 additional source of turbulence and vertical mixing within the boundary layer (Egerer et al.,  
698 2023). During the descent, the wind speed profile clearly revealed the presence of a low-level  
699 jet, with a wind speed maximum at least  $2 \text{ m s}^{-1}$  higher than the minimum values both above  
700 and below. This low-level jet is a significant additional source of turbulence and vertical mixing  
701 within the boundary layer (Egerer et al., 2023).

hat formatiert: Hochgestellt

702 At the ground,  $N_{150}$  was around  $60 \text{ cm}^{-3}$ , and gradually decreased to  $45 \text{ cm}^{-3}$  at the balloon's  
703 sampling height, indicating a fairly uniform aerosol distribution dominated by primary  
704 emissions indicating a fairly uniform aerosol number distribution and a dominant influence of  
705 primary ground-level emissions. Combined with nearly constant specific humidity ( $\sim 0.7\text{--}0.8 \text{ g}$   
706  $\text{kg}^{-1}$ ), a slight wind speed increase with altitude, the low-level jet during descent, and  
707 consistent wind direction (Figure 4a), these suggest a largely well-mixed boundary layer.

hat formatiert: Schriftart: 12 Pt.

hat formatiert: Schriftart: 12 Pt.

hat formatiert: Schriftart: 12 Pt., Fett

hat formatiert: Schriftart: 12 Pt.

708 HALFBAC samples from ground and balloon showed similar concentrations of inorganic ions  
709 ( $\text{Na}_{\text{aer}}^+$ : 240 & 223,  $\text{Cl}_{\text{aer}}^-$ : 586 & 543,  $\text{SO}_4^-$ : 336 & 330,  $\text{Ca}_{\text{aer}}^{2+}$ : 87 & 92,  $\text{Mg}_{\text{aer}}^{2+}$ : 9.5 & 7.8,  
710  $\text{K}_{\text{aer}}^+$ : 34 & 30  $\text{ng m}^{-3}$ ), oxalate<sub>aer</sub> (34 & 37  $\text{ng m}^{-3}$ ), and major CCHO-bound monosaccharides  
711 ( $\text{Glc}_{\text{CCHO,aer}}$ : 17 & 9.1,  $\text{Xyl}_{\text{CCHO,aer}}$ : 5.0 & 4.7,  $\text{Ara}_{\text{CCHO,aer}}$ : 1.2 & 0.9  $\text{ng m}^{-3}$ ), supporting a well-mixed  
712 layer. Despite diverse sources (SSA, dust, anthropogenic, secondary), vertical aerosol  
713 composition remained uniform. Zeppelin Observatory 24 h measurements of  $\text{Na}_{\text{aer}}^+$ ,  $\text{Cl}_{\text{aer}}^-$   
714 and  $\text{SO}_4^{2-}$  showed slightly lower concentrations but agreed with balloon results. Combined with  
715 the nearly constant specific humidity ( $\sim 0.7\text{--}0.8 \text{ g kg}^{-1}$ ), a slight increase of wind speed with  
716 altitude measured during the balloon's ascent, the low-level jet observed at the decent and a  
717 consistent wind direction on the measurement day (Figure 3a), these observations suggest  
718 that the boundary layer was largely well-mixed.

hat formatiert: Hochgestellt, Nicht Hervorheben

hat formatiert: Tiefgestellt

hat formatiert: Hochgestellt, Nicht Hervorheben

hat formatiert: Tiefgestellt

hat formatiert: Tiefgestellt

hat formatiert: Tiefgestellt

hat formatiert: Nicht Hervorheben

719 For this event, chemical analyses from both HALFBACs (Figure 3a) showed similar, sometimes  
720 almost identical, concentrations of almost all inorganic ions (sodium: 240 & 223  $\text{ng m}^{-3}$ ,  
721 chloride: 586 & 543  $\text{ng m}^{-3}$ , sulfate: 336 & 330  $\text{ng m}^{-3}$ , calcium: 87 & 92  $\text{ng m}^{-3}$ , magnesium:  
722 9.5 & 7.8  $\text{ng m}^{-3}$ , potassium: 34 & 30  $\text{ng m}^{-3}$ ), oxalate (34 & 37  $\text{ng m}^{-3}$ ) and major CCHO-bound  
723 monosaccharide compounds ( $\text{Glc}_{\text{CCHO}}$ : 17 & 9.1  $\text{ng m}^{-3}$ ,  $\text{Xyl}_{\text{CCHO}}$ : 5.0 & 4.7  $\text{ng m}^{-3}$ ,  $\text{Ara}_{\text{CCHO}}$ : 1.2 &  
724 0.9  $\text{ng m}^{-3}$ ) at the ground and at the balloon. As outlined above, there are clear indications for  
725 a well-mixed boundary layer, as evidenced by the similar concentrations of all these  
726 compounds, including marine CCHO<sub>aer</sub>, at both the ground and balloon. Despite their  
727 potentially diverse origins—such as SSA, terrestrial dust, anthropogenic emissions, and

~~secondary formation processes—the vertical distribution of aerosol particle constituents remained uniform. The major inorganic compounds sodium, chloride, and sulfate were also measured at the Zeppelin Observatory with a 24-hour time resolution, showing only slightly lower concentrations and good agreement with the chemical results from the balloon.~~

Back-trajectory analysis ~~revealed that air masses for three arrival heights—at ground level, the balloon, and Zeppelin Observatory (Figure 64, Case I)—revealed that air masses at all levels~~ followed the same path ~~during the~~ within the 48 hours before sampling. Originating from the Arctic pack ice, they crossed the marginal ice zone with a short residence time before passing over the ice-free ocean and Kongsfjorden, where most SSA compounds were likely taken up. The back-trajectory heights indicate a vertical connection between the three air masses, confirming a similar transport history, influenced by the same emission sources.

This case demonstrates that major SSA constituents ( $\text{Na}^+_{\text{aer}}$ ,  $\text{Cl}^-_{\text{aer}}$ , and  $\text{CCHO}_{\text{aer}}$ ) can mix effectively within the boundary layer, reaching altitudes relevant to cloud formation with concentrations nearly identical to ground level, and that such a mixing state can persist during temporarily decoupled conditions.

~~This case demonstrates that major SSA particle constituents, including  $\text{Na}^+_{\text{aer}}$ ,  $\text{Cl}^-_{\text{aer}}$ , and  $\text{CCHO}_{\text{aer}}$ , can mix effectively within the boundary layer. Under favorable meteorological conditions, this mixing allows these compounds to reach elevated altitudes relevant to cloud formation, maintaining concentrations nearly identical to those at the ground. Moreover, such a mixed state can persist even during temporarily decoupled conditions,~~ provided there is no additional aerosol particle source at the ground or aloft.

#### **Case II: Free troposphere decoupled from the ground**

On 27 September 2021, balloon measurements were conducted at a median altitude of 1112 m, above both the Zeppelin Observatory and the altitude range of Case I, i.e. in the free troposphere above the boundary layer. A strong increase of the potential temperature between 700 m ( $\theta \approx 274$  K) and 900 m ( $\theta \approx 280$  K) indicates a pronounced inversion (Figure 5b).  $\text{N}_{150}$  peaked near the ground, remained stable in the lowest 200 m, decreased up to  $\sim 700$  m, and slightly increased toward 1112 m, suggesting sources other than the ground. Specific humidity varied strongly ( $2.6\text{--}4$  g  $\text{kg}^{-1}$ ), confirming a decoupled atmospheric layer.

During ground sampling, mean conditions were 3 °C, 89 % RH, and 0.7 m  $\text{s}^{-1}$  wind from the southwest (Table S5). At balloon altitude, air was colder ( $-1.9$  °C), slightly drier (87 % RH), and

hat formatiert: Schriftart: Nicht Fett

hat formatiert: Tiefgestellt

hat formatiert: Schriftart: Fett

759 much windier ( $5.5 \text{ m s}^{-1}$ ), primarily from the south and southwest (Table S4). IWV increased  
760 from 13 to  $\sim 15 \text{ kg m}^{-2}$  during sampling (Figure S5b). A dense warm-front cloud layer (2–8 km)  
761 with mainly cloud ice (IWP up to  $1.4 \text{ kg m}^{-2}$ ) was present (Figure S5b). Precipitation reached  
762 the balloon as snowfall only in the last 15–30 min of sampling. On 27 September 2021, balloon  
763 measurements were conducted at a median altitude of 1112 m—significantly higher than  
764 both the Zeppelin Observatory and the balloon in Case I. At this altitude, the balloon had  
765 ascended beyond the boundary layer and into the free troposphere. This observation is  
766 supported by the strong increase of potential temperature between 700 m ( $\theta \sim 274 \text{ K}$ ) and  
767 900 m ( $\theta \sim 280 \text{ K}$ ) in the vertical profile (Figure 3b), indicating a significant temperature  
768 inversion.  $\text{N}_{150}$  concentrations were highest near the ground and remained stable within the  
769 lower 200 m. Above this layer, values gradually decreased up to around 700 m. From there,  
770 they increased slightly toward 1112 m, likely indicating influence from sources other than the  
771 ground. Specific humidity also showed substantial variability, fluctuating between 2.6 and  
772  $4 \text{ g kg}^{-1}$ , further confirming the decoupled state of the sampled layer.

773  
774 During active aerosol particle sampling at the ground, the average temperature was  $3^\circ\text{C}$ , with  
775 a relative humidity of 89% and a mean wind speed of  $0.7 \text{ m s}^{-1}$ , predominantly from the  
776 southwest (Table S5). In contrast, at balloon altitude, the air was slightly colder, with a mean  
777 temperature of  $-1.9^\circ\text{C}$ , a relative humidity of 87%, and a significantly higher average wind  
778 speed of  $5.5 \text{ m s}^{-1}$ , primarily from the south and southwest (Table S4). On that day, IWV was  
779 high increasing from  $13 \text{ kg m}^{-2}$  to about  $15 \text{ kg m}^{-2}$  during the balloon sampling (Figure S6b). A  
780 dense layer of warm front clouds was present between 2 and 8 km, mainly consisting of cloud  
781 ice with IWP values up to  $1.4 \text{ kg m}^{-2}$  (Figure S6b). No precipitation reached the balloon or the  
782 ground up to the last 15–30 minutes of sampling, when snowfall reached the balloon and  
783 sampling was stopped.

784 On this date, we observed a strong vertical gradient in both  $\text{Na}_{\text{aer}}^+$  and  $\text{CCHO}_{\text{aer}}$   
785 concentrations (Figure 53b), starting from the winch ( $\text{Na}_{\text{aer}}^+$ :  $1840 \text{ ng m}^{-3}$ ,  $\text{CCHO}_{\text{aer}}$ :  
786  $199 \text{ ng m}^{-3}$ ), decreasing at the Zeppelin Observatory ( $\text{Na}_{\text{aer}}^+$ :  $850 \text{ ng m}^{-3}$ ), and dropping  
787 sharply at the balloon's altitude ( $\text{Na}_{\text{aer}}^+$ :  $23 \text{ ng m}^{-3}$ ,  $\text{CCHO}_{\text{aer}}$ :  $8.6 \text{ ng m}^{-3}$ ). Similar declines  
788 occurred by, decreasing trends with altitude were observed for other constituents, including  
789  $\text{SO}_4^{2-}$  sulfate (580; 220;  $76 \text{ ng m}^{-3}$ ),  $\text{Cl}_{\text{aer}}^-$  chloride (4230; 1500;  $60 \text{ ng m}^{-3}$ ), and  $\text{Ca}_{\text{aer}}^{2+}$  calcium

hat formatiert: Schriftart: Fett

hat formatiert: Schriftart: Fett

hat formatiert: Schriftart: Fett

hat formatiert: Schriftart: +Textkörper (Calibri), Englisch (Vereinigtes Königreich)

hat formatiert: Englisch (Vereinigtes Königreich)

hat formatiert: Englisch (Vereinigtes Königreich)

hat formatiert: Englisch (Vereinigtes Königreich)

hat formatiert: Englisch (Vereinigtes Königreich)

hat formatiert: Englisch (Vereinigtes Königreich)

hat formatiert: Englisch (Vereinigtes Königreich)

hat formatiert: Englisch (Vereinigtes Königreich)

hat formatiert: Englisch (Vereinigtes Königreich)

hat formatiert: Englisch (Vereinigtes Königreich)

hat formatiert: Englisch (Vereinigtes Königreich)

hat formatiert: Englisch (Vereinigtes Königreich)

hat formatiert: Englisch (Vereinigtes Königreich)

hat formatiert: Englisch (Vereinigtes Königreich)

hat formatiert: Englisch (Vereinigtes Königreich)

hat formatiert: Englisch (Vereinigtes Königreich)

hat formatiert: Englisch (Vereinigtes Königreich)

hat formatiert: Englisch (Vereinigtes Königreich)

hat formatiert: Englisch (Vereinigtes Königreich)

hat formatiert: Englisch (Vereinigtes Königreich)

hat formatiert: Englisch (Vereinigtes Königreich)

hat formatiert: Englisch (Vereinigtes Königreich)

790 (165; 32; 28 ng m<sup>-3</sup>). This pronounced decrease with altitude indicates separation between  
791 ground-level and elevated air masses, making fresh local SSA from Kongsfjorden or the west  
792 coast of Svalbard an unlikely source for the substances detected at 1112 m. This pronounced  
793 decline in major inorganic ions and CCHO<sub>aer</sub> concentrations with increasing altitude suggests  
794 a separation of ground-level air masses and those at higher elevations. It is unlikely that the  
795 substances detected at 1112 m originated primarily from fresh local sea-spray emissions from  
796 Kongsfjorden or the west coast of Svalbard.

797 ▲  
798 This assumption is supported by back-trajectory analysis (**Figure 64b**): air masses at 50 m and  
799 474 m arrival height originated from Arctic pack ice and crossed the ice-free Fram Strait,  
800 whereas the 1112 m air mass followed a different path over the Barents Sea near Franz Josef  
801 Land. After contact with the marine boundary layer and possibly the sea surface about 48 h  
802 before sampling, it remained mainly between 1000 and 1800 m. This indicates that the SSA  
803 observed at 1112 m in Ny-Ålesund likely originated from this distant source region.

804 While air masses arriving at 50 m and 474 m originated from the pack ice region in the central  
805 Arctic Ocean with a subsequent residence time over the ice-free Fram Strait, the air mass  
806 arriving at 1112 m followed a different pathway, passing over the Barents Sea near Franz Josef  
807 Land. 48 hours before sampling, this air mass had come into contact with the ground and the  
808 marine boundary layer in that region. However, after leaving the vicinity of Franz Josef Land,  
809 it remained predominantly at altitudes between 1000 and 1800 m. This suggests that SSA  
810 emissions contributing to the measured concentrations at 1112 m in Ny-Ålesund likely  
811 originated from that distant region.

812 In summary, Case II demonstrates that in the presence of an atmospheric inversion, major SSA  
813 constituents, including (Na<sub>aer</sub><sup>+</sup> sodium, Ca<sub>aer</sub><sup>2+</sup> calcium, Cl<sub>aer</sub><sup>-</sup> chloride, SO<sub>4aer</sub><sup>2-</sup> sulfate and  
814 CCHO<sub>aer</sub> (CCHO<sub>7</sub>)) can be present in the free troposphere and likely originate from a distant  
815 source at higher altitudes. However, they appear at different concentrations above the  
816 temperature inversion than in the mixed boundary layer below, where concentrations, like in  
817 Case I, are similar. However, in contrast to the mixed boundary layer (Case I), they occur at  
818 concentrations different from those at the ground and likely originate from more distant  
819 emission sources through long-range transport.

820 **Case III: Inside and below a drizzling cloud**

hat formatiert: Nicht Hervorheben

hat formatiert: Englisch (Vereinigtes Königreich)

hat formatiert: Englisch (Vereinigtes Königreich)

hat formatiert: Englisch (Vereinigtes Königreich)

hat formatiert: Englisch (Vereinigtes Königreich)

hat formatiert: Englisch (Vereinigtes Königreich)

hat formatiert: Englisch (Vereinigtes Königreich)

hat formatiert: Englisch (Vereinigtes Königreich)

hat formatiert: Englisch (Vereinigtes Königreich)

hat formatiert: Englisch (Vereinigtes Königreich)

hat formatiert: Englisch (Vereinigtes Königreich)

hat formatiert: Englisch (Vereinigtes Königreich)

hat formatiert: Englisch (Vereinigtes Königreich)

hat formatiert: Schriftart: (Standard) + Textkörper (Calibri), Englisch (Vereinigtes Königreich)

hat formatiert: Nicht Hervorheben

hat formatiert: Nicht Hervorheben

821 On 03 October 2021, the ground temperature was 3°C with a high relative humidity of 89%.  
822 Winds were light, shifting between east, south, and west at 0.7 m s<sup>-1</sup> during sampling. At the  
823 balloon's altitude of 666 m, the average temperature was -1.3°C, the relative humidity 96%  
824 and the wind speed 6.8 m s<sup>-1</sup> from the east and northeast. The day was overcast, with  
825 continuous drizzle from a 2 km deep mixed-phase cloud layer with LWP values of up to  
826 300 g m<sup>-2</sup> and IWV of around 13 to 14 kg m<sup>-2</sup>. The balloon's altitude was close to the melting  
827 layer.

828 During the balloon's ascent and descent to ~~the aerosol sampling height of~~ 666 m, a positive  
829 gradient in potential temperature ~~was observed~~ (272 K at the ground vs. 278 K at the balloon,  
830 **Figure 53c**) ~~indicating~~ a stably stratified boundary layer. ~~Specific humidity was uniform (3.2–~~  
831 ~~3.8 g kg<sup>-1</sup>), while N<sub>150</sub> was lower than in Case I (3–10 cm<sup>-3</sup>) with higher relative variability, likely~~  
832 ~~influenced by low counting statistics at these low concentrations. Overall, mixing conditions~~  
833 ~~in Case III were similar to Case I, but sampling occurred partly within or below a drizzling low-~~  
834 ~~level cloud. Similar to Case I, the specific humidity remained relatively uniform throughout the~~  
835 ~~vertical column, with values between 3.2 and 3.8 g kg<sup>-1</sup>. The vertical N<sub>150</sub> distribution showed~~  
836 ~~generally lower aerosol number concentrations compared to Case I, ranging between 3 and~~  
837 ~~10 cm<sup>-3</sup>, and exhibited greater relative fluctuation. In summary, the boundary layer mixing~~  
838 ~~conditions on 03 October 2021 (Case III) appeared similar to those in Case I. The key~~  
839 ~~difference, however, was that in this case, aerosol sampling occurred partially inside or below~~  
840 ~~a drizzling low-level cloud.~~

841  
842 Back-trajectory analysis ~~for ground, balloon, and Zeppelin Observatory (Figure 64, Case III)~~  
843 ~~showed that air masses at the altitudes of ground, balloon, and Zeppelin Observatory~~  
844 ~~followed the same 48-h path from the ice-free ocean south of Svalbard. all arrival heights~~  
845 ~~followed the same path within the 48 hours before sampling, originating from the ice-free~~  
846 ~~ocean south of Svalbard. Vertical trajectory heights indicate shared transport history and~~  
847 ~~influence by the same emission sources, consistent with Case I.~~

848 ~~As observed in Case I, trajectory heights indicate a vertical movement during this period,~~  
849 ~~suggesting that air masses at all three levels shared a similar transport history and were~~  
850 ~~influenced by the same emission sources.~~

hat formatiert: Englisch (Vereinigtes Königreich),  
Tiefgestellt

851 In line with the lower aerosol number concentrations, offline measurements of chemical  
852 constituents were also generally lower than in the previous cases. Furthermore, major  
853 inorganic ions (**Figure 53c**) were ~~generally similar or slightly higher at at the ground and than~~  
854 ~~at the balloon~~ ( $\text{Cl}_{\text{aer}}^-$  chloride: 289 & 252 ng m<sup>-3</sup>;  $\text{SO}_4^{2-}$  sulfate: 66 & 59 ng m<sup>-3</sup>;  $\text{Na}^+$ : 53 &  
855 ~~35 ng m<sup>-3</sup>~~;  $\text{K}_{\text{aer}}^+$   $\text{K}^+$ : 23 & 20 ng m<sup>-3</sup>), with  $\text{Na}_{\text{aer}}^+$  (53 & 35 ng m<sup>-3</sup>) somewhat higher at the  
856 ~~ground.~~ At the Zeppelin Observatory, only  $\text{Na}_{\text{aer}}^+$   ~~$\text{Na}^+$  was measured above~~ exceeded the  
857 detection limit, with a concentration of ~~which was quantified at~~ 38 ng m<sup>-3</sup>, ~~very similar to the~~  
858 ~~value almost identical to~~ ~~observed~~ the concentration measured at the balloon. This  
859 consistency indicates a rather mixed boundary layer. Creamean et al. (2021) analyzed three  
860 years of Arctic aerosol vertical distributions using a tethered balloon in Alaska and found that,  
861 when a uniform aerosol distribution below clouds was observed, it primarily occurred in  
862 autumn, aligning well with Case III.

863 Interestingly, despite the same levels of major inorganic ions, some chemical constituents  
864 exhibited increased concentrations at higher altitudes. These included major  
865 monosaccharides bound within CCHO (ground & balloon:  $\text{Gl}_{\text{CCHO,aer}}$ : 12.6 & 34 ng m<sup>-3</sup>;  
866  $\text{Xyl}_{\text{CCHO,aer}}$ : 0.57 & 4.4 ng m<sup>-3</sup>;  $\text{Ara}_{\text{CCHO,aer}}$ : below detection limit & 0.97 ng m<sup>-3</sup>), as well as  
867 oxalate<sub>aer</sub> (5.5 & 24 ng m<sup>-3</sup>),  $\text{Ca}_{\text{aer}}^{2+}$   $\text{Ca}^{2+}$  (47 & 187 ng m<sup>-3</sup>), and  $\text{Mg}_{\text{aer}}^{2+}$   $\text{Mg}^{2+}$  (0.97 & 2.6 ng m<sup>-3</sup>).  
868 ~~These elevated concentrations cannot be explained by direct local sea spray emissions or~~  
869 ~~remote source contributions alone, suggesting the involvement of cloud-related enrichment~~  
870 ~~and transformation processes. The origin of these elevated concentrations remains unclear, as~~  
871 ~~neither local sea spray emissions nor remote sources appeared suitable to account for the~~  
872 ~~observed patterns.~~

873  
874 ~~Soluble. While organics like CCHO<sub>aer</sub> and oxalate<sub>aer</sub> might originate through secondary in-situ~~  
875 ~~atmospheric chemical or microbial processes — particularly in the aqueous phase, as discussed~~  
876 ~~more in detail in the following section — this does not  $\text{Ca}_{\text{aer}}^{2+}$  and  $\text{Mg}_{\text{aer}}^{2+}$  apply for inorganic~~  
877 ~~elements such as calcium and magnesium. possibly derived from preexisting organic~~  
878 ~~structures in SSA, becoming soluble and detectable after chemical aging. Instead, their ionic~~  
879 ~~forms were possibly released from preexisting complex organic structures in SSA particles,~~  
880 ~~becoming soluble and thus detectable by our analytical methods.~~ OM-bound Ca<sup>2+</sup>, as already  
881 found in Antarctic SSA (Su et al., 2023), may originate from SML-derived polysaccharide gels

hat formatiert: Englisch (Vereinigtes Königreich)

hat formatiert: Englisch (Vereinigtes Königreich)

hat formatiert: Englisch (Vereinigtes Königreich)

hat formatiert: Englisch (Vereinigtes Königreich)

hat formatiert: Englisch (Vereinigtes Königreich)

hat formatiert: Englisch (Vereinigtes Königreich)

hat formatiert: Englisch (Vereinigtes Königreich)

hat formatiert: Englisch (Vereinigtes Königreich)

hat formatiert: Englisch (Vereinigtes Königreich)

hat formatiert: Englisch (Vereinigtes Königreich)

hat formatiert: Nicht Hochgestellt/ Tiefgestellt

hat formatiert: Englisch (Vereinigtes Königreich)

hat formatiert: Englisch (Vereinigtes Königreich)

hat formatiert: Englisch (Vereinigtes Königreich)

hat formatiert: Englisch (Vereinigtes Königreich),  
Tiefgestellt

hat formatiert: Englisch (Vereinigtes Königreich)

hat formatiert: Englisch (Vereinigtes Königreich)

hat formatiert: Englisch (Vereinigtes Königreich)

hat formatiert: Englisch (Vereinigtes Königreich)

hat formatiert: Englisch (Vereinigtes Königreich)

hat formatiert: Englisch (Vereinigtes Königreich)

hat formatiert: Englisch (Vereinigtes Königreich)

hat formatiert: Englisch (Vereinigtes Königreich)

hat formatiert: Englisch (Vereinigtes Königreich)

hat formatiert: Nicht Hervorheben

hat formatiert: Nicht Hervorheben

882 such as TEPs, and airborne algal cells or fragments, which can release Ca<sup>2+</sup> and Mg<sup>2+</sup> through  
883 gel dispersion or cell dissolution under the acidic conditions of chemically aged SSA aerosol  
884 particles (Aller et al., 2017; Angle et al., 2021; Orellana and Leck, 2015; van Pinxteren et al.,  
885 2022; Trainic et al., 2018; Zhu et al., 2014). Since these particles were sampled in cloud water,  
886 which contains abundant TEP (van Pinxteren et al., 2022), this mechanism may also explain  
887 the elevated CCHO concentrations. Ca<sub>aer</sub><sup>2+</sup> can form complexes with oxalate<sub>aer</sub> (Furukawa and  
888 Takahashi, 2011), and oxalic acid increases hygroscopicity, potentially accounting for the high  
889 values observed at the balloon in Case III. In addition, secondary in-situ atmospheric or  
890 microbial origins, particularly in the aqueous phase, may contribute to CCHO<sub>aer</sub> and oxalate<sub>aer</sub>,  
891 and is discussed in the following section.

892 In summary, Case III demonstrates that certain SSA constituents can vary with altitude due to  
893 atmospheric processing following primary emissions and vertical transport. In summary, Case  
894 III, demonstrates that certain organic SSA constituents can change within the vertical column  
895 due to atmospheric aging after primary emissions and vertical transport.

898 The three cases show that meteorological conditions can produce similar, lower, or higher  
899 chemical concentrations at different altitudes. Porter et al. (2022) observed similar patterns  
900 for ice-nucleating particles at the North Pole. They combined their measurements with  
901 trajectory analyses and heat sensitivity tests to conclude on aerosol sources. While this effect-  
902 based approach gives insights into particle properties, direct chemical analyses, as performed  
903 in this study, can further enhance certainty about particle origin and composition relevant for  
904 cloud formation.

905 Overall, the three cases presented highlight distinct meteorological scenarios that can lead to  
906 similar, lower, or even higher concentrations of chemical constituents at different altitudes.  
907 Interestingly, comparable patterns, with higher, lower, or similar levels at ground and balloon  
908 altitude, were also observed at the North Pole by Porter et al. (2022), who measured INP  
909 concentrations and combined these with trajectory analyses and heat sensitivity tests to  
910 conclude on their sources. While this effect-based approach provides valuable insights into  
911 aerosol particle properties, direct chemical analyses, as performed in this study, can further

**hat formatiert:** Schriftart: 12 Pt., Nicht Fett, Schriftfarbe: Automatisch, Nicht Hervorheben

**hat formatiert:** Schriftart: 12 Pt., Nicht Fett, Schriftfarbe: Automatisch, Nicht Hervorheben

**hat formatiert:** Schriftfarbe: Automatisch, Tiefgestellt

**hat formatiert:** Schriftart: 12 Pt., Nicht Fett, Schriftfarbe: Automatisch, Nicht Hervorheben

**hat formatiert:** Schriftart: 12 Pt., Nicht Fett, Schriftfarbe: Automatisch, Nicht Hervorheben

**hat formatiert:** Schriftart: 12 Pt., Nicht Fett, Schriftfarbe: Automatisch, Nicht Hervorheben

**hat formatiert:** Schriftfarbe: Automatisch, Tiefgestellt

**hat formatiert:** Schriftart: 12 Pt., Nicht Fett, Schriftfarbe: Automatisch, Nicht Hervorheben

**hat formatiert:** Schriftfarbe: Automatisch, Tiefgestellt

**hat formatiert:** Schriftart: 12 Pt., Nicht Fett, Schriftfarbe: Automatisch, Tiefgestellt, Nicht Hervorheben

**hat formatiert:** Schriftart: 12 Pt., Nicht Fett, Schriftfarbe: Automatisch, Nicht Hervorheben

**hat formatiert:** Schriftart: 11 Pt., Fett

912 ~~enhance certainty regarding the origin and composition of particles relevant for cloud droplet~~  
913 ~~and cloud ice formation.~~

914 **3.3 Factors affecting SSA constituents beyond local sea-air transfer**

915 ***Long-range transport and size-dependent deposition***

916 SSA particles originate from both local and remote marine regions. However, our sampling  
917 methods make it challenging to determine the relative contribution of long-range transported  
918 SSA constituents, particularly when a local marine source, such as the Kongsfjorden is adjacent  
919 to the sampling site and may dominate other marine emissions.

920 As demonstrated in Case II, long-range transport of SSA can become dominant when air  
921 masses at elevated altitudes are decoupled from those at the ground. In this case, vertical and  
922 horizontal trajectory analysis suggests that the measured SSA constituents may have been  
923 emitted and incorporated into the atmosphere approximately 48 hours earlier over the  
924 Barents Sea, near Franz Josef Land. ~~Atmospheric processes, such as the removal of larger  
925 supermicron particles, cloud activation, and precipitation,~~Typical removal processes of  
926 supermicron particles, such as dry and wet deposition or cloud droplet activation, likely  
927 reduced their ~~absolute mass~~atmospheric concentrations of major inorganic ions and  $CCHO_{aer}$   
928 by one to two orders of magnitude before the arrival of the air masses in Ny-Ålesund (Figure  
929 5b).

930 In several balloon-borne TSP filter samples, ~~however,~~an elevated  $CCHO_{aer}/Na^+_{aer}$   ~~$CCHO/Na^+$~~   
931 ratio was observed, most notably on 24 September 2021; 03 October 2021 (Case III) and 03  
932 April 2022 (see **Figure 2d**). These values far exceeded both ground-based aerosol  
933 measurements from this study and previously reported values (Zeppenfeld et al., 2021, 2023),  
934 particularly for supermicron SSA particles that dominate the TSP mass. A slight increase of this  
935 ratio may be explained by a longer atmospheric residence time of these particles. ~~This leads,~~  
936 ~~leading~~ to a relative reduction of supermicron aerosol particles, ~~typically dominated by sea~~  
937 salt (O'Dowd and de Leeuw, 2007), through deposition (Croft et al., 2009; Hoppel et al.,  
938 2002); ~~In contrast, which are typically dominated by sea salt (O'Dowd and de Leeuw, 2007),~~  
939 ~~while~~ submicron aerosol particles, ~~which are~~ rich in surface-active  $CCHO$ , remain. This  
940 process could lead to a shift of the  $CCHO_{aer}/Na^+_{aer}$   ~~$CCHO/Na^+$~~  ratios more ~~similar~~  
941 ~~to~~characteristic of submicron than supermicron particles in the TSP samples of this study, as  
942 seen in Case II.

hat formatiert: Tiefgestellt

hat formatiert: Schriftart: Fett

hat formatiert: Schriftart: Fett

hat formatiert: Nicht Hervorheben

hat formatiert: Nicht Hervorheben

943 However, ~~in-for~~ the three cases with the most pronounced increases ~~in-of-the~~ CCHO<sub>aer</sub>/Na<sup>+</sup><sub>aer</sub>  
944 ratios in TSP at higher altitudes (24 September 2021; 03 October 2021; 03 April 2022), absolute  
945 CCHO<sub>aer</sub> concentrations were also elevated ~~as well~~ (compare **Figures 2b and 2d**). Such  
946 increases ~~in-of~~ absolute concentrations cannot be explained by ~~the selective selective~~ removal  
947 ~~of supermicron particles as hypothesized above~~ processes. This raises the question of whether  
948 the observed CCHO<sub>aer</sub> concentrations could result from the long-range transport of SSA  
949 compounds from a distant marine source with significantly higher CCHO levels ~~in-the-seawater~~  
950 than the local Kongsfjorden.

951 Model simulations using FESOM2.1-REcoM3 (Gürses et al., 2023) (**Figure S67**) and field data  
952 (Assmy et al., 2023; Feltracco et al., 2021; Grosse et al., 2021; Wietz et al., 2024) confirm that  
953 the eastern Fram Strait as well as coastal Svalbard waters are productive and polysaccharide-  
954 rich regions. While the FESOM2.1-REcoM3 model does not resolve the SML separately,  
955 previous studies have shown significant CCHO enrichment in this layer (Compiano et al., 1993;  
956 Engel and Galgani, 2016; Gao et al., 2012; Zäncker et al., 2021), particularly in the productive  
957 marginal ice zone (Zeppenfeld et al., 2023). However, in ~~the~~ cases of high CCHO<sub>aer</sub> at  
958 ~~higher~~ elevated altitudes in ~~the current~~ this study, air mass trajectories did not ~~pass over~~ ~~cross~~  
959 ~~the marginal ice zone within any of these productive marine regions~~ ~~48~~ within 48 hours before  
960 reaching Svalbard (**Figure S78**). These findings suggest that long-range transport of SSA from  
961 more productive remote marine sources is unlikely to ~~explain~~ ~~explain~~ ~~elevated~~ ~~the elevated~~  
962 CCHO<sub>aer</sub> concentrations at elevated altitudes within the lower troposphere in Ny-Ålesund,  
963 further supporting a ~~rather~~ predominantly local source or atmospheric in-situ formation.

964 In summary, while long-range transport of SSA constituents at elevated altitudes appears  
965 relevant in cases of decoupled atmospheric layers such as in Case II, it may not explain the  
966 significantly higher CCHO<sub>aer</sub> concentrations at high altitudes compared to ground levels.  
967 Instead, in-situ formation of CCHO<sub>aer</sub> could be a more plausible explanation for these  
968 observations.

969 **Atmospheric in-situ formation of marine CCHO<sub>aer</sub>**  
970 *Atmospheric in-situ formation of marine CCHO<sub>aer</sub>*  
971 Bacteria can be transported into and persist in the Arctic atmosphere (Jensen et al., 2022;  
972 Šantl-Temkiv et al., 2018), with sources including terrestrial environments and surface  
973 seawater, particularly the SML (Aller et al., 2005). Our complementary microbiological

hat formatiert: Nicht Hervorheben

hat formatiert: Schriftart: (Standard) + Textkörper (Calibri)

hat formatiert: Schriftart: (Standard) + Textkörper (Calibri)

hat formatiert: Schriftart: (Standard) + Textkörper (Calibri), Englisch (Vereinigtes Königreich)

974 ~~sampling during our campaign supported such dynamics by detecting diverse marine bacteria~~  
975 ~~in aerosol particles. Our field study confirmed such dynamics by finding diverse marine and~~  
976 ~~terrestrial bacteria in aerosol particles collected at the Old Pier~~ (Wietz et al., ~~to be~~  
977 ~~submitted~~2025). Some aerosolized taxa, for instance *Polaribacter*, encode multiple genes for  
978 CCHO metabolism (Avci et al., 2020) and consistently occur in ~~both the~~ Kongsfjorden ~~seawater~~  
979 ~~and atmosphere~~ during the spring bloom (Feltracco et al., 2021). These observations might  
980 underpin microbial CCHO transformations in the atmosphere, for instance the production of  
981 ~~sticky,~~ polysaccharide-based gels as protection against temperature fluctuations, salinity  
982 changes, and desiccation (Aller et al., 2005; Ramasamy et al., 2023; Šantl-Temkiv et al., 2022).  
983 Under highly humid conditions, ~~—~~especially in the presence of liquid water (such as in Case  
984 III), ~~—~~airborne bacteria can become metabolically active (Ervens and Amato, 2020; Haddrell  
985 and Thomas, 2017). Atmospheric OM formation, including CCHO, through microbial activity  
986 has been documented for cloud water and aerosol particles (Bianco et al., 2019; Klein et al.,  
987 2016; Matulová et al., 2014). Consequently, metabolically active bacteria in the atmosphere  
988 could explain the increased CCHO<sub>aer</sub> concentrations observed within or near drizzling clouds  
989 in Case III of this study.

#### 990 ***CCHO<sub>aer</sub> versus oxalate<sub>aer</sub>: Co-production or atmospheric processing?***

991 Since both combined glucose and combined xylose were consistently detected in CCHO<sub>aer</sub> of  
992 nearly all aerosol samples, we examined their correlation with other atmospheric chemical  
993 parameters. We observed a strong correlation between atmospheric xylose in CCHO<sub>aer</sub> and  
994 oxalate<sub>aer</sub> with an R=0.78 (p<0.001) across all sampling locations and heights (**Figure 75**).  
995 Oxalate, the ionic form of oxalic acid, is the most abundant dicarboxylic acid in aerosol  
996 particles (Kerminen et al., 1999; Rinaldi et al., 2011), with atmospheric concentrations in this  
997 study between <1 and 67 ng m<sup>-3</sup>. The strong correlation raised the question of whether oxalic  
998 acid could be chemically linked to combined carbohydrates in aerosol particles.

999 Oxalate<sub>aer</sub> is known to originate from several primary sources and secondary formation  
1000 pathways in both terrestrial and anthropogenic environments (Kawamura and Bikkina, 2016;  
1001 Yang et al., 2022). In remote marine environments, the atmospheric formation of oxalic acid  
1002 was proposed by Warneck (2003) through the aqueous-phase oxidation of glyoxal and  
1003 glycolaldehyde, a process also investigated by field measurements inside and above marine  
1004 clouds (Crahan et al., 2004; Sorooshian et al., 2007) and modeling (Herrmann et al., 2005;

hat formatiert: Schriftart: (Standard) +Textkörper (Calibri), Englisch (Vereinigtes Königreich)

hat formatiert: Schriftart: (Standard) +Textkörper (Calibri)

hat formatiert: Schriftart: (Standard) +Textkörper (Calibri)

hat formatiert: Schriftart: (Standard) +Textkörper (Calibri)

1005 Tilgner and Herrmann, 2010). The possible aqueous-phase formation was supported by Case  
1006 III of this study, where higher oxalate<sub>aer</sub> concentrations were observed within and in vicinity of  
1007 clouds compared to ground level. In contrast, in the drier conditions of Cases I and II, oxalate<sub>aer</sub>  
1008 levels remained vertically uniform. Additionally, since overall oxalate<sub>aer</sub> levels at the Old Pier  
1009 (1.1–10.1 ng m<sup>-3</sup>; mean=4.3±3.5 ng m<sup>-3</sup>) were relatively low compared to the more inland  
1010 Winch (<1–58 ng m<sup>-3</sup>; mean=19.8±16.2 ng m<sup>-3</sup>) and elevated altitudes samples (4.6–67 ng m<sup>-3</sup>;  
1011 mean=29.6±17.8 ng m<sup>-3</sup>), direct primary oceanic emission was likely not its dominant source.

1012

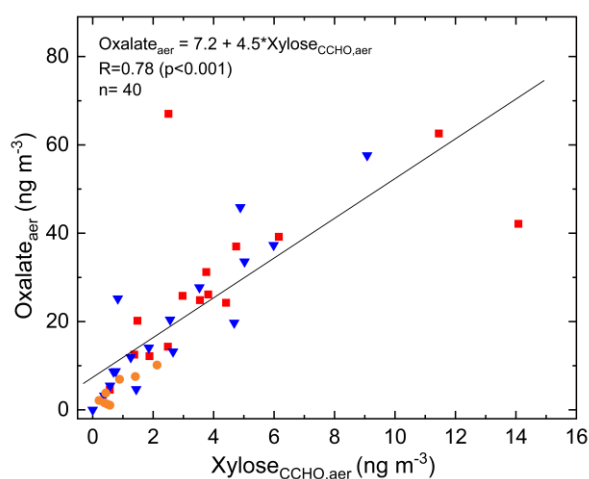


Figure 75. Atmospheric oxalate as a function of xylose in CCHO<sub>aer</sub> (R=0.78; p<0.001) measured in TSP from the Old Pier (orange circles), the winch site (blue triangles) and at elevated altitudes (red squares).

1021 But what are the precursors of oxalic acid's precursors? While Warneck (2003) suggested that  
1022 the anthropogenic volatile organic compounds acetylene and ethene can be transformed to  
1023 atmospheric glyoxal, other studies suggest the photochemical degradation of marine OM  
1024 (McNeill, 2015; Sinreich et al., 2010; Turekian et al., 2003; Zhou et al., 2014), with oligo- and  
1025 polysaccharides representing a known subclass. Although not explicitly measured in this  
1026 study, previous findings have shown that both CCHO<sub>aer</sub> (Leck et al., 2013; Zeppenfeld et al.,  
1027 2021, 2023) and oxalate<sub>aer</sub> (Guo et al., 2016; Rinaldi et al., 2011; Turekian et al., 2003) are  
1028 present across both the accumulation and coarse size modes. However, no consistently  
1029 dominant size mode has been identified, which may support a common mechanism of  
1030 formation or similar atmospheric processing pathways.

1031 Here, based on known chemical reactions, we propose possible atmospheric pathways linking  
 1032 xylose-containing oligo- and polysaccharides as the precursors to oxalate as the final product  
 1033 (Figure 86). The initial depolymerization of CCHO presumably occurs either via enzymatic  
 1034 degradation, e.g. by glycoside hydrolases, or acid hydrolysis (Panagiotopoulos and Sempéré,  
 1035 2005), both of which are plausible in the atmospheric context. Active microbial enzymes have  
 1036 been detected in SSA, often exhibiting activities 1–2 orders of magnitude higher than in bulk  
 1037 seawater (Malfatti et al., 2019). Additionally, SSA particles are known for reaching very low pH  
 1038 levels within minutes after their emissions due to the uptake and reactions with acidic gases,  
 1039 as well as water loss (Angle et al., 2022, 2021). Furthermore, although not explicitly  
 1040 investigated in an atmospheric context, Zhu et al. (2023) observed rapid depolymerization of  
 1041 xylose-containing oligosaccharides into the monosaccharide xylose within minutes in a  
 1042 UV/H<sub>2</sub>O<sub>2</sub> system, which generates hydroxyl radicals, generating hydroxyl radicals.

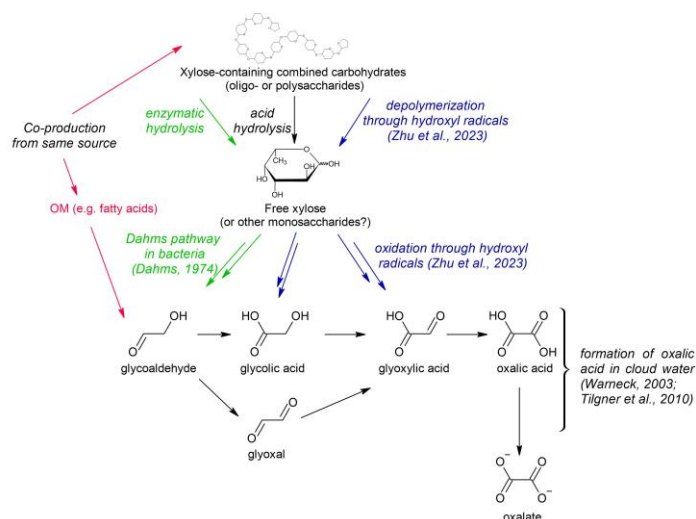


Figure 86. Possible pathways for the formation of atmospheric oxalate from xylose in combined carbohydrates in marine aerosol particles.

1053 With one exception, Free xylose was ~~with one exception~~ never detected in any aerosol  
 1054 sample of this study. This, suggests ~~sting~~ two possible explanations. First, xylose may have  
 1055 remained bound within the CCHO<sub>aer</sub> fraction and was not released into its free form. In this  
 1056 case, it would indicate co-emission without a chemical pathway leading to oxalate. Second,

hat formatiert: Tiefgestellt

1057 free xylose may have been rapidly processed in the atmosphere via reactions described  
1058 below.that it is rapidly processed in the atmosphere.

1059 Two potential pathways may link monomeric xylose to precursors of Warneck's oxalate  
1060 formation: (1) a follow-up reaction with hydroxyl radicals, where the pyranose ring of xylose  
1061 is cleaved after the more susceptible glycosidic bonds have been readily broken. Zhu et al.  
1062 (2023) observed glycolic acid and glyoxylic acid among other products following the UV/H<sub>2</sub>O<sub>2</sub>  
1063 treatment of xylooligosaccharides. (2) Bacterial metabolism via the Dahms pathway  
1064 converting free xylose into pyruvate and glycolaldehyde (Dahms, 1974). However, only few  
1065 bacteria encode this pathway; and it is highly questionable whether these occur in sufficient  
1066 atmospheric concentrations for a measurable effect.

1067 One indication that direct formation from xylose-containing oligo- and polysaccharides cannot  
1068 be the sole source of atmospheric oxalate in the marine environment is the discrepancy in  
1069 concentrations: atmospheric oxalate levels were seven times higher than those of combined  
1070 xylose. This confirms the involvement of additional precursors or a co-production/co-emission  
1071 of combined xylose with gaseous precursors, such as isoprene (Carlton et al., 2009; Kawamura  
1072 and Bikkina, 2016), or other primary marine organic matter, such as phytoplankton-derived  
1073 fatty acids (Kawamura et al., 1996b, a) undergoing photo-oxidation. Further targeted  
1074 laboratory and modeling studies are needed for clarity.

#### 1075 **4. Summary and Atmospheric Implications**

1076 In autumn 2021 and spring 2022, we performed balloon-borne measurements of major SSA  
1077 constituents at Ny-Ålesund (Svalbard). Our evidence demonstrated that both sodium and  
1078 marine CCHO reach elevated altitudes within the boundary layer, and even the free  
1079 troposphere as part of aerosol particles. The relationship between ground-level and high-  
1080 altitude measurements was strongly influenced by meteorological conditions and the mixing  
1081 state of the lower atmosphere, as discussed in three representative cases. Long-range  
1082 transport of  $\text{Na}^+_{\text{aer}}$  and  $\text{CCHO}_{\text{aer}}$  from remote marine sources is presumably relevant for high-  
1083 altitude measurements, especially when the upper air masses were decoupled from the  
1084 ground. However, in cases of a well-mixed lower atmosphere, the local marine source (here,  
1085 the Kongsfjorden) was the dominant contributor for atmospheric  $\text{Na}^+_{\text{aer}}$  and  $\text{CCHO}_{\text{aer}}$ . Under  
1086 very humid conditions particularly in the presence of liquid precipitating clouds, in-situ  
1087 formation of  $\text{CCHO}_{\text{aer}}$  was observed, possibly linked to microbial metabolism. To establish  
1088 more generalizable patterns, we recommend further field studies using airborne platforms.

1089 The significant correlation between combined xylose within  $\text{CCHO}_{\text{aer}}$ , and oxalate<sub>aer</sub> suggests  
1090 underlying pathways for oxalic acid formation from combined xylose and other  
1091 monosaccharide units within  $\text{CCHO}_{\text{aer}}$ ; alternatively, a co-production of xylose-containing  
1092 oligo- and polysaccharides alongside oxalate precursors.

1093 ~~CCNs~~ Cloud condensation nuclei and ~~INPs~~ ice-nucleating particles are key drivers in cloud  
1094 formation, influencing radiative and precipitation properties and, consequently, climate  
1095 processes. Considerable uncertainties remain regarding the origin and chemical composition  
1096 of these particles, particularly in remote Arctic regions, which affects the accuracy of climate  
1097 models. Since marine polysaccharides have been identified as relevant ice-nucleating  
1098 molecules in the remote marine atmosphere (Hartmann et al., 2025), our findings have  
1099 implications for cloud microphysics, especially given that these carbohydrates are transported  
1100 to altitudes relevant for cloud formation. Furthermore, atmospheric processing, as observed  
1101 here, may alter the ice-nucleating properties of these macromolecules, potentially creating  
1102 new ~~INPs~~ ice-nucleating particles in-situ or deactivating existing ones.

1103 As the Arctic continues to change, expanding ice-free ocean areas will serve as emission  
1104 sources for SSA particles, influencing cloud properties, and finally the radiative budget.

1105 Consequently, our findings contribute to an improved understanding of the complex interplay  
1106 of environmental processes resulting in Arctic amplification (Wendisch et al., 2017, 2023).

## 1107 **Author contributions**

1108 SZ wrote the manuscript with input from all co-authors. SZ, JS, CP, HS, BW, MW, and MvP  
1109 collected field samples in Ny-Ålesund. HS and BW served as principal investigators for balloon  
1110 operations during the field campaign. SZ conducted the laboratory carbohydrate analyses and  
1111 data processing. MZ and AB carried out the FESOM2.1-REcoM3 simulations. KE assessed cloud  
1112 conditions for the case studies using remote sensing data. All co-authors reviewed and  
1113 commented on the manuscript.

1114

## 1115 **Acknowledgments**

1116 We would like to express our gratitude to Kings Bay and the AWIPEV staff, with special thanks  
1117 to the station leader Grégory Tran, for their invaluable support to make this field study  
1118 possible. We furthermore thank the AWIPEV station's scientific staff in ensuring the  
1119 availability of high-quality meteorological data. In this context, we like to give special thanks  
1120 to Fieke Rader and Marion Maturilli. The cloud observations were taken within the project  
1121 AWIPEV\_0016.

1122 We also thank the scientific team at the Zeppelin Observatory from NILU and NPI, with special  
1123 appreciation to Wenche Aas, for their dedicated work in monitoring aerosol data.

1124 Furthermore, we acknowledge the entire BELUGA team for their contributions during both  
1125 the autumn 2021 and spring 2022 campaigns, with special thanks to Thomas Conrath. We also  
1126 thank Michel Michalkow for preprocessing the CAMP and standard meteorological data  
1127 collected at BELUGA as part of his Master's thesis. We are grateful to René Rabe for preparing  
1128 the campaign equipment and to Leon Schmidt for conducting the chemical analysis of  
1129 inorganic ions.

1130 For the FESOM2.1-REcoM3 simulation for this research, the authors gratefully acknowledge  
1131 the computing time granted by the Resource Allocation Board and provided on the  
1132 supercomputer Lise and Emmy at NHR@ZIB and NHR@Göttingen as part of the NHR

1133 infrastructure. The calculations for this research were conducted with computing resources  
1134 under the project hbk00084.

1135 This research has been supported by the Deutsche Forschungsgemeinschaft (DFG, German  
1136 Research Foundation, project no. 268020496-TRR 172) within the Transregional Collaborative  
1137 Research Center “Arctic Amplification: Climate Relevant Atmospheric and SurfaCe Processes,  
1138 and Feedback Mechanisms (AC)3” in subprojects A02, B04, C03 and E02. MW was supported  
1139 by the DFG Priority Program SPP 1158 “Antarctic Research with comparative investigations in  
1140 Arctic ice areas” (grant 522416631). We thank Johannes Röttenbacher for his constructive  
1141 feedback on the manuscript.

1142

### 1143 **Competing interests**

1144 All authors declare no financial or non-financial competing interests. Some authors are  
1145 members of the editorial board of ACP.

1146

### 1147 **Data availability**

1148 Chemical data from offline TSP filters are publicly available in PANGAEA for seawater  
1149 (Zeppenfeld and Schmidt, 2025) and aerosol particles (Zeppenfeld et al., 2025). The  
1150 microwave radiometer LWP and IWV data are available in PANGAEA (Ebell and Ritter, 2022).  
1151 The Cloudnet classification and ice water content products (Ebell et al., 2025) can be  
1152 downloaded via the ACTRIS Cloudnet data portal (<https://cloudnet.fmi.fi>).

hat formatiert: Nicht Hervorheben

hat formatiert: Englisch (Vereinigtes Königreich)

## 1153 References

- 1154 Aas, W., Berglen, T. F., Eckhardt, S., Fiebig, M., Solberg, S., and Yttri, K. E.: Monitoring of long-range transported air pollutants  
1155 in Norway. Annual Report 2021., NILU, 2022.
- 1156 Aas, W., Eckhardt, S., Solberg, S., and Yttri, K. E.: Monitoring of long-range transported air pollutants in Norway. Annual Report  
1157 2022., NILU, 2023.
- 1158 Akansu, E. F., Dahlke, S., Siebert, H., and Wendisch, M.: Evaluation of methods to determine the surface mixing layer height  
1159 of the atmospheric boundary layer in the central Arctic during polar night and transition to polar day in cloudless and cloudy  
1160 conditions, *Atmospheric Chemistry and Physics*, 23, 15473–15489, <https://doi.org/10.5194/acp-23-15473-2023>, 2023.
- 1161 Aller, J. Y., Kuznetsova, M. R., Jahns, C. J., and Kemp, P. F.: The sea surface microlayer as a source of viral and bacterial  
1162 enrichment in marine aerosols, *Journal of Aerosol Science*, 36, 801–812, <https://doi.org/10.1016/j.jaerosci.2004.10.012>,  
1163 2005.
- 1164 Aller, J. Y., Radway, J. C., Kiltthau, W. P., Bothe, D. W., Wilson, T. W., Vaillancourt, R. D., Quinn, P. K., Coffman, D. J., Murray,  
1165 B. J., and Knopf, D. A.: Size-resolved characterization of the polysaccharidic and proteinaceous components of sea spray  
1166 aerosol, *Atmospheric Environment*, 154, 331–347, <https://doi.org/10.1016/j.atmosenv.2017.01.053>, 2017.
- 1167 Alpert, P. A., Kiltthau, W. P., O'Brien, R. E., Moffet, R. C., Gilles, M. K., Wang, B., Laskin, A., Aller, J. Y., and Knopf, D. A.: Ice-  
1168 nucleating agents in sea spray aerosol identified and quantified with a holistic multimodal freezing model, *Science Advances*,  
1169 8, eabq6842, <https://doi.org/10.1126/sciadv.abq6842>, 2022.
- 1170 Aluwihare, L. I., Repeta, D. J., and Chen, R. F.: A major biopolymeric component to dissolved organic carbon in surface sea  
1171 water, *Nature*, 387, 166–169, <https://doi.org/10.1038/387166a0>, 1997.
- 1172 Amore, A., Giardi, F., Becagli, S., Caiazzo, L., Mazzola, M., Severi, M., and Traversi, R.: Source apportionment of sulphate in  
1173 the High Arctic by a 10 yr-long record from Gruebadet Observatory (Ny-Ålesund, Svalbard Islands), *Atmospheric  
1174 Environment*, 270, 118890, <https://doi.org/10.1016/j.atmosenv.2021.118890>, 2022.
- 1175 Angle, K., Grassian, V. H., and Ault, A. P.: The rapid acidification of sea spray aerosols, *Physics today*, 75, 58–59,  
1176 <https://doi.org/10.1063/PT.3.4926>, 2022.
- 1177 Angle, K. J., Crocker, D. R., Simpson, R. M. C., Mayer, K. J., Garofalo, L. A., Moore, A. N., Garcia, S. L. M., Or, V. W., Srinivasan,  
1178 S., Farhan, M., Sauer, J. S., Lee, C., Pothier, M. A., Farmer, D. K., Martz, T. R., Bertram, T. H., Cappa, C. D., Prather, K. A., and  
1179 Grassian, V. H.: Acidity across the interface from the ocean surface to sea spray aerosol, *PNAS*, 118, 1–6,  
1180 <https://doi.org/10.1073/pnas.2018397118>, 2021.
- 1181 Arnosti, C., Wietz, M., Brinkhoff, T., Hehemann, J.-H., Probandt, D., Zeugner, L., and Amann, R.: The Biogeochemistry of  
1182 Marine Polysaccharides: Sources, Inventories, and Bacterial Drivers of the Carbohydrate Cycle, *Ann Rev Mar Sci*, 13, 81–108,  
1183 <https://doi.org/10.1146/annurev-marine-032020-012810>, 2021.
- 1184 Assmy, P., Cecilie Kvernvik, A., Hop, H., Hoppe, C. J. M., Chierici, M., David T., D., Duarte, P., Fransson, A., García, L. M., Patula,  
1185 W., Kwaśniewski, S., Maturilli, M., Pavlova, O., Tatarek, A., Wiktor, J. M., Wold, A., Wolf, K. K. E., and Bailey, A.: Seasonal  
1186 plankton dynamics in Kongsfjorden during two years of contrasting environmental conditions, *Progress in Oceanography*,  
1187 213, 102996, <https://doi.org/10.1016/j.pocean.2023.102996>, 2023.
- 1188 Avci, B., Krüger, K., Fuchs, B. M., Teeling, H., and Amann, R. I.: Polysaccharide niche partitioning of distinct *Polaribacter* clades  
1189 during North Sea spring algal blooms, *ISME J*, 14, 1369–1383, <https://doi.org/10.1038/s41396-020-0601-y>, 2020.
- 1190 Barthelmeß, T., Cristi, A., Deppeler, S., Safi, K., Sellegri, K., Law, C. S., and Engel, A.: Pronounced Diel Cycling of Dissolved  
1191 Carbohydrates and Amino Acids in the Surface Ocean and across Diverse Regimes, *Environ. Sci. Technol.*, 59, 419–429,  
1192 <https://doi.org/10.1021/acs.est.4c00491>, 2025.
- 1193 Becker, S., Tebben, J., Coffinet, S., Wiltshire, K., Iversen, M. H., Harder, T., Hinrichs, K.-U., and Hehemann, J.-H.: Laminarin is  
1194 a major molecule in the marine carbon cycle, *PNAS*, 117, 6599–6607, <https://doi.org/10.1073/pnas.1917001117>, 2020.
- 1195 Bianco, A., Deguillaume, L., Chaumerliac, N., Vaïtilingom, M., Wang, M., Delort, A.-M., and Bridoux, M. C.: Effect of  
1196 endogenous microbiota on the molecular composition of cloud water: a study by Fourier-transform ion cyclotron resonance  
1197 mass spectrometry (FT-ICR MS), *Sci Rep*, 9, 1–12, <https://doi.org/10.1038/s41598-019-44149-8>, 2019.
- 1198 Bischof, K., Convey, P., Duarte, P., Gattuso, J.-P., Granberg, M., Hop, H., Hoppe, C., Jiménez, C., Lisitsyn, L., Martínez, B.,  
1199 Røleda, M. Y., Thor, P., Wiktor, J. M., and Gabrielsen, G. W.: Kongsfjorden as Harbinger of the Future Arctic: Knowns,  
1200 Unknowns and Research Priorities, in: *The Ecosystem of Kongsfjorden, Svalbard*, edited by: Hop, H. and Wiencke, C., Springer  
1201 International Publishing, Cham, 537–562, [https://doi.org/10.1007/978-3-319-46425-1\\_14](https://doi.org/10.1007/978-3-319-46425-1_14), 2019.
- 1202 Bivand, R., Pebesma, E., and Gomez-Rubio, V.: *Applied spatial data analysis with R*, Springer, 2013.
- 1203 Bivand, R., Keitt, T., and Rowlingson, B.: *rgdal: Bindings for the “Geospatial” Data Abstraction Library*, R package version 1.5-  
1204 32, 2022.

1205 Borch, N. H. and Kirchman, D. L.: Concentration and composition of dissolved combined neutral sugars (polysaccharides) in  
1206 seawater determined by HPLC-PAD, *Marine Chemistry*, 57, 85–95, [https://doi.org/10.1016/S0304-4203\(97\)00002-9](https://doi.org/10.1016/S0304-4203(97)00002-9), 1997.

1207 Brownrigg, M. R.: Package ‘mapdata’, R package version 2.3.1, 2013.

1208 Brownrigg, M. R.: maps: Draw Geographical Maps, R package version 3.4.2, 2023.

1209 Browse, J., Carslaw, K. S., Mann, G. W., Birch, C. E., Arnold, S. R., and Leck, C.: The complex response of Arctic aerosol to sea-  
1210 ice retreat, *Atmospheric Chemistry and Physics*, 14, 7543–7557, <https://doi.org/10.5194/acp-14-7543-2014>, 2014.

1211 Burns, W. G., Marchetti, A., and Ziervogel, K.: Enhanced formation of transparent exopolymer particles (TEP) under  
1212 turbulence during phytoplankton growth, *J Plankton Res*, 41, 349–361, <https://doi.org/10.1093/plankt/fbz018>, 2019.

1213 Burrows, S. M., Ogunro, O., Frossard, A., Russell, L. M., Rasch, P. J., and Elliott, S.: A Physically Based Framework for Modelling  
1214 the Organic Fractionation of Sea Spray Aerosol from Bubble Film Langmuir Equilibria, *Atmospheric Chemistry and Physics*,  
1215 14(24):13601–13629, <https://doi.org/10.5194/acp-14-13601-2014>, 2014.

1216 Cai, Q., Wang, J., Beletsky, D., Overland, J., Ikeda, M., and Wan, L.: Accelerated decline of summer Arctic sea ice during 1850–  
1217 2017 and the amplified Arctic warming during the recent decades, *Environ. Res. Lett.*, 16, 034015,  
1218 <https://doi.org/10.1088/1748-9326/abdb5f>, 2021.

1219 Carlton, A. G., Wiedinmyer, C., and Kroll, J. H.: A review of Secondary Organic Aerosol (SOA) formation from isoprene,  
1220 *Atmospheric Chemistry and Physics*, 9, 4987–5005, <https://doi.org/10.5194/acp-9-4987-2009>, 2009.

1221 Carslaw, D. C. and Ropkins, K.: openair --- An R package for air quality data analysis, *Environmental Modelling & Software*,  
1222 27–28, 52–61, 2012.

1223 Chang, L., Song, S., Feng, G., Zhang, Y., and Gao, G.: Assessment of the Uncertainties in Arctic Low-Level Temperature  
1224 Inversion Characteristics in Radio Occultation Observations, *IEEE Transactions on Geoscience and Remote Sensing*, 55, 1793–  
1225 1803, <https://doi.org/10.1109/TGRS.2016.2633461>, 2017.

1226 Chi, J. W., Li, W. J., Zhang, D. Z., Zhang, J. C., Lin, Y. T., Shen, X. J., Sun, J. Y., Chen, J. M., Zhang, X. Y., Zhang, Y. M., and Wang,  
1227 W. X.: Sea salt aerosols as a reactive surface for inorganic and organic acidic gases in the Arctic troposphere, *Atmospheric  
1228 Chemistry and Physics*, 15, 11341–11353, <https://doi.org/10.5194/acp-15-11341-2015>, 2015.

1229 Compiano, A.-M., Romano, J.-C., Garabetian, F., Laborde, P., and de la Giraudière, I.: Monosaccharide composition of  
1230 particulate hydrolysable sugar fraction in surface microlayers from brackish and marine waters, *Marine Chemistry*, 42, 237–  
1231 251, [https://doi.org/10.1016/0304-4203\(93\)90015-G](https://doi.org/10.1016/0304-4203(93)90015-G), 1993.

1232 Crahan, K. K., Hegg, D., Covert, D. S., and Jonsson, H.: An exploration of aqueous oxalic acid production in the coastal marine  
1233 atmosphere, *Atmospheric Environment*, 38, 3757–3764, <https://doi.org/10.1016/j.atmosenv.2004.04.009>, 2004.

1234 Creamean, J. M., de Boer, G., Telg, H., Mei, F., Dexheimer, D., Shupe, M. D., Solomon, A., and McComiskey, A.: Assessing the  
1235 vertical structure of Arctic aerosols using balloon-borne measurements, *Atmospheric Chemistry and Physics*, 21, 1737–1757,  
1236 <https://doi.org/10.5194/acp-21-1737-2021>, 2021.

1237 Croft, B., Lohmann, U., Martin, R. V., Stier, P., Wurzel, S., Feichter, J., Posselt, R., and Ferrachat, S.: Aerosol size-dependent  
1238 below-cloud scavenging by rain and snow in the ECHAM5-HAM, *Atmospheric Chemistry and Physics*, 9, 4653–4675,  
1239 <https://doi.org/10.5194/acp-9-4653-2009>, 2009.

1240 Cunliffe, M. and Wurl, O.: Guide to best practices to study the ocean’s surface., *Marine Biological Association of the United  
1241 Kingdom for SCOR*, 2014.

1242 Dahms, A. S.: 3-Deoxy-D-pentulonic acid aldolase and its role in a new pathway of D-xylose degradation, *Biochemical and  
1243 Biophysical Research Communications*, 60, 1433–1439, [https://doi.org/10.1016/0006-291X\(74\)90358-1](https://doi.org/10.1016/0006-291X(74)90358-1), 1974.

1244 Dekhtyareva, A., Holmén, K., Maturilli, M., Hermansen, O., and Gravensen, R.: Effect of seasonal mesoscale and microscale  
1245 meteorological conditions in Ny-Ålesund on results of monitoring of long-range transported pollution, *Polar Research*, 2018.

1246 DeMott, P. J., Hill, T. C. J., McCluskey, C. S., Prather, K. A., Collins, D. B., Sullivan, R. C., Ruppel, M. J., Mason, R. H., Irish, V. E.,  
1247 Lee, T., Hwang, C. Y., Rhee, T. S., Snider, J. R., McMeeking, G. R., Dhaniyala, S., Lewis, E. R., Wentzell, J. J. B., Abbatt, J., Lee,  
1248 C., Sultana, C. M., Ault, A. P., Axson, J. L., Martinez, M. D., Venero, I., Santos-Figueroa, G., Stokes, M. D., Deane, G. B., Mayol-  
1249 Bracero, O. L., Grassian, V. H., Bertram, T. H., Bertram, A. K., Moffett, B. F., and Franc, G. D.: Sea spray aerosol as a unique  
1250 source of ice nucleating particles, *PNAS*, 113, 5797–5803, <https://doi.org/10.1073/pnas.1514034112>, 2016.

1251 Dusek, U., Frank, G. P., Hildebrandt, L., Curtius, J., Schneider, J., Walter, S., Chand, D., Drewnick, F., Hings, S., Jung, D.,  
1252 Borrmann, S., and Andreae, M. O.: Size Matters More Than Chemistry for Cloud-Nucleating Ability of Aerosol Particles,  
1253 *Science*, 312, 1375–1378, <https://doi.org/10.1126/science.1125261>, 2006.

1254 Ebell, K. and Ritter, C.: HATPRO microwave radiometer measurements at AWIPEV, Ny-Ålesund (2019–2021), *PANGAEA*,  
1255 <https://doi.org/10.1594/PANGAEA.943004>, 2022.

1256 Ebell, K., Maturilli, M., Ritter, C., and O’Connor, E.: Custom collection of classification, and ice water content data from Ny-  
1257 Ålesund between 27 Sep and 12 Nov 2021, ACTRIS Cloud remote sensing data centre unit (CLU),  
1258 <https://doi.org/10.60656/5598100185854c01>, 2025.

- 1259 Egerer, U., Ehrlich, A., Gottschalk, M., Griesche, H., Neggers, R. A. J., Siebert, H., and Wendisch, M.: Case study of a humidity  
1260 layer above Arctic stratocumulus and potential turbulent coupling with the cloud top, *Atmospheric Chemistry and Physics*,  
1261 21, 6347–6364, <https://doi.org/10.5194/acp-21-6347-2021>, 2021.
- 1262 Egerer, U., Siebert, H., Hellmuth, O., and Sørensen, L. L.: The role of a low-level jet for stirring the stable atmospheric surface  
1263 layer in the Arctic, *Atmospheric Chemistry and Physics*, 23, 15365–15373, <https://doi.org/10.5194/acp-23-15365-2023>, 2023.
- 1264 Engel, A.: Distribution of transparent exopolymer particles (TEP) in the northeast Atlantic Ocean and their potential  
1265 significance for aggregation processes, *Deep Sea Research Part I: Oceanographic Research Papers*, 51, 83–92,  
1266 <https://doi.org/10.1016/j.dsr.2003.09.001>, 2004.
- 1267 Engel, A. and Galgani, L.: The organic sea-surface microlayer in the upwelling region off the coast of Peru and potential  
1268 implications for air–sea exchange processes, *Biogeosciences (BG)*, 13, 989–1007, <https://doi.org/10.5194/bg-13-989-2016>,  
1269 2016.
- 1270 Engel, A. and Händel, N.: A novel protocol for determining the concentration and composition of sugars in particulate and in  
1271 high molecular weight dissolved organic matter (HMW-DOM) in seawater, *Marine Chemistry*, 127, 180–191,  
1272 <https://doi.org/10.1016/j.marchem.2011.09.004>, 2011.
- 1273 Engel, A., Thoms, S., Riebesell, U., Rochelle-Newall, E., and Zondervan, I.: Polysaccharide aggregation as a potential sink of  
1274 marine dissolved organic carbon, *Nature*, 428, 929–932, <https://doi.org/10.1038/nature02453>, 2004.
- 1275 Engel, A., Harlay, J., Piontek, J., and Chou, L.: Contribution of combined carbohydrates to dissolved and particulate organic  
1276 carbon after the spring bloom in the northern Bay of Biscay (North-Eastern Atlantic Ocean), *Continental Shelf Research*, 45,  
1277 42–53, <https://doi.org/10.1016/j.csr.2012.05.016>, 2012.
- 1278 Ervens, B. and Amato, P.: The global impact of bacterial processes on carbon mass, *Atmospheric Chemistry & Physics*, 20,  
1279 1777–1794, <https://doi.org/10.5194/acp-20-1777-2020>, 2020.
- 1280 Esau, I. and Repina, I.: Wind Climate in Kongsfjorden, Svalbard, and Attribution of Leading Wind Driving Mechanisms through  
1281 Turbulence-Resolving Simulations, *Advances in Meteorology*, 2012, 568454, <https://doi.org/10.1155/2012/568454>, 2012.
- 1282 Fabiano, M., Povero, P., and Danovaro, R.: Distribution and composition of particulate organic matter in the Ross Sea  
1283 (Antarctica), *Polar Biol*, 13, 525–533, <https://doi.org/10.1007/BF00236394>, 1993.
- 1284 Facchini, M. C., Rinaldi, M., Decesari, S., Carbone, C., Finessi, E., Mircea, M., Fuzzi, S., Ceburnis, D., Flanagan, R., Nilsson, E. D.,  
1285 Leeuw, G. de, Martino, M., Woeltjen, J., and O'Dowd, C. D.: Primary submicron marine aerosol dominated by insoluble organic  
1286 colloids and aggregates, *Geophysical Research Letters*, 35, 1–5, <https://doi.org/10.1029/2008GL034210>, 2008.
- 1287 Farmer, D. K., Cappa, C. D., and Kreidenweis, S. M.: Atmospheric Processes and Their Controlling Influence on Cloud  
1288 Condensation Nuclei Activity, *Chem. Rev.*, 115, 4199–4217, <https://doi.org/10.1021/cr5006292>, 2015.
- 1289 Farmer, D. K., Boedicker, E. K., and DeBolt, H. M.: Dry Deposition of Atmospheric Aerosols: Approaches, Observations, and  
1290 Mechanisms, *Annual Review of Physical Chemistry*, 72, 375–397, <https://doi.org/10.1146/annurev-physchem-090519-034936>, 2021.
- 1291  
1292 Feltracco, M., Barbaro, E., Hoppe, C. J. M., Wolf, K. K. E., Spolaor, A., Layton, R., Keuschnig, C., Barbante, C., Gambaro, A., and  
1293 Larose, C.: Airborne bacteria and particulate chemistry capture Phytoplankton bloom dynamics in an Arctic fjord, *Atmospheric  
1294 Environment*, 256, 118458, <https://doi.org/10.1016/j.atmosenv.2021.118458>, 2021.
- 1295 Fomba, K. W., Müller, K., van Pinxteren, D., Poulain, L., van Pinxteren, M., and Herrmann, H.: Long-term chemical  
1296 characterization of tropical and marine aerosols at the Cape Verde Atmospheric Observatory (CVAO) from 2007 to 2011,  
1297 *Atmospheric Chemistry and Physics*, 14, 8883–8904, <https://doi.org/10.5194/acp-14-8883-2014>, 2014.
- 1298 Francis, J. A. and Wu, B.: Why has no new record-minimum Arctic sea-ice extent occurred since September 2012?, *Environ.  
1299 Res. Lett.*, 15, 114034, <https://doi.org/10.1088/1748-9326/abc047>, 2020.
- 1300 Freud, E., Krejci, R., Tunved, P., Leaitch, R., Nguyen, Q. T., Massling, A., Skov, H., and Barrie, L.: Pan-Arctic aerosol number size  
1301 distributions: seasonality and transport patterns, *Atmospheric Chemistry and Physics*, 17, 8101–8128,  
1302 <https://doi.org/10.5194/acp-17-8101-2017>, 2017.
- 1303 [Furukawa, T. and Takahashi, Y.: Oxalate metal complexes in aerosol particles: implications for the hygroscopicity of oxalate-](https://doi.org/10.5194/acp-11-4289-2011)  
1304 [containing particles, \*Atmos. Chem. Phys.\*, 11, 4289–4301, <https://doi.org/10.5194/acp-11-4289-2011>, 2011.](https://doi.org/10.5194/acp-11-4289-2011)
- 1305 Gantt, B., Meskhidze, N., Facchini, M. C., Rinaldi, M., Ceburnis, D., and O'Dowd, C. D.: Wind speed dependent size-resolved  
1306 parameterization for the organic mass fraction of sea spray aerosol, *Atmospheric Chemistry and Physics*, 11, 8777–8790,  
1307 <https://doi.org/10.5194/acp-11-8777-2011>, 2011.
- 1308 Gao, Q., Leck, C., Rauschenberg, C., and Matrai, P. A.: On the chemical dynamics of extracellular polysaccharides in the high  
1309 Arctic surface microlayer, *Ocean Science*, 8, 401–418, <https://doi.org/10.5194/os-8-401-2012>, 2012.
- 1310 Gierens, R., Kneifel, S., Shupe, M. D., Ebell, K., Maturilli, M., and Löhnert, U.: Low-level mixed-phase clouds in a complex Arctic  
1311 environment, *Atmospheric Chemistry and Physics*, 20, 3459–3481, <https://doi.org/10.5194/acp-20-3459-2020>, 2020.

hat formatiert: Schriftart: 9 Pt.

Formatiert: Standard, Links, Abstand Nach: 0 Pt.

1312 Goldberg, S. J., Carlson, C. A., Brzezinski, M., Nelson, N. B., and Siegel, D. A.: Systematic removal of neutral sugars within  
1313 dissolved organic matter across ocean basins, *Geophysical Research Letters*, 38, 1–7,  
1314 <https://doi.org/10.1029/2011GL048620>, 2011.

1315 Grawe, S., Jentsch, C., Schaefer, J., Wex, H., Mertes, S., and Stratmann, F.: Next-generation ice-nucleating particle sampling  
1316 on board aircraft: characterization of the High-volume flow aERosol particle filter sAmplifier (HERA), *Atmospheric Measurement  
1317 Techniques*, 16, 4551–4570, <https://doi.org/10.5194/amt-16-4551-2023>, 2023.

1318 Grolemond, G. and Wickham, H.: Dates and Times Made Easy with lubridate, *Journal of Statistical Software*, 40, 1–25, 2011.

1319 Grosse, J., Nöthig, E.-M., Torres-Valdés, S., and Engel, A.: Summertime Amino Acid and Carbohydrate Patterns in Particulate  
1320 and Dissolved Organic Carbon Across Fram Strait, *Front. Mar. Sci.*, 8, <https://doi.org/10.3389/fmars.2021.684675>, 2021.

1321 Guo, T., Li, K., Zhu, Y., Gao, H., and Yao, X.: Concentration and size distribution of particulate oxalate in marine and coastal  
1322 atmospheres – Implication for the increased importance of oxalate in nanometer atmospheric particles, *Atmospheric  
1323 Environment*, 142, 19–31, <https://doi.org/10.1016/j.atmosenv.2016.07.026>, 2016.

1324 Gürses, Ö., Oziel, L., Karakuş, O., Sidorenko, D., Völker, C., Ye, Y., Zeising, M., Butzin, M., and Hauck, J.: Ocean biogeochemistry  
1325 in the coupled ocean–sea ice–biogeochemistry model FESOM2.1–REcoM3, *Geoscientific Model Development*, 16, 4883–  
1326 4936, <https://doi.org/10.5194/gmd-16-4883-2023>, 2023.

1327 Haddrell, A. E. and Thomas, R. J.: Aerobiology: Experimental Considerations, Observations, and Future Tools, *Appl. Environ.  
1328 Microbiol.*, 83, 1–15, <https://doi.org/10.1128/AEM.00809-17>, 2017.

1329 Hansell, D. A.: Recalcitrant Dissolved Organic Carbon Fractions, *Annual Review of Marine Science*, 5, 421–445,  
1330 <https://doi.org/10.1146/annurev-marine-120710-100757>, 2013.

1331 Hara, K., Yamagata, S., Yamanouchi, T., Sato, K., Herber, A., Iwasaka, Y., Nagatani, M., and Nakata, H.: Mixing states of  
1332 individual aerosol particles in spring Arctic troposphere during ASTAR 2000 campaign, *Journal of Geophysical Research:  
1333 Atmospheres*, 108, 1–12, <https://doi.org/10.1029/2002JD002513>, 2003.

1334 Hartmann, S., Schrödner, R., Hassett, B. T., Hartmann, M., van Pinxteren, M., Fomba, K. W., Stratmann, F., Herrmann, H.,  
1335 Pöhler, M., and Zeppenfeld, S.: Polysaccharides–Important Constituents of Ice-Nucleating Particles of Marine Origin,  
1336 *Environ. Sci. Technol.*, 59, 5098–5108, <https://doi.org/10.1021/acs.est.4c08014>, 2025.

1337 Hasenecz, E., Jayarathne, T., Pendergraft, M. A., Santander, M. V., Mayer, K. J., Sauer, J., Lee, C., Gibson, W. S., Kruse, S. M.,  
1338 Malfatti, F., Prather, K. A., and Stone, E. A.: Marine bacteria affect saccharide enrichment in sea spray aerosol during a  
1339 phytoplankton bloom, *ACS Earth Space Chem.*, 4, 1638–1649, <https://doi.org/10.1021/acsearthspacechem.0c00167>, 2020.

1340 Hasenecz, E. S., Kaluarachchi, C. P., Lee, H. D., Tivanski, A. V., and Stone, E. A.: Saccharide Transfer to Sea Spray Aerosol  
1341 Enhanced by Surface Activity, Calcium, and Protein Interactions, *ACS Earth Space Chem.*, 3, 2539–2548,  
1342 <https://doi.org/10.1021/acsearthspacechem.9b00197>, 2019.

1343 Herrmann, H., Tilgner, A., Barzaghi, P., Majdik, Z., Gligorovski, S., Poulain, L., and Monod, A.: Towards a more detailed  
1344 description of tropospheric aqueous phase organic chemistry: CAPRAM 3.0, *Atmospheric Environment*, 39, 4351–4363,  
1345 <https://doi.org/10.1016/j.atmosenv.2005.02.016>, 2005.

1346 Heutte, B., Bergner, N., Angot, H., Pernov, J. B., Dada, L., Mirrielees, J. A., Beck, I., Baccarini, A., Boyer, M., Creamean, J. M.,  
1347 Daellenbach, K. R., El Haddad, I., Frey, M. M., Henning, S., Laurila, T., Moschos, V., Petäjä, T., Pratt, K. A., Quéléver, L. L. J.,  
1348 Shupe, M. D., Zieger, P., Jokinen, T., and Schmale, J.: Observations of high-time-resolution and size-resolved aerosol chemical  
1349 composition and microphysics in the central Arctic: implications for climate-relevant particle properties, *Atmospheric  
1350 Chemistry and Physics*, 25, 2207–2241, <https://doi.org/10.5194/acp-25-2207-2025>, 2025.

1351 Hijmans, R. J.: raster: Geographic Data Analysis and Modeling, R package version 3.6-26, 2023.

1352 Hill, T. C. J., Malfatti, F., McCluskey, C. S., Schill, G. P., Santander, M. V., Moore, K. A., Rauker, A. M., Perkins, R. J., Celussi, M.,  
1353 Levin, E. J. T., Suski, K. J., Cornwell, G. C., Lee, C., Negro, P. D., Kreidenweis, S. M., Prather, K. A., and DeMott, P. J.: Resolving  
1354 the controls over the production and emission of ice-nucleating particles in sea spray, *Environ. Sci.: Atmos.*,  
1355 <https://doi.org/10.1039/D2EA00154C>, 2023.

1356 Hoffman, E. J. and Duce, R. A.: Factors influencing the organic carbon content of marine aerosols: A laboratory study, *Journal  
1357 of Geophysical Research (1896-1977)*, 81, 3667–3670, <https://doi.org/10.1029/JC081i021p03667>, 1976.

1358 Hogan, R. J., Mittermaier, M. P., and Illingworth, A. J.: The Retrieval of Ice Water Content from Radar Reflectivity Factor and  
1359 Temperature and Its Use in Evaluating a Mesoscale Model, *Journal of Applied Meteorology and Climatology*, 45, 301–317,  
1360 <https://doi.org/10.1175/JAM2340.1>, 2006.

1361 Hoppel, W. A., Frick, G. M., and Fitzgerald, J. W.: Surface source function for sea-salt aerosol and aerosol dry deposition to  
1362 the ocean surface, *Journal of Geophysical Research: Atmospheres*, 107, AAC 7-1-AAC 7-17,  
1363 <https://doi.org/10.1029/2001JD002014>, 2002.

1364 Illingworth, A. J., Hogan, R. J., O’Connor, E. J., Bouniol, D., Brooks, M. E., Delanoé, J., Donovan, D. P., Eastment, J. D., Gaussiat,  
1365 N., Goddard, J. W. F., Haeffelin, M., Baltink, H. K., Krasnov, O. A., Pelon, J., Piriou, J.-M., Protat, A., Russchenberg, H. W. J.,  
1366 Seifert, A., Tompkins, A. M., Zadelhoff, G.-J. van, Vinit, F., Willén, U., Wilson, D. R., and Wrench, C. L.: Cloudnet: Continuous

1367 Evaluation of Cloud Profiles in Seven Operational Models Using Ground-Based Observations, *Bulletin of the American*  
1368 *Meteorological Society*, 88, 883–898, <https://doi.org/10.1175/BAMS-88-6-883>, 2007.

1369 Ittekkot, V., Brockmann, U., Michaelis, W., and Degens, E. T.: Dissolved free and combined carbohydrates during a  
1370 phytoplankton bloom in the northern North Sea, *Marine Ecology Progress Series*, 4, 299–305, 1981.

1371 Jayarathne, T., Sultana, C. M., Lee, C., Malfatti, F., Cox, J. L., Pendergraft, M. A., Moore, K. A., Azam, F., Tivanski, A. V., Cappa,  
1372 C. D., Bertram, T. H., Grassian, V. H., Prather, K. A., and Stone, E. A.: Enrichment of Saccharides and Divalent Cations in Sea  
1373 Spray Aerosol During Two Phytoplankton Blooms, *Environ Sci Technol*, 50, 11511–11520,  
1374 <https://doi.org/10.1021/acs.est.6b02988>, 2016.

1375 Jensen, L. Z., Glasius, M., Gryning, S.-E., Massling, A., Finster, K., and Šantl-Temkiv, T.: Seasonal Variation of the Atmospheric  
1376 Bacterial Community in the Greenlandic High Arctic Is Influenced by Weather Events and Local and Distant Sources, *Front.*  
1377 *Microbiol.*, 13, <https://doi.org/10.3389/fmicb.2022.909980>, 2022.

1378 Kang, H., Jung, C. H., Lee, B. Y., Krejci, R., Heslin-Rees, D., Aas, W., and Yoon, Y. J.: Aerosol hygroscopicity influenced by  
1379 seasonal chemical composition variations in the Arctic region, *Journal of Aerosol Science*, 106551,  
1380 <https://doi.org/10.1016/j.jaerosci.2025.106551>, 2025.

1381 Kanji, Z. A., Ladino, L. A., Wex, H., Boose, Y., Burkert-Kohn, M., Cziczo, D. J., and Krämer, M.: Overview of Ice Nucleating  
1382 Particles, *Meteorological Monographs*, 58, 1.1-1.33, <https://doi.org/10.1175/AMSMONOGRAPH5-D-16-0006.1>, 2017.

1383 Karl, M., Leck, C., Rad, F. M., Bäcklund, A., Lopez-Aparicio, S., and Heintzenberg, J.: New insights in sources of the sub-  
1384 micrometre aerosol at Mt. Zeppelin observatory (Spitsbergen) in the year 2015, *Tellus B: Chemical and Physical Meteorology*,  
1385 71, 1613143, <https://doi.org/10.1080/16000889.2019.1613143>, 2019.

1386 Kawamura, K. and Bikkina, S.: A review of dicarboxylic acids and related compounds in atmospheric aerosols: Molecular  
1387 distributions, sources and transformation, *Atmospheric Research*, 170, 140–160,  
1388 <https://doi.org/10.1016/j.atmosres.2015.11.018>, 2016.

1389 Kawamura, K., Kasukabe, H., and Barrie, L. A.: Source and reaction pathways of dicarboxylic acids, ketoacids and dicarbonyls  
1390 in arctic aerosols: One year of observations, *Atmospheric Environment*, 30, 1709–1722, [https://doi.org/10.1016/1352-2310\(95\)00395-9](https://doi.org/10.1016/1352-2310(95)00395-9), 1996a.

1392 Kawamura, K., Sempéré, R., Imai, Y., Fujii, Y., and Hayashi, M.: Water soluble dicarboxylic acids and related compounds in  
1393 Antarctic aerosols, *Journal of Geophysical Research: Atmospheres*, 101, 18721–18728, <https://doi.org/10.1029/96JD01541>,  
1394 1996b.

1395 Keene, W. C., Pszenny, A. A. P., Galloway, J. N., and Hawley, M. E.: Sea-salt corrections and interpretation of constituent ratios  
1396 in marine precipitation, *Journal of Geophysical Research*, 91, 6647–6658, <https://doi.org/10.1029/JD091iD06p06647>, 1986.

1397 Keene, W. C., Long, M. S., Reid, J. S., Frossard, A. A., Kieber, D. J., Maben, J. R., Russell, L. M., Kinsey, J. D., Quinn, P. K., and  
1398 Bates, T. S.: Factors That Modulate Properties of Primary Marine Aerosol Generated From Ambient Seawater on Ships at Sea,  
1399 *Journal of Geophysical Research: Atmospheres*, 122, 11,961-11,990, <https://doi.org/10.1002/2017JD026872>, 2017.

1400 Kerminen, V.-M., Teinilä, K., Hillamo, R., and Mäkelä, T.: Size-segregated chemistry of particulate dicarboxylic acids in the  
1401 Arctic atmosphere, *Atmospheric Environment*, 33, 2089–2100, [https://doi.org/10.1016/S1352-2310\(98\)00350-1](https://doi.org/10.1016/S1352-2310(98)00350-1), 1999.

1402 Khadem, H. E.: *Carbohydrate Chemistry: Monosaccharides and Their Oligomers*, Elsevier, 267 pp., 2012.

1403 Kharbush, J. J., Close, H. G., Van Mooy, B. A. S., Arnosti, C., Smittenberg, R. H., Le Moigne, F. A. C., Mollenhauer, G., Scholz-  
1404 Böttcher, B., Obrecht, I., Koch, B. P., Becker, K., Iversen, M. H., and Mohr, W.: Particulate Organic Carbon Deconstructed:  
1405 Molecular and Chemical Composition of Particulate Organic Carbon in the Ocean, *Frontiers in Marine Science*, 7, Art.Nr. 518,  
1406 <https://doi.org/10.3389/fmars.2020.00518>, 2020.

1407 Kirchman, D. L., Meon, B., Ducklow, H. W., Carlson, C. A., Hansell, D. A., and Steward, G. F.: Glucose fluxes and concentrations  
1408 of dissolved combined neutral sugars (polysaccharides) in the Ross Sea and Polar Front Zone, Antarctica, *Deep Sea Research*  
1409 *Part II: Topical Studies in Oceanography*, 48, 4179–4197, [https://doi.org/10.1016/S0967-0645\(01\)00085-6](https://doi.org/10.1016/S0967-0645(01)00085-6), 2001.

1410 Klein, A. M., Bohannan, B. J. M., Jaffe, D. A., Levin, D. A., and Green, J. L.: Molecular Evidence for Metabolically Active Bacteria  
1411 in the Atmosphere, *Front. Microbiol.*, 7, 772, <https://doi.org/10.3389/fmicb.2016.00772>, 2016.

1412 Köllner, F., Schneider, J., Willis, M. D., Klimach, T., Helleis, F., Bozem, H., Kunkel, D., Hoor, P., Burkart, J., Leaitch, W. R.,  
1413 Aliabadi, A. A., Abbatt, J. P. D., Herber, A. B., and Borrmann, S.: Particulate trimethylamine in the summertime Canadian high  
1414 Arctic lower troposphere, *Atmospheric Chemistry and Physics*, 17, 13747–13766, [https://doi.org/10.5194/acp-17-13747-](https://doi.org/10.5194/acp-17-13747-2017)  
1415 2017, 2017.

1416 Leck, C., Gao, Q., Mashayekhy Rad, F., and Nilsson, U.: Size-resolved atmospheric particulate polysaccharides in the high  
1417 summer Arctic, *Atmospheric Chemistry and Physics*, 13, 12573–12588, <https://doi.org/10.5194/acp-13-12573-2013>, 2013.

1418 Leon-Marcos, A., Zeising, M., van Pinxteren, M., Zeppenfeld, S., Bracher, A., Barbaro, E., Engel, A., Feltracco, M., Tegen, I., and  
1419 Heinold, B.: Modelling emission and transport of key components of primary marine organic aerosol using the global aerosol-  
1420 climate model ECHAM6.3–HAM2.3, *Geoscientific Model Development*, 18, 4183–4213, [https://doi.org/10.5194/gmd-18-](https://doi.org/10.5194/gmd-18-4183-2025)  
1421 4183-2025, 2025.

1422 Li, J., Han, Z., Fu, P., Yao, X., and Liang, M.: Seasonal characteristics of emission, distribution, and radiative effect of marine  
1423 organic aerosols over the western Pacific Ocean: an investigation with a coupled regional climate aerosol model, *Atmospheric  
1424 Chemistry and Physics*, 24, 3129–3161, <https://doi.org/10.5194/acp-24-3129-2024>, 2024.

1425 Lohmann, U. and Feichter, J.: Global indirect aerosol effects: a review, *Atmospheric Chemistry and Physics*, 5, 715–737,  
1426 <https://doi.org/10.5194/acp-5-715-2005>, 2005.

1427 Madry, W. L., Toon, O. B., and O’Dowd, C. D.: Modeled optical thickness of sea-salt aerosol, *Journal of Geophysical Research:  
1428 Atmospheres*, 116, <https://doi.org/10.1029/2010JD014691>, 2011.

1429 Malfatti, F., Lee, C., Tinta, T., Pendergraft, M. A., Celussi, M., Zhou, Y., Sultana, C. M., Rotter, A., Axson, J. L., Collins, D. B.,  
1430 Santander, M. V., Anides Morales, A. L., Aluwihare, L. I., Riemer, N., Grassian, V. H., Azam, F., and Prather, K. A.: Detection of  
1431 Active Microbial Enzymes in Nascent Sea Spray Aerosol: Implications for Atmospheric Chemistry and Climate, *Environ. Sci.  
1432 Technol. Lett.*, 6, 171–177, <https://doi.org/10.1021/acs.estlett.8b00699>, 2019.

1433 Manders, A. M. M., Schaap, M., Querol, X., Albert, M. F. M. A., Vercauteren, J., Kuhlbusch, T. A. J., and Hoogerbrugge, R.: Sea  
1434 salt concentrations across the European continent, *Atmospheric Environment*, 44, 2434–2442,  
1435 <https://doi.org/10.1016/j.atmosenv.2010.03.028>, 2010.

1436 Matulová, M., Husárová, S., Capek, P., Sancelme, M., and Delort, A.-M.: Biotransformation of Various Saccharides and  
1437 Production of Exopolymeric Substances by Cloud-Borne *Bacillus* sp. 3B6, *Environ. Sci. Technol.*, 48, 14238–14247,  
1438 <https://doi.org/10.1021/es501350s>, 2014.

1439 Maturilli, M.: Continuous meteorological observations at station Ny-Ålesund (2011-08 et seq), Alfred Wegener Institute -  
1440 Research Unit Potsdam, <https://doi.org/10.1594/PANGAEA.914979>, 2020.

1441 Maturilli, M., Herber, A., and König-Langlo, G.: Climatology and time series of surface meteorology in Ny-Ålesund, Svalbard,  
1442 *Earth System Science Data*, 5, 155–163, <https://doi.org/10.5194/essd-5-155-2013>, 2013.

1443 Maturilli, M., Herber, A., and König-Langlo, G.: Surface radiation climatology for Ny-Ålesund, Svalbard (78.9° N), basic  
1444 observations for trend detection, *Theor Appl Climatol*, 120, 331–339, <https://doi.org/10.1007/s00704-014-1173-4>, 2015.

1445 Mayot, N., Matrai, P., Ellingsen, I. H., Steele, M., Johnson, K., Riser, S. C., and Swift, D.: Assessing Phytoplankton Activities in  
1446 the Seasonal Ice Zone of the Greenland Sea Over an Annual Cycle, *Journal of Geophysical Research: Oceans*, 123, 8004–8025,  
1447 <https://doi.org/10.1029/2018JC014271>, 2018.

1448 McNeill, V. F.: Aqueous Organic Chemistry in the Atmosphere: Sources and Chemical Processing of Organic Aerosols, *Environ.  
1449 Sci. Technol.*, 49, 1237–1244, <https://doi.org/10.1021/es5043707>, 2015.

1450 Mirrielees, J. A., Kirpes, R. M., Costa, E. J., Porter, G. C. E., Murray, B. J., Lata, N. N., Boschi, V., China, S., Grannas, A. M., Ault,  
1451 A. P., Matrai, P. A., and Pratt, K. A.: Marine aerosol generation experiments in the High Arctic during summertime, *Elementa:  
1452 Science of the Anthropocene*, 12, 00134, <https://doi.org/10.1525/elementa.2023.00134>, 2024.

1453 Müller, K., Lehmann, S., Pinxteren, D. van, Gnauk, T., Niedermeier, N., Wiedensohler, A., and Herrmann, H.: Particle  
1454 characterization at the Cape Verde atmospheric observatory during the 2007 RHaMBLe intensive, *Atmospheric Chemistry  
1455 and Physics*, 10, 2709–2721, <https://doi.org/10.5194/acp-10-2709-2010>, 2010.

1456 Neuwirth, E.: RColorBrewer: ColorBrewer Palettes, R package version 1.1-3, 2022.

1457 Nomokonova, T., Ebell, K., Löhnert, U., Maturilli, M., Ritter, C., and O’Connor, E.: Statistics on clouds and their relation to  
1458 thermodynamic conditions at Ny-Ålesund using ground-based sensor synergy, *Atmospheric Chemistry and Physics*, 19, 4105–  
1459 4126, <https://doi.org/10.5194/acp-19-4105-2019>, 2019.

1460 O’Dowd, C. D. and de Leeuw, G.: Marine aerosol production: a review of the current knowledge, *Philos Trans A Math Phys  
1461 Eng Sci*, 365, 1753–1774, <https://doi.org/10.1098/rsta.2007.2043>, 2007.

1462 O’Dowd, C. D., Smith, M. H., Consterdine, I. E., and Lowe, J. A.: Marine aerosol, sea-salt, and the marine sulphur cycle: a short  
1463 review, *Atmospheric Environment*, 31, 73–80, [https://doi.org/10.1016/S1352-2310\(96\)00106-9](https://doi.org/10.1016/S1352-2310(96)00106-9), 1997.

1464 Ooki, A., Uematsu, M., Miura, K., and Nakae, S.: Sources of sodium in atmospheric fine particles, *Atmospheric Environment*,  
1465 36, 4367–4374, [https://doi.org/10.1016/S1352-2310\(02\)00341-2](https://doi.org/10.1016/S1352-2310(02)00341-2), 2002.

1466 Orellana, M. V. and Leck, C.: Chapter 9 - Marine Microgels, in: *Biogeochemistry of Marine Dissolved Organic Matter (Second  
1467 Edition)*, edited by: Hansell, D. A. and Carlson, C. A., Academic Press, Boston, 451–480, <https://doi.org/10.1016/B978-0-12-405940-5.00009-1>, 2015.

1469 Orellana, M. V., Matrai, P. A., Leck, C., Rauschenberg, C. D., Lee, A. M., and Coz, E.: Marine microgels as a source of cloud  
1470 condensation nuclei in the high Arctic, *PNAS*, 108, 13612–13617, <https://doi.org/10.1073/pnas.1102457108>, 2011.

1471 Oziel, L., Schourup-Kristensen, V., Wekerle, C., and Hauck, J.: The Pan-Arctic Continental Slope as an Intensifying Conveyor  
1472 Belt for Nutrients in the Central Arctic Ocean (1985–2015), *Global Biogeochemical Cycles*, 36, e2021GB007268,  
1473 <https://doi.org/10.1029/2021GB007268>, 2022.

1474 Panagiotopoulos, C. and Sempéré, R.: Analytical methods for the determination of sugars in marine samples: A historical  
1475 perspective and future directions, *Limnology and Oceanography: Methods*, 3, 419–454,  
1476 <https://doi.org/10.4319/lom.2005.3.419>, 2005.

1477 Penner, J. E., Andreae, M. O., Annegarn, H., Barrie, L., Feichter, J., Hegg, D., Jayaraman, A., Leaitch, R., Murphy, D., Nganga,  
1478 J., and Pitari, G.: Aerosols, their Direct and Indirect Effects, *Climate Change 2001: The Scientific Basis. Contribution of Working  
1479 Group I to the Third Assessment Report of the Intergovernmental Panel on Climate Change*, 289–348, 2001.

1480 Pierce, D.: ncd4: Interface to Unidata netCDF (Version 4 or Earlier) Format Data, R package version 1.22, 2023.

1481 Pilinis, C., Pandis, S. N., and Seinfeld, J. H.: Sensitivity of direct climate forcing by atmospheric aerosols to aerosol size and  
1482 composition, *Journal of Geophysical Research*, 100, 18,739–18,754, <https://doi.org/10.1029/95JD02119>, 1995.

1483 Pilz, C., Düsing, S., Wehner, B., Müller, T., Siebert, H., Voigtländer, J., and Lonardi, M.: CAMP: an instrumented platform for  
1484 balloon-borne aerosol particle studies in the lower atmosphere, *Atmospheric Measurement Techniques*, 15, 6889–6905,  
1485 <https://doi.org/10.5194/amt-15-6889-2022>, 2022.

1486 Pilz, C., Lonardi, M., Egerer, U., Siebert, H., Ehrlich, A., Heymsfield, A. J., Schmitt, C. G., Shupe, M. D., Wehner, B., and  
1487 Wendisch, M.: Profile observations of the Arctic atmospheric boundary layer with the BELUGA tethered balloon during  
1488 MOSAiC, *Sci Data*, 10, 534, <https://doi.org/10.1038/s41597-023-02423-5>, 2023.

1489 Pilz, C., Cassano, J. J., de Boer, G., Kirbus, B., Lonardi, M., Pöhlker, M., Shupe, M. D., Siebert, H., Wendisch, M., and Wehner,  
1490 B.: Tethered balloon measurements reveal enhanced aerosol occurrence aloft interacting with Arctic low-level clouds,  
1491 *Elementa: Science of the Anthropocene*, 12, 00120, <https://doi.org/10.1525/elementa.2023.00120>, 2024.

1492 van Pinxteren, M., Müller, C., Iinuma, Y., Stolle, C., and Herrmann, H.: Chemical Characterization of Dissolved Organic  
1493 Compounds from Coastal Sea Surface Microlayers (Baltic Sea, Germany), *Environmental Science & Technology*, 46, 10455–  
1494 10462, <https://doi.org/10.1021/es204492b>, 2012.

1495 van Pinxteren, M., Barthel, S., Fomba, K. W., Müller, K., Von Tümpling, W., and Herrmann, H.: The influence of environmental  
1496 drivers on the enrichment of organic carbon in the sea surface microlayer and in submicron aerosol particles – measurements  
1497 from the Atlantic Ocean, *Elem Sci Anth*, 5, 1–21, <https://doi.org/10.1525/elementa.225>, 2017.

1498 van Pinxteren, M., Robinson, T.-B., Zeppenfeld, S., Gong, X., Bahlmann, E., Fomba, K. W., Triesch, N., Stratmann, F., Wurl, O.,  
1499 Engel, A., Wex, H., and Herrmann, H.: High number concentrations of transparent exopolymer particles in ambient aerosol  
1500 particles and cloud water – a case study at the tropical Atlantic Ocean, *Atmospheric Chemistry and Physics*, 22, 5725–5742,  
1501 <https://doi.org/10.5194/acp-22-5725-2022>, 2022.

1502 van Pinxteren, M., Zeppenfeld, S., Fomba, K. W., Triesch, N., Frka, S., and Herrmann, H.: Amino acids, carbohydrates, and  
1503 lipids in the tropical oligotrophic Atlantic Ocean: sea-to-air transfer and atmospheric in situ formation, *Atmospheric Chemistry  
1504 and Physics*, 23, 6571–6590, <https://doi.org/10.5194/acp-23-6571-2023>, 2023.

1505 Platt, S. M., Hov, Ø., Berg, T., Breivik, K., Eckhardt, S., Eleftheriadis, K., Evangeliou, N., Fiebig, M., Fisher, R., Hansen, G.,  
1506 Hansson, H.-C., Heintzenberg, J., Hermansen, O., Heslin-Rees, D., Holmén, K., Hudson, S., Kallenborn, R., Krejci, R., Krognes,  
1507 T., Larssen, S., Lowry, D., Lund Myhre, C., Lunder, C., Nisbet, E., Nizzetto, P. B., Park, K.-T., Pedersen, C. A., Aspö Pfaffhuber,  
1508 K., Röckmann, T., Schmidbauer, N., Solberg, S., Stohl, A., Ström, J., Svendby, T., Tunved, P., Tørnkvist, K., van der Veen, C.,  
1509 Vratolis, S., Yoon, Y. J., Yttri, K. E., Zieger, P., Aas, W., and Tørseth, K.: Atmospheric composition in the European Arctic and  
1510 30 years of the Zeppelin Observatory, Ny-Ålesund, *Atmospheric Chemistry and Physics*, 22, 3321–3369,  
1511 <https://doi.org/10.5194/acp-22-3321-2022>, 2022.

1512 van de Poll, W. H., Maat, D. S., Fischer, P., Visser, R. J. W., Brussaard, C. P. D., and Buma, A. G. J.: Solar radiation and solar  
1513 radiation driven cycles in warming and freshwater discharge control seasonal and inter-annual phytoplankton chlorophyll a  
1514 and taxonomic composition in a high Arctic fjord (Kongsfjorden, Spitsbergen), *Limnology and Oceanography*, 66, 1221–1236,  
1515 <https://doi.org/10.1002/lno.11677>, 2021.

1516 Porter, G. C. E., Adams, M. P., Brooks, I. M., Ickes, L., Karlsson, L., Leck, C., Salter, M. E., Schmale, J., Siegel, K., Sikora, S. N. F.,  
1517 Tarn, M. D., Vüllers, J., Wernli, H., Zieger, P., Zinke, J., and Murray, B. J.: Highly Active Ice-Nucleating Particles at the Summer  
1518 North Pole, *Journal of Geophysical Research: Atmospheres*, 127, e2021JD036059, <https://doi.org/10.1029/2021JD036059>,  
1519 2022.

1520 Quinn, P. K., Collins, D. B., Grassian, V. H., Prather, K. A., and Bates, T. S.: Chemistry and Related Properties of Freshly Emitted  
1521 Sea Spray Aerosol, *Chemical Reviews*, 115, 4383–4399, <https://doi.org/10.1021/cr500713g>, 2015.

1522 Ramasamy, K. P., Mahawar, L., Rajasabapathy, R., Rajeshwari, K., Miceli, C., and Pucciarelli, S.: Comprehensive insights on  
1523 environmental adaptation strategies in Antarctic bacteria and biotechnological applications of cold adapted molecules, *Front.  
1524 Microbiol.*, 14, <https://doi.org/10.3389/fmicb.2023.1197797>, 2023.

1525 Rinaldi, M., Decesari, S., Carbone, C., Finessi, E., Fuzzi, S., Ceburnis, D., O'Dowd, C. D., Sciare, J., Burrows, J. P., Vrekoussis, M.,  
1526 Ervens, B., Tsigaridis, K., and Facchini, M. C.: Evidence of a natural marine source of oxalic acid and a possible link to glyoxal,  
1527 *Journal of Geophysical Research: Atmospheres*, 116, <https://doi.org/10.1029/2011JD015659>, 2011.

1528 Robinson, T.-B., Stolle, C., and Wurl, O.: Depth is relative: the importance of depth for transparent exopolymer particles in  
1529 the near-surface environment, *Ocean Science*, 15, 1653–1666, <https://doi.org/10.5194/os-15-1653-2019>, 2019a.

- 1530 Robinson, T.-B., Wurl, O., Bahlmann, E., Jürgens, K., and Stolle, C.: Rising bubbles enhance the gelatinous nature of the air–  
1531 sea interface, *Limnology and Oceanography*, 64, 2358–2372, <https://doi.org/10.1002/lno.11188>, 2019b.
- 1532 Rocchi, A., von Jackowski, A., Welti, A., Li, G., Kanji, Z. A., Povazhnyy, V., Engel, A., Schmale, J., Nenes, A., Berdalet, E., Simó,  
1533 R., and Dall’Osto, M.: Glucose Enhances Salinity-Driven Sea Spray Aerosol Production in Eastern Arctic Waters, *Environ. Sci.*  
1534 *Technol.*, 58, 8748–8759, <https://doi.org/10.1021/acs.est.4c02826>, 2024.
- 1535 Russell, L. M., Hawkins, L. N., Frossard, A. A., Quinn, P. K., and Bates, T. S.: Carbohydrate-like composition of submicron  
1536 atmospheric particles and their production from ocean bubble bursting, *Proc. Natl. Acad. Sci. U.S.A.*, 107, 6652–6657,  
1537 <https://doi.org/10.1073/pnas.0908905107>, 2010.
- 1538 Sander, R., Keene, W. C., Pszenny, A. a. P., Arimoto, R., Ayers, G. P., Baboukas, E., Cainey, J. M., Crutzen, P. J., Duce, R. A.,  
1539 Hönninger, G., Huebert, B. J., Maenhaut, W., Mihalopoulos, N., Turekian, V. C., and Van Dingenen, R.: Inorganic bromine in  
1540 the marine boundary layer: a critical review, *Atmospheric Chemistry and Physics*, 3, 1301–1336, <https://doi.org/10.5194/acp-3-1301-2003>, 2003.
- 1542 Šantl-Temkiv, T., Gosewinkel, U., Starnawski, P., Lever, M., and Finster, K.: Aeolian dispersal of bacteria in southwest  
1543 Greenland: their sources, abundance, diversity and physiological states, *FEMS Microbiol Ecol*, 94,  
1544 <https://doi.org/10.1093/femsec/fiy031>, 2018.
- 1545 Šantl-Temkiv, T., Amato, P., Casamayor, E. O., Lee, P. K. H., and Pointing, S. B.: Microbial ecology of the atmosphere, *FEMS*  
1546 *Microbiology Reviews*, 46, fuac009, <https://doi.org/10.1093/femsre/fuac009>, 2022.
- 1547 Schartau, M., Engel, A., Schröter, J., Thoms, S., Völker, C., and Wolf-Gladrow, D.: Modelling carbon overconsumption and the  
1548 formation of extracellular particulate organic carbon, *Biogeosciences*, 4, 433–454, <https://doi.org/10.5194/bg-4-433-2007>,  
1549 2007.
- 1550 Schill, S. R., Burrows, S. M., Hasenecz, E. S., Stone, E. A., and Bertram, T. H.: The Impact of Divalent Cations on the Enrichment  
1551 of Soluble Saccharides in Primary Sea Spray Aerosol, *Atmosphere*, 9, 476, <https://doi.org/10.3390/atmos9120476>, 2018.
- 1552 Schmale, J., Zieger, P., and Ekman, A. M. L.: Aerosols in current and future Arctic climate, *Nature Climate Change*, 11, 95–105,  
1553 <https://doi.org/10.1038/s41558-020-00969-5>, 2021.
- 1554 Schmale, J., Sharma, S., Decesari, S., Pernov, J., Massling, A., Hansson, H.-C., von Salzen, K., Skov, H., Andrews, E., Quinn, P.  
1555 K., Upchurch, L. M., Eleftheriadis, K., Traversi, R., Gilardoni, S., Mazzola, M., Laing, J., and Hopke, P.: Pan-Arctic seasonal cycles  
1556 and long-term trends of aerosol properties from 10 observatories, *Atmospheric Chemistry and Physics*, 22, 3067–3096,  
1557 <https://doi.org/10.5194/acp-22-3067-2022>, 2022.
- 1558 Sharma, S., Barrie, L. a., Magnusson, E., Brattström, G., Leaitch, W. r., Steffen, A., and Landsberger, S.: A Factor and Trends  
1559 Analysis of Multidecadal Lower Tropospheric Observations of Arctic Aerosol Composition, Black Carbon, Ozone, and Mercury  
1560 at Alert, Canada, *Journal of Geophysical Research: Atmospheres*, 124, 14133–14161, <https://doi.org/10.1029/2019JD030844>,  
1561 2019.
- 1562 Shestakova, A., Chechin, D., Lüpkes, C., Hartmann, J., and Maturilli, M.: Foehn effect during easterly flow over Svalbard,  
1563 <https://doi.org/10.5194/acp-2021-478>, 2021.
- 1564 [Simon, D. J., Hartmann, J., Schaefer, J., Zeppenfeld, S., Lüpkes, C., Hartmann, M., Wetzel, B., Heinold, B., Jurányi, Z., Schulz,  
1565 A., Köhler, L., Jörss, A.-M., Herber, A., Henning, S., Pöhlker, M. L., Roberts, G. C., and Stratmann, F.: Turbulent aerosol fluxes  
1566 from airborne measurements over the Arctic Ocean, \*Geophys. Res. Lett.\*, 52, e2025GL117094,  
1567 <https://doi.org/10.1029/2025GL117094>, 2025](https://doi.org/10.1029/2025GL117094)
- 1568
- 1569 Sinreich, R., Coburn, S., Dix, B., and Volkamer, R.: Ship-based detection of glyoxal over the remote tropical Pacific Ocean,  
1570 *Atmospheric Chemistry and Physics*, 10, 11359–11371, <https://doi.org/10.5194/acp-10-11359-2010>, 2010.
- 1571 Sorooshian, A., Lu, M.-L., Brechtel, F. J., Jonsson, H., Feingold, G., Flagan, R. C., and Seinfeld, J. H.: On the Source of Organic  
1572 Acid Aerosol Layers above Clouds, *Environ. Sci. Technol.*, 41, 4647–4654, <https://doi.org/10.1021/es0630442>, 2007.
- 1573 Stein, A. F., Draxler, R. R., Rolph, G. D., Stunder, B. J. B., Cohen, M. D., and Ngan, F.: NOAA’s HYSPLIT Atmospheric Transport  
1574 and Dispersion Modeling System, *Bull. Amer. Meteor. Soc.*, 96, 2059–2077, <https://doi.org/10.1175/BAMS-D-14-00110.1>,  
1575 2015.
- 1576 Struthers, H., Ekman, A. M. L., Glantz, P., Iversen, T., Kirkevåg, A., Mårtensson, E. M., Seland, Ø., and Nilsson, E. D.: The effect  
1577 of sea ice loss on sea salt aerosol concentrations and the radiative balance in the Arctic, *Atmospheric Chemistry and Physics*,  
1578 11, 3459–3477, <https://doi.org/10.5194/acp-11-3459-2011>, 2011.
- 1579 Su, B., Bi, X., Zhang, Z., Liang, Y., Song, C., Wang, T., Hu, Y., Li, L., Zhou, Z., Yan, J., Wang, X., and Zhang, G.: Enrichment of  
1580 calcium in sea spray aerosol: insights from bulk measurements and individual particle analysis during the R/V *Xuelong* cruise  
1581 in the summertime in Ross Sea, Antarctica, *Atmospheric Chemistry and Physics*, 23, 10697–10711,  
1582 <https://doi.org/10.5194/acp-23-10697-2023>, 2023.
- 1583 Theodosi, C., Im, U., Bougiatioti, A., Zarmas, P., Yenigun, O., and Mihalopoulos, N.: Aerosol chemical composition over  
1584 Istanbul, *Science of The Total Environment*, 408, 2482–2491, <https://doi.org/10.1016/j.scitotenv.2010.02.039>, 2010.

hat formatiert: Schriftart: 11 Pt.

Formatiert: Standard, Abstand Nach: 0 Pt.

1585 Thyng, K., Greene, C. A., Hetland, R. D., Zimmerle, H. M., and DiMarco, S.: True colors of oceanography: Guidelines for effective  
1586 and accurate colormap selection, *Oceanography*, 3, <https://doi.org/10.5670/oceanog.2016.66>, 2016.

1587 Tilgner, A. and Herrmann, H.: Radical-driven carbonyl-to-acid conversion and acid degradation in tropospheric aqueous  
1588 systems studied by CAPRAM, *Atmospheric Environment*, 44, 5415–5422, <https://doi.org/10.1016/j.atmosenv.2010.07.050>,  
1589 2010.

1590 Tørseth, K., Aas, W., Breivik, K., Fjæraa, A. M., Fiebig, M., Hjellbrekke, A. G., Lund Myhre, C., Solberg, S., and Yttri, K. E.:  
1591 Introduction to the European Monitoring and Evaluation Programme (EMEP) and observed atmospheric composition change  
1592 during 1972–2009, *Atmospheric Chemistry and Physics*, 12, 5447–5481, <https://doi.org/10.5194/acp-12-5447-2012>,  
1593 2012.

1594 Trainic, M., Koren, I., Sharoni, S., Frada, M., Segev, L., Rudich, Y., and Vardi, A.: Infection Dynamics of a Bloom-Forming Alga  
1595 and Its Virus Determine Airborne Coccolith Emission from Seawater, *iScience*, 6, 327–335,  
1596 <https://doi.org/10.1016/j.isci.2018.07.017>, 2018.

1597 Triesch, N., van Pinxteren, M., Engel, A., and Herrmann, H.: Concerted measurements of free amino acids at the Cabo Verde  
1598 islands: high enrichments in submicron sea spray aerosol particles and cloud droplets, *Atmospheric Chemistry and Physics*,  
1599 21, 163–181, <https://doi.org/10.5194/acp-21-163-2021>, 2021.

1600 Turekian, V. C., Macko, S. A., and Keene, W. C.: Concentrations, isotopic compositions, and sources of size-resolved,  
1601 particulate organic carbon and oxalate in near-surface marine air at Bermuda during spring, *Journal of Geophysical Research:*  
1602 *Atmospheres*, 108, <https://doi.org/10.1029/2002JD002053>, 2003.

1603 Veron, F.: Ocean Spray, *Annual Review of Fluid Mechanics*, 47, 507–538, <https://doi.org/10.1146/annurev-fluid-010814-014651>, 2015.

1605 Vihtakari, M.: PlotSvalbard: PlotSvalbard-Plot research data from Svalbard on maps, R package version 0.9 2, 2020.

1606 Warneck, P.: In-cloud chemistry opens pathway to the formation of oxalic acid in the marine atmosphere, *Atmospheric*  
1607 *Environment*, 37, 2423–2427, [https://doi.org/10.1016/S1352-2310\(03\)00136-5](https://doi.org/10.1016/S1352-2310(03)00136-5), 2003.

1608 Wendisch, M., Brückner, M., Burrows, J. P., Crewell, S., Dethloff, K., Ebell, K., Lüpkes, C., Macke, A., Notholt, J., and Quaas, J.:  
1609 Understanding causes and effects of rapid warming in the Arctic, *Eos*, 98, 2017.

1610 Wendisch, M., Brückner, M., Crewell, S., Ehrlich, A., Notholt, J., Lüpkes, C., Macke, A., Burrows, J. P., Rinke, A., Quaas, J.,  
1611 Maturilli, M., Schemann, V., Shupe, M. D., Akansu, E. F., Barrientos-Velasco, C., Bärfuss, K., Blechschmidt, A.-M., Block, K.,  
1612 Bougoudis, I., Bozem, H., Böckmann, C., Bracher, A., Bresson, H., Bretschneider, L., Buschmann, M., Chechin, D. G., Chyllik, J.,  
1613 Dahlke, S., Deneke, H., Dethloff, K., Donth, T., Dorn, W., Dupuy, R., Ebell, K., Egerer, U., Engelmann, R., Eppers, O., Gerdes, R.,  
1614 Gierens, R., Gorodetskaya, I. V., Gottschalk, M., Griesche, H., Gryanik, V. M., Handorf, D., Harm-Altstädter, B., Hartmann, J.,  
1615 Hartmann, M., Heinold, B., Herber, A., Herrmann, H., Heygster, G., Höschel, I., Hofmann, Z., Hölemann, J., Hünerbein, A.,  
1616 Jafariserajehlou, S., Jäkel, E., Jacobi, C., Janout, M., Jansen, F., Jourdan, O., Jurányi, Z., Kalesse-Los, H., Kanzow, T., Kätthner,  
1617 R., Kliesch, L. L., Klingebiel, M., Knudsen, E. M., Kovács, T., Körtke, W., Krampe, D., Kretzschmar, J., Kreyling, D., Kulla, B.,  
1618 Kunkel, D., Lampert, A., Lauer, M., Lelli, L., Lerber, A. von, Linke, O., Löhnert, U., Lonardi, M., Losa, S. N., Losch, M., Maahn,  
1619 M., Mech, M., Mei, L., Mertes, S., Metzner, E., Mewes, D., Michaelis, J., Mioche, G., Moser, M., Nakoudi, K., Negggers, R.,  
1620 Neuber, R., Nomokonova, T., Oelker, J., Papakonstantinou-Presvelou, I., et al.: Atmospheric and Surface Processes, and  
1621 Feedback Mechanisms Determining Arctic Amplification: A Review of First Results and Prospects of the (AC)3 Project, *Bulletin*  
1622 *of the American Meteorological Society*, 104, E208–E242, <https://doi.org/10.1175/BAMS-D-21-0218.1>, 2023.

1623 White, W. H.: Chemical markers for sea salt in IMPROVE aerosol data, *Atmospheric Environment*, 42, 261–274,  
1624 <https://doi.org/10.1016/j.atmosenv.2007.09.040>, 2008.

1625 Wickham, H.: Reshaping Data with the reshape Package, *Journal of Statistical Software*, 21, 1–20, 2007.

1626 Wickham, H.: ggplot2: Elegant Graphics for Data Analysis, Springer-Verlag New York, [https://doi.org/10.1007/978-3-319-24277-4\\_2](https://doi.org/10.1007/978-3-319-24277-4_2), 2016.

1628 Wickham, H., François, R., Henry, L., Müller, K., and Vaughan, D.: dplyr: A Grammar of Data Manipulation, R package version  
1629 1.1.4, 2023a.

1630 Wickham, H., Pedersen, T. L., and Seidel, D.: scales: Scale Functions for Visualization, R package version 1.3.0, 2023b.

1631 Wietz, M., Engel, A., Ramondenc, S., Niwano, M., von Appen, W.-J., Priest, T., von Jackowski, A., Metfies, K., Bienhold, C., and  
1632 Boetius, A.: The Arctic summer microbiome across Fram Strait: Depth, longitude, and substrate concentrations structure  
1633 microbial diversity in the euphotic zone, *Environmental Microbiology*, 26, e16568, <https://doi.org/10.1111/1462-1634.2920.16568>, 2024.

1635 Wietz, M., van Pinxteren, M., Freese, H. M., Sproer, C., and Zeppenfeld, S.: Seasonal connectivity of microbes and  
1636 carbohydrates between ocean, atmosphere, and cryosphere in Kongsfjorden (Svalbard, Arctic Ocean), preprint,  
1637 <https://doi.org/10.64898/2025.12.01.691664>, uploaded on 2 December 2025.

hat formatiert: Schriftart: 9 Pt.

Formatiert: Block

1638 ~~Wietz, M., van Pinxteren, M., Freese, H. M., Spröer, C., and Zeppenfeld, S.: Seasonal connectivity of microbes and~~  
1639 ~~carbohydrates between ocean, cryosphere and atmosphere in Kongsfjorden (Svalbard, Arctic Ocean), to be submitted as~~  
1640 ~~preprint, 2025.~~

1641 Willis, M. D., Leaitch, W. R., and Abbatt, J. P. D.: Processes Controlling the Composition and Abundance of Arctic Aerosol,  
1642 *Reviews of Geophysics*, 56, 621–671, <https://doi.org/10.1029/2018RG000602>, 2018.

1643 Wong, J. P. S., Tsagkaraki, M., Tsiodra, I., Mihalopoulos, N., Violaki, K., Kanakidou, M., Sciare, J., Nenes, A., and Weber, R. J.:  
1644 Effects of Atmospheric Processing on the Oxidative Potential of Biomass Burning Organic Aerosols, *Environ. Sci. Technol.*, 53,  
1645 6747–6756, <https://doi.org/10.1021/acs.est.9b01034>, 2019.

1646 Wurl, O. and Holmes, M.: The gelatinous nature of the sea-surface microlayer, *Marine Chemistry*, 110, 89–97,  
1647 <https://doi.org/10.1016/j.marchem.2008.02.009>, 2008.

1648 Xu, W., Ovadnevaite, J., Fossum, K. N., Lin, C., Huang, R.-J., Ceburnis, D., and O'Dowd, C.: Sea spray as an obscured source for  
1649 marine cloud nuclei, *Nat. Geosci.*, 15, 282–286, <https://doi.org/10.1038/s41561-022-00917-2>, 2022.

1650 Yang, C., Zhou, S., Zhang, C., Yu, M., Cao, F., and Zhang, Y.: Atmospheric Chemistry of Oxalate: Insight Into the Role of Relative  
1651 Humidity and Aerosol Acidity From High-Resolution Observation, *Journal of Geophysical Research: Atmospheres*, 127,  
1652 e2021JD035364, <https://doi.org/10.1029/2021JD035364>, 2022.

1653 Yttri, K. E., Bäcklund, A., Conen, F., Eckhardt, S., Evangelou, N., Fiebig, M., Kasper-Giebl, A., Gold, A., Gundersen, H., Myhre,  
1654 C. L., Platt, S. M., Simpson, D., Surratt, J. D., Szidat, S., Rauber, M., Tørseth, K., Ytre-Eide, M. A., Zhang, Z., and Aas, W.:  
1655 Composition and sources of carbonaceous aerosol in the European Arctic at Zeppelin Observatory, Svalbard (2017 to 2020),  
1656 *Atmospheric Chemistry and Physics*, 24, 2731–2758, <https://doi.org/10.5194/acp-24-2731-2024>, 2024.

1657 Yu, H., Kaufman, Y. J., Chin, M., Feingold, G., Remer, L. A., Anderson, T. L., Balkanski, Y., Bellouin, N., Boucher, O., Christopher,  
1658 S., DeCola, P., Kahn, R., Koch, D., Loeb, N., Reddy, M. S., Schulz, M., Takemura, T., and Zhou, M.: A review of measurement-  
1659 based assessments of the aerosol direct radiative effect and forcing, *Atmospheric Chemistry and Physics*, 6, 613–666,  
1660 <https://doi.org/10.5194/acp-6-613-2006>, 2006.

1661 Zäncker, B., Cunliffe, M., and Engel, A.: Eukaryotic community composition in the sea surface microlayer across an east–west  
1662 transect in the Mediterranean Sea, *Biogeosciences*, 18, 2107–2118, <https://doi.org/10.5194/bg-18-2107-2021>, 2021.

1663 Zeppenfeld, S. and Schmidt, L.: Dissolved and particulate carbohydrates and inorganic ions in the sea surface microlayer and  
1664 bulk water of Kongsfjorden (Autumn 2021/Spring 2022), <https://doi.org/10.1594/PANGAEA.982606>, 2025.

1665 Zeppenfeld, S., van Pinxteren, M., Engel, A., and Herrmann, H.: A protocol for quantifying mono- and polysaccharides in  
1666 seawater and related saline matrices by electro-dialysis (ED) – combined with HPAEC-PAD, *Ocean Science*, 16, 817–830,  
1667 <https://doi.org/10.5194/os-16-817-2020>, 2020.

1668 Zeppenfeld, S., van Pinxteren, M., van Pinxteren, D., Wex, H., Berdalet, E., Vaqué, D., Dall'Osto, M., and Herrmann, H.: Aerosol  
1669 Marine Primary Carbohydrates and Atmospheric Transformation in the Western Antarctic Peninsula, *ACS Earth Space Chem.*,  
1670 5, 1032–1047, <https://doi.org/10.1021/acsearthspacechem.0c00351>, 2021.

1671 Zeppenfeld, S., van Pinxteren, M., Hartmann, M., Zeising, M., Bracher, A., and Herrmann, H.: Marine carbohydrates in Arctic  
1672 aerosol particles and fog – diversity of oceanic sources and atmospheric transformations, *Atmospheric Chemistry and Physics*,  
1673 23, 15561–15587, <https://doi.org/10.5194/acp-23-15561-2023>, 2023.

1674 Zeppenfeld, S., Schaefer, J., van Pinxteren, M., and Schmidt, L.: Marine combined carbohydrates and inorganic ions in  
1675 atmospheric total suspended particles across altitudes in the lower troposphere of Ny-Ålesund, Svalbard,  
1676 <https://doi.org/10.1594/PANGAEA.982703>, 2025.

1677 Zhou, S., Gonzalez, L., Leithead, A., Finewax, Z., Thalman, R., Vlasenko, A., Vagle, S., Miller, L. A., Li, S.-M., Bureekul, S.,  
1678 Furutani, H., Uematsu, M., Volkamer, R., and Abbatt, J.: Formation of gas-phase carbonyls from heterogeneous oxidation of  
1679 polyunsaturated fatty acids at the air–water interface and of the sea surface microlayer, *Atmospheric Chemistry and Physics*,  
1680 14, 1371–1384, <https://doi.org/10.5194/acp-14-1371-2014>, 2014.

1681 Zhu, B., Sun-Waterhouse, D., and You, L.: Insights into the mechanisms underlying the degradation of xylooligosaccharides in  
1682 UV/H<sub>2</sub>O<sub>2</sub> system, *Carbohydrate Polymers*, 317, 121091, <https://doi.org/10.1016/j.carbpol.2023.121091>, 2023.

1683 Zhu, Y.-S., Connolly, A., Guyon, A., and FitzGerald, R. J.: Solubilisation of calcium and magnesium from the marine red algae  
1684 *Lithothamnion calcareum*, *International Journal of Food Science and Technology*, 49, 1600–1606,  
1685 <https://doi.org/10.1111/ijfs.12459>, 2014.